R-662

INTERIM REPORT
SPACE SHUTTLE TRAJECTORY MANAGEMENT, NAVIGATION, GUIDANCE, AND CONTROL DURING APPROACH AND LANDING

by

George W. Cherry, Mukund Desai, Barton DeWolf,
Donald Keene, Duncan MacKinnon, Paul Madden

MAY 1970

CHARLES STARK DRAPER LABORATORY

MASSACHUSETTS INSTITUTE OF TECHNOLOGY

CAMBRIDGE, MASSACHUSETTS, 02139

NASA CR 108501

R-662

INTERIM REPORT
SPACE SHUTTLE TRAJECTORY MANAGEMENT, NAVIGATION, GUIDANCE, AND CONTROL DURING APPROACH AND LANDING

by

George W. Cherry
Mukund Desai
Barton DeWolf
Donald Keene
Duncan MacKinnon
Paul Madden

MAY 1970

Submitted by: George W Cherry Date: 5/27/70
G. W. CHERRY, DEPUTY ASSOCIATE DIRECTOR
CHARLES STARK DRAPER LABORATORY

Approved: D. G. Hoag Date: 28 May 70
D. G. HOAG, DIRECTOR
APOLLO GUIDANCE AND NAVIGATION PROGRAM

Approved: Ralph R. Ragan Date: 28 May 70
R. R. RAGAN, DEPUTY DIRECTOR
CHARLES STARK DRAPER LABORATORY

ACKNOWLEDGEMENT

This report was prepared under DSR Project 55-40800, sponsored by the Manned Spacecraft Center of the National Aeronautics and Space Administration through Contract NAS 9-10268 with the Massachusetts Institute of Technology.

The authors would gratefully like to acknowledge the support and direction of Dr. Kenneth Cox of the Manned Spacecraft Center.

Published by the Charles Stark Draper Laboratory of the Massachusetts Institute of Technology.
Printed in Cambridge, Massachusetts, U.S.A., 1970

TABLE OF CONTENTS

TABLE OF CONTENTS

CHAPTER 1
INTRODUCTION

by

George W. Cherry

This report describes a great deal of the work done at the Draper Laboratory in the last three months devising and testing tools and techniques for trajectory planning and management and navigation, guidance, and control of the Space Shuttle vehicle during the approach and landing phase of its mission. This reporting period of the work has emphasized the synthesis and creation of trajectory planning concepts, guidance laws, filter equations, control parameter optimization algorithms and programs, etcetera. Therefore, while the motivation for the work was application to the Space Shuttle vehicle, there has been virtually no simulation of the invented techniques on Space Shuttle trajectories and dynamics. (In fact, in order to test some of the techniques devised for the shuttle, known available jet transport dynamics were used: for example, Chapter 5 tested its tools on the Convair 880.) It is planned that the next period of activity on this project will correct this deficiency.

In order to obtain an over-view of the major thrust of this report, the reader should consider the factors which could limit the ability of the Space Shuttle to follow a given path.

1. Navigation sensor noise, bias, and drift.
2. Environmental disturbances.
   a. steady winds
   b. wind shear
   c. wind gust
3. Space Shuttle dynamics.
4. Operational limitations such as air speed, power, fuel, maximum bank angle, maximum roll rate, etc.
5. Limitations on control forces, moments, activities and energy.

The block diagram in Fig. 1-1 summarizes the problem areas and references the chapters and appendixes where discussions and, hopefully, solutions of the problems can be found.

Chapter 2 deals directly with problem area 1. above and lays the foundation for dealing with 2.a. and 2.b. by providing estimates of the steady wind and, hopefully,

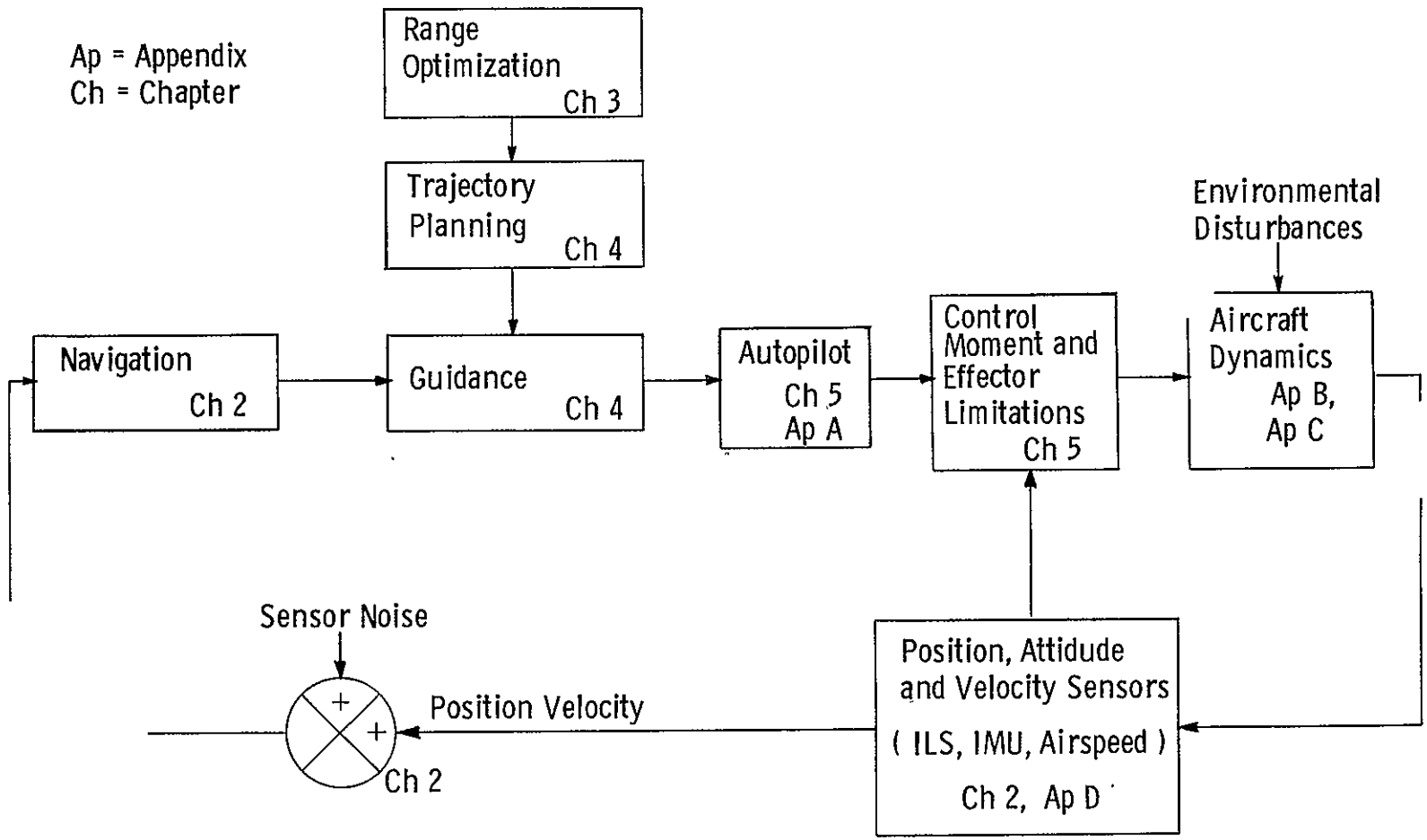

Fig. 1-1 Factors Affecting the Attainment of Precise Path Following

the wind-shear. If the wind velocity and wind shear can be estimated, then the guidance equations can provide feedforward commands to cancel their effects. For example, the crab angle required to follow a ground track can easily be computed by the guidance equations if the state estimator provides a wind estimate. The alternative is the less desirable technique of preventing increasing course deviation by integral compensation of position error.

Although no simulation results are available yet, preliminary computations predict that even at a range of 6 miles and using the coarse ILS, the optimal combination of IMU and scanning beam ILS data will result in position and velocity RMS errors of about 15 feet and 0.5 feet/second. Over the runway threshold the errors will be much smaller and certainly small enough for zero-zero landings without a radar altimeter.

Chapter 3 deals with aspects of problem area 4. above. It addresses itself to maximizing range subject to the constraint of a limited fuel quantity and includes the glider case by allowing the specification of zero fuel quantity available. While re-entry planning for the Space Shuttle vehicle should obviate the need for requiring SSV maximum range capability, contingencies such as accidents at the intended airport or an Apollo 13 type mishap, may make this capability a desirable contingency tool.

Chapter 4 deals with problem areas 2.a., 3., and 4. above. There are two key concepts in this chapter.

1. The first key concept is the design of reference paths and trajectories whose derivatives (velocity), second derivatives (acceleration), and third derivatives (jerk), take into account the Space Shuttle vehicle's dynamics, maneuver limitations, maneuver rate limitations, air speed restrictions, and so on. Such trajectories offer the significant advantage that the SSV, with a suitable control system, can fly such paths extremely accurately.
2. The second key concept is the provision of feedforward signals designed to make a simple model of the SSV fly the reference trajectory. (The simple problem includes the computation of feedforward signals which compensate for the steady wind.) The combination of an essentially flyable reference path with feedforward compensation results in close adherence of the space shuttle to the reference trajectory. The problem of dealing with wind gusts and errors in estimates of the wind velocity as well as effects due to the departure of the SSV's transfer function from the model's, is delegated to the feedback control system, whose

bandwidth and response can be optimized for its share of the control problem. In order to understand the relationship of the SSV to the simple model, the reader might consider the following analogy: The model is the lead aircraft (with perhaps different dynamics and a somewhat different environment from the SSV) in a formation, and the SSV flies wing on the model.

Chapter 5 deals with problem areas 2., 3., and 5. above and closes the loop in Fig. 1-1. This chapter describes the theory and a computer program (and some results) which can be used to optimize the parameters in the feedback path control system. The objective is to provide close adherence to the reference path in a turbulent aerodynamic environment without excessive control surface (or wheel) motion. The results are for the Convair 880 but can be extended to the SSV.

The appendixes contain material on several subsidiary topics, including (Appendix D) an error model and coordinate transformation equations for the scanning beam instrument landing system.

Chapter 1 References

1. MacKinnon, D., Improving Automatic Landing System Performances Using Modern Control Theory and Inertial Measurements, MIT Instrumentation Laboratory Report R-628, January 1969.
2. MacKinnon, D., Some Applications of Mathematical Optimization to Automatic Landing Systems, MIT Instrumentation Laboratory Report R-651, November 1969.
3. Cherry, G.W., MacKinnon, D., DeWolf, B., A New Approach and Landing System: Help For Our Troubled Terminal Areas, MIT Charles Stark Draper Laboratory Report R-654, March 1970.

CHAPTER 2

SPACE SHUTTLE STATE ESTIMATION DURING APPROACH AND LANDING

by
Donald W. Keene

2.0 Introduction

The fundamental problem of navigation is to provide accurate indications of position and velocity of a vehicle so that it can be guided accurately to its destination. For the Space Shuttle vehicles the position and velocity estimates must be extremely accurate to permit automatic landings under adverse weather conditions. To meet this objective, one proposed navigation system for the Space Shuttle vehicles includes both an inertial subsystem and a scanning beam microwave ILS receiver which interface with the guidance and navigation computer. The inertial system provides a self-contained navigation capability that affords extremely accurate short-term position and velocity information but which is subject to long-term drift. The scanning beam microwave ILS,* on the other hand, provides accurate drift-free measurements of position but is incapable of supplying the same high quality velocity data as the inertial system. To take advantage of the unique qualities of each system, the data from both systems can be combined in optimum fashion to yield results superior to either system alone.

The filtering approach which is used to optimally combine these data is presented in Section 2.3. The procedure to be followed here in the estimation of the position and velocity is to estimate the errors in these quantities rather than the quantities themselves. This indirect method is used since the position and velocity errors change slowly with time and a linear model for the inertial navigator can be utilized. The basic philosophy employed in the design of the navigation filters is to estimate only those quantities which are slowly varying with time such as position and velocity errors, instrument biases, and wind velocities.

There will be, of course, a need to estimate other dynamic variables such as vehicle angular rates and accelerations which are needed for control purposes, but

*As described in Appendix D.

undoubtedly these variables will be required at higher rates than are normally necessary for navigational purposes. Therefore, the estimation of these quantities would be incorporated more effectively in the design of the control system.

Accurate estimates of the wind velocity will be required for two reasons: first so that the guidance can plan optimal maneuver strategies and secondly to reduce the undesired effects of the wind on the ground track. In order to estimate the wind velocities it is necessary that the vehicle be equipped with a true airspeed indicator which interfaces with the guidance computer. Procedures for the optimal estimation of wind velocity are outlined in Section 2.4.

2.1 The Equations of Motion

In this section the equations of motion of the aircraft will be derived relative to the runway coordinate system. In Section 2.2 the equations defining the inertial navigation system estimates of position and velocity will be derived and compared with the results of this section to define the equations for the errors in the indicated position and velocity. The error equations will then be used to formulate the navigation filter equations for incorporating the microwave ILS position fix data.

Since the runway coordinate system is an earth-fixed reference frame, it is both accelerating and rotating relative to inertial space; thus the acceleration of the aircraft can be expressed as:

$$\underline{a} = \underline{a}_I - 2\underline{\omega}_e \times \underline{V} - \underline{\omega}_e \times \underline{\omega}_e \times \underline{R} - \underline{\omega}_e \times \underline{\omega}_e \times \underline{R}_r \qquad (2.1\text{-}1)$$

and the equation for the position and velocity of the aircraft are:

$$\dot{\underline{R}} = \underline{V} \qquad (2.1\text{-}2)$$

$$\dot{\underline{V}} = \underline{a} \qquad (2.1\text{-}3)$$

where

- $\underline{a}$ = acceleration of the aircraft relative to the runway coordinate frame
- $\underline{a}_I$ = inertial acceleration of the aircraft
- $\underline{V}$ = velocity of the aircraft relative to the runway coordinate frame
- $\underline{R}$ = position of the aircraft relative to the runway coordinate frame

$\underline{R}_r$ = position vector of the origin of the runway coordinate frame relative to the center of the earth

$\underline{\omega}_e$ = angular velocity of the earth.

In runway coordinates the components of these vectors can be written as:

$$\underline{R} = \begin{bmatrix} x \\ y \\ z \end{bmatrix} \qquad \underline{V} = \begin{bmatrix} x \\ y \\ z \end{bmatrix} \qquad \underline{a} = \begin{bmatrix} x \\ y \\ z \end{bmatrix}$$

$$\underline{R}_r = \begin{bmatrix} 0 \\ 0 \\ -R_e \end{bmatrix} \qquad \underline{a}_I = \begin{bmatrix} a_{Ix} \\ a_{Iy} \\ a_{Iz} \end{bmatrix}$$

$$\underline{\omega}_e = \omega_e \begin{bmatrix} \cos L \cos\psi_r \\ -\cos L \cos\psi_r \\ -\sin L \end{bmatrix}$$

where

L = latitude of the airport

ψ_r = angle of the runway centerline with respect to true north

R_e = radius of the earth

For convenience, define the matrix ω_x such that

$$\underline{\omega}_e \ \underline{V} = \omega_x \ \underline{V}$$

It can be easily verified that

$$\omega_x = \omega_e \begin{bmatrix} 0 & \sin L & -\cos L \sin\psi_r \\ -\sin L & 0 & -\cos L \cos\psi_r \\ \cos L \sin\psi_r & \cos L \cos\psi_r & 0 \end{bmatrix}$$

The centrifugal accelerations can then be written as:

$$\underline{\omega}_e \times \underline{\omega}_e \times \underline{R} = \left[\omega_x\right]^2 \begin{bmatrix} x \\ y \\ z \end{bmatrix}$$

$$\underline{\omega}_e \times \underline{\omega}_e \times \underline{R}_r = \left[\omega_x\right]^2 \begin{bmatrix} 0 \\ 0 \\ -R_e \end{bmatrix}$$

2.2 Modeling the Inertial System

In this section the equations describing the output of the inertial navigation system are derived. It should be emphasized that the equations presented here do not necessarily represent the mechanization of the equations employed in the inertial navigator; they simply represent a model of the system for use in defining the error propagation.

For the purposes of this analysis we can assume that the accelerometer measurements are resolved into a reference frame which is approximately aligned with the runway coordinate system. The misalignment between the runway coordinate frame and the reference frame is assumed to be small and is represented by the matrix:

$$E = \begin{bmatrix} 1 & -\epsilon_z & \epsilon_y \\ \epsilon_z & 1 & -\epsilon_x \\ -\epsilon_y & \epsilon_x & 1 \end{bmatrix}$$

Thus, the accelerometer measurements resolved into the platform frame are

$$\underline{f} = [E]\left(\underline{a}_I - \underline{g}(x,y,z)\right) + \underline{b} + \underline{w}_a \qquad (2.2\text{-}1)$$

where

$\underline{g}$ = acceleration due to gravity
$\underline{b}$ = uncompensated accelerometer bias
$\underline{w}_a$ = accelerometer noise

The inertially derived aircraft acceleration is given by

$$\underline{a}' = \underline{f} + \underline{g}(x', y', z') - 2(\underline{\omega}_e \times \underline{V}') - \underline{\omega}_e \times \underline{\omega}_e \times \underline{R}' - \underline{\omega}_e \times \underline{\omega}_e \times \underline{R}_r \qquad (2.2\text{-}2)$$

and the corresponding position and velocity is given by

$$\dot{\underline{R}}' = \underline{V}' \qquad (2.2\text{-}3)$$

$$\dot{\underline{V}}' = \underline{a}' \qquad (2.2\text{-}4)$$

In the equations above

$$\underline{R}' = \begin{bmatrix} x' \\ y' \\ z' \end{bmatrix} = \text{inertially derived position of the aircraft relative to the runway coordinates}$$

$$\underline{V}' = \begin{bmatrix} \dot{x}' \\ \dot{y}' \\ \dot{z}' \end{bmatrix} = \text{inertially derived velocity of the aircraft relative to the runway coordinates}$$

Also,

$$\underline{\omega}_e \times \underline{V}' = \begin{bmatrix} \omega_x \end{bmatrix} \begin{bmatrix} x' \\ y' \\ z' \end{bmatrix}$$

$$\underline{\omega}_e \times \underline{\omega}_e \times \underline{R}' = \begin{bmatrix} \omega_x \end{bmatrix} \begin{bmatrix} \omega_x \end{bmatrix} \begin{bmatrix} x' \\ y' \\ z' \end{bmatrix}$$

$$\underline{\omega}_e \times \underline{\omega}_e \times \underline{R}_r = \begin{bmatrix} \omega_x \end{bmatrix} \begin{bmatrix} \omega_x \end{bmatrix} \begin{bmatrix} 0 \\ 0 \\ -R_e \end{bmatrix}$$

To obviate the need of modeling the aircraft accelerations in the state equations used to define the navigation filter, we will use the equations which define the inertial system errors. These equations are obtained by subtracting Eq. 2.1-1 from Eq. 2.2-2 to yield

$$\Delta\dot{\underline{R}} = \Delta\underline{V} \tag{2.2-5}$$

$$\Delta\dot{\underline{V}} = [E - I]\left((\underline{a}_I - \underline{g}(x,y,z)\right) - \underline{g}(x,y,z) + \underline{g}(x', y', z') - 2\begin{bmatrix} \omega_x \end{bmatrix} \Delta\underline{V} - \begin{bmatrix} \omega_x \end{bmatrix} \begin{bmatrix} \omega_x \end{bmatrix} \Delta\underline{R} + \underline{b} + \underline{w}_a \tag{2.2-6}$$

where

I = identity matrix

$$\Delta\underline{R} = \begin{bmatrix} x' - x \\ y' - y \\ z' - z \end{bmatrix} = \begin{bmatrix} \Delta x \\ \Delta y \\ \Delta z \end{bmatrix}$$

$$\Delta\underline{V} = \begin{bmatrix} V'_x - V_x \\ V'_y - V_y \\ V'_z - V_z \end{bmatrix} = \begin{bmatrix} \Delta V_x \\ \Delta V_y \\ \Delta V_z \end{bmatrix}$$

The gravity term g (x', y', z') can be expanded about the actual aircraft position to give

$$\underline{g}(x',y',z') \simeq \underline{g}(x, y, z) - \frac{GM}{\left|\underline{R}_{ae}\right|^3}\left(\Delta R - \frac{3\underline{R}_{ae} \cdot \Delta\underline{R}}{\left|\underline{R}_{ae}\right|^2} \underline{R}_{ae}\right) \tag{2.2-7}$$

where

G = gravitational constant

M = mass of the earth

$\underline{R}_{ae}$ = position vector of the aircraft related to the center of the earth

Near the airport

$$\underline{R}_{ae} = \begin{bmatrix} 0 \\ 0 \\ -R_e \end{bmatrix}$$

so that

$$\underline{g}(x',y',z') = \underline{g}(x,y,z) + \frac{g}{R_e} \begin{bmatrix} -1 & 0 & 0 \\ 0 & -1 & 0 \\ 0 & 0 & +2 \end{bmatrix} \Delta\underline{R} \qquad (2.2\text{-}8)$$

Thus Eq. 2.2-6 can be rewritten as

$$\Delta\dot{\underline{V}} = [E - I]\left(\underline{a}_I - \underline{g}(x,y,z)\right) + \frac{g}{R_e} \begin{bmatrix} -1 & 0 & 0 \\ 0 & -1 & 0 \\ 0 & 0 & +2 \end{bmatrix} \Delta\underline{R}$$
$$-2\left[\omega_x\right]\Delta\underline{V} - \left[\omega_x\right]\left[\omega_x\right]\Delta\underline{R} + \underline{b} + \underline{w}_a \qquad (2.2\text{-}9)$$

If we assume that the misalignments are small and that the inertial accelerations of the aircraft are small compared to g, the term involving platform misalignments can be rewritten as

$$[E - I]\left(\underline{a}_I - \underline{g}(x,y,z)\right) \simeq g \begin{bmatrix} 0 & -1 & 0 \\ 1 & 0 & 0 \\ 0 & 0 & 0 \end{bmatrix} \underline{\epsilon} \qquad (2.2\text{-}10)$$

where

$$\underline{\epsilon} = \begin{bmatrix} \epsilon_x \\ \epsilon_y \\ \epsilon_z \end{bmatrix}$$

If we assume that the uncompensated gyro drift can be modeled as a random-walk process then

$$\dot{\underline{\epsilon}} = \underline{d} + [I - E]\,\omega_e \qquad (2.2\text{-}11)$$

$$\dot{\underline{d}} = \underline{w}_d \qquad (2.2\text{-}12)$$

where

$\underline{d}$ = gyro drift

$\underline{w}_d$ = white-noise source of gyro drift

If high-quality external position data are available for correcting the output of the inertial system, then most of the terms appearing in Eq. 2.2-6 can be neglected. For example, if

ϵ ~ 0.0001 rad

ΔR ~ 100 ft (with microwave ILS data)

ΔV ~ 2 ft/sec (with microwave ILS data)

R_e ~ 400 m

ω_e ~ $7.29 \quad 10^{-5}$ rad/sec

b ~ 0.001 ft/sec^2. (the effect of accelerometer scale factor errors would be of the same magnitude)

then,

$$g = 0.0322 \text{ ft/sec}^2$$

$$\frac{g}{R_e}\Delta R = 0.00015 \text{ ft/sec}^2$$

$$2\omega_e \Delta V = 0.00029 \text{ ft/sec}^2$$

$$\omega_e^2 \Delta R = 0.0000000001 \text{ ft/sec}^2$$

It is apparent that the platform misalignment will be the dominant error source under these circumstances. Thus, a reasonable model for the INS is provided by the following equations:

$$\Delta\dot{\underline{R}} = \Delta\underline{V} \tag{2.2-13}$$

$$\Delta\dot{\underline{V}} = g \begin{bmatrix} 0 & -1 & 0 \\ 1 & 0 & 0 \\ 0 & 0 & 0 \end{bmatrix} \underline{\epsilon} + \underline{w}_a \tag{2.2-14}$$

$$\dot{\underline{\epsilon}} = \underline{d} \tag{2.2-15}$$

$$\dot{\underline{d}} = \underline{w}_d \tag{2.2-16}$$

where the earth rate term $[I\text{-}E]\ \underline{\omega}_e$ can be neglected.

Hollister[1] has shown that, if external position data are available at intervals less than one tenth the Schuler period, it is necessary to estimate the platform misalignments (the microwave ILS data rate is 15 times/sec). Even though the angles may become large, the filter is continuously estimating the velocity error which they produce. The main reason for estimating the misalignment angles is to be able to navigate accurately in the event that the external position information is lost. Thus, if we assume that microwave data are continuously available during the approach and landing phase, the equations for the error propagations become simply

$$\Delta\dot{\underline{R}} = \Delta\underline{V} \tag{2.2-17}$$

$$\Delta\dot{\underline{V}} = \underline{w}_a \tag{2.2-18}$$

For this model the effects of platform misalignments, accelerometer errors, and computational errors would be treated as an equivalent white noise process w_a.

2.3 Optimum Mixing of INS and Microwave ILS Data

The method to be used in filtering the microwave ILS data is based on the minimum variance estimator as derived by Kalman and Bucy.[2] For this approach the measurements are considered to be linear combinations of the state variables for the system which are corrupted by additive white noise. Thus

$$\underline{m} = H\underline{x} + \underline{\nu} \tag{2.3-1}$$

For the scanning beam microwave ILS the measurements are considered to be

$$\underline{m} = \begin{bmatrix} EL' & -EL \\ AZ' & -AZ \\ d' & -d \end{bmatrix} \tag{2.3-2}$$

where

EL' = elevation angle predicted by the inertial navigator
AZ' = azimuth angle predicted by the inertial navigator
d' = range to the runway predicted by the inertial navigator

and EL, AZ, and d are the actual elevation, azimuth, and range measurements.

Since the measurements are functions of position

$$\underline{m} = H\Delta\underline{R} + \underline{\nu} \tag{2.3-3}$$

and

$$H = \frac{\partial h}{\partial \underline{R}}$$

where $\frac{\partial h}{\partial R}$ is given in Appendix D.

The covariance of the measurement noise is defined to be

$$\overline{\nu\nu}^T = \left[V_n\right]$$

where $\left[V_n\right]$ is also given in Appendix D.

It is assumed that the measurements will be made and processed at 1-second intervals and that the measurement errors are uncorrelated at this sampling rate.

The equation of state can be represented in the form

$$\dot{\underline{x}} = F\underline{x} + \underline{w} \tag{2.3-4}$$

If we use Eq. 2.2-13 through 2.2-16 as a model for the system, then

$$\underline{x} = \begin{bmatrix} \Delta x \\ \Delta y \\ \Delta z \\ \Delta V_x \\ \Delta V_y \\ \Delta V_z \\ \epsilon_x \\ \epsilon_y \\ \epsilon_z \\ d_x \\ d_y \\ d_z \end{bmatrix} \qquad F = \begin{bmatrix} 0 & 0 & 0 & 1 & 0 & 0 & 0 & 0 & 0 & 0 & 0 & 0 \\ 0 & 0 & 0 & 0 & 1 & 0 & 0 & 0 & 0 & 0 & 0 & 0 \\ 0 & 0 & 0 & 0 & 0 & 1 & 0 & 0 & 0 & 0 & 0 & 0 \\ 0 & 0 & 0 & 0 & 0 & 0 & 0 & -g & 0 & 0 & 0 & 0 \\ 0 & 0 & 0 & 0 & 0 & 0 & g & 0 & 0 & 0 & 0 & 0 \\ 0 & 0 & 0 & 0 & 0 & 0 & 0 & 0 & 0 & 0 & 0 & 0 \\ 0 & 0 & 0 & 0 & 0 & 0 & 0 & 0 & 0 & 1 & 0 & 0 \\ 0 & 0 & 0 & 0 & 0 & 0 & 0 & 0 & 0 & 0 & 1 & 0 \\ 0 & 0 & 0 & 0 & 0 & 0 & 0 & 0 & 0 & 0 & 0 & 1 \\ 0 & 0 & 0 & 0 & 0 & 0 & 0 & 0 & 0 & 0 & 0 & 0 \\ 0 & 0 & 0 & 0 & 0 & 0 & 0 & 0 & 0 & 0 & 0 & 0 \\ 0 & 0 & 0 & 0 & 0 & 0 & 0 & 0 & 0 & 0 & 0 & 0 \end{bmatrix} \tag{2.3-5}$$

$$\underline{w} = \begin{bmatrix} 0 \\ 0 \\ 0 \\ w_{ax} \\ w_{ay} \\ w_{az} \\ 0 \\ 0 \\ 0 \\ w_{dx} \\ w_{dy} \\ w_{dz} \end{bmatrix}$$

If the simpler model (Eq. 2.2-17, 2.2-18) is used, then the state equations can be decoupled into three independent relations of the form:

$$\underline{x} = \begin{bmatrix} \Delta x \\ \Delta V_x \end{bmatrix} \qquad F = \begin{bmatrix} 0 & 1 \\ 0 & 0 \end{bmatrix} \qquad \underline{w} = \begin{bmatrix} 0 \\ w_a \end{bmatrix} \tag{2.3-6}$$

For either model an estimate of the state and the covariance of the state-vector errors are propagated between measurements as

$$\dot{\underline{\hat{x}}} = F\underline{\hat{x}} \tag{2.3-7}$$

$$\dot{P} = FP + PF^T + Q \tag{2.3-8}$$

where Q is the power density of the system-noise matrix.

At the time of each measurement the new estimate is given by

$$\underline{\hat{x}}^+ = \underline{\hat{x}}^- + K(\underline{m} - H\underline{\hat{x}}^-) \tag{2.3-9}$$

where

$$K = PH^T \left[HPH^T + V_n \right]^{-1} \tag{2.3-10}$$

$$P^+ = \left[I - KH \right] P^- \tag{2.3-11}$$

$\underline{\hat{x}}^+$ = estimate of the state after incorporation of the measurement

$\underline{\hat{x}}^-$ = estimate of the state before incorporation of the measurement

and

P^+ = covariance just after the measurement.

P^- = covariance just before the measurement

At this point a few statements can be made concerning the selection of the INS model. If Eq. 2.3-5 is used, it should be noted that the platform azimuthal misalignment, ϵ_z, is unobservable. This implies that additional instrumentation such as a stabilized magnetic compass or radio direction finder would have to be incorporated into the navigation system for estimation of azimuthal misalignment. Alternatively, ϵ_z could be estimated if the aircraft accelerations could be modeled as a function of the applied maneuver commands. The accuracy of this approach depends on how well the aircraft accelerations can be modeled and upon the magnitude of the vehicle-disturbance accelerations. A similar statement can be made concerning estimating the vertical misalignments. However, in view of the anticipated magnitude of the misalignments ($\approx$1 milliradian) and the rather low accuracy of the magnetic or radio direction indicators and in view of the limited amount of time in the approach phase available to filter these data, it does not appear desirable to estimate these quantities. The magnetic or radio-compass data could be used instead as a gross check on the platform orientation rather than as a means of estimating the misalignments. The ultimate decision as to whether or not to incorporate the estimation of the platform misalignments depends on the answers to the following questions:

1) What is the expected value of the misalignments at the beginning of the approach phase?
2) How well can the misalignments be estimated?
3) How accurate is the inertial navigator without ILS data?
4) Is there a requirement to perform an automatic landing without ILS data?
5) How accurate does the platform alignment need to be in order to adequately perform the decrab and roll-out maneuvers?

Irregardless of which model is selected for the navigation filter, it is still possible to estimate the accuracy of the position and velocity estimates when microwave ILS data are available. Hollister[1] has shown that, if the sampling interval ΔT is less than the response time for the resultant filter $(1/\omega_n)$, the continuous approximation to the discrete filter can be used to predict the performance of the navigation system. For the continuous measurement case the estimates of position and velocity errors are given by

$$\dot{\hat{\underline{x}}} = F\hat{\underline{x}} + PH^T R_n^{-1} (\underline{m} - H\underline{x}) \tag{2.3-12}$$

and the covariance matrix propagates as

$$\dot{P} = FP + PF^T + Q - PH^T R_n^{-1} H P \tag{2.3-13}$$

where R_n = power spectral density of the external measurement noise.

If the simplified model is used (2.3-6), the steady-state variances in the position and velocity estimates for one axis are given by

$$\sigma_r^2 = \sqrt{2}\, N^{1/4} R_n^{3/4} \tag{2.3-14}$$

$$\sigma_v^2 = \sqrt{2}\, N^{3/4} R_n^{1/4} \tag{2.3-15}$$

where N = power spectral density of the equivalent accelerometer noise

The natural frequency of the filter is given by

$$\omega_n^4 = \frac{N}{R_n}$$

and the steady-state gains are

$$\underline{K} = PH^T R_n^{-1} = \begin{bmatrix} \sqrt{2}\,\omega_n \\ \omega_n^2 \end{bmatrix}$$

The structure of this filter is illustrated in Fig. 2.3-1. If we assume that

$N = 0.001 \text{ ft}^2/\text{sec}^3$ (this corresponds to a platform misalignment of 1 mr)

$R_n = 10^4 \text{ ft}^2 \text{ sec}$ (this corresponds to a measurement taken at 5.5 miles from the airport using the c-band data)

then

$$\sigma_r = 15.9 \text{ ft}$$

$$\sigma_v = 0.282 \text{ ft/sec}$$

$$\omega_n = 0.0178 \text{ sec}^{-1}$$

$$\frac{1}{\omega_n} = 56 \text{ sec}$$

According to Hollister[1] a more realistic value of equivalent accelerometer noise is:

$$N = 10^{-2} \text{ ft}^2/\text{sec}^3$$

In which case,

$$\sigma_r = 21.2 \text{ ft}$$

$$\sigma_v = 0.68 \text{ ft/sec}$$

$$\omega_n = 0.0316 \text{ sec}^{-1}$$

$$\frac{1}{\omega_n} = 31.6 \text{ sec}$$

It should be emphasized that, as the aircraft approaches the runway, the errors in the position and velocity estimates will decrease. The ultimate accuracy of the complemented inertial system would seem to depend on the correlation time of the ILS measurement noise. For this analysis it was assumed that the correlation time was less than one second. This assumption should be checked as soon as data on the microwave ILS is available.

2.4 Estimating the Wind Velocity

One of the primary reasons for estimating the wind velocity is to allow the guidance to plan optimal aircraft maneuver strategies. It is also desirable to estimate the wind velocity so that open-loop or feed-forward commands can be used to cancel the undesirable effects of the wind on the ground track. Without the wind estimates the guidance and control system would typically develop positional errors to compensate for the effects of the wind.

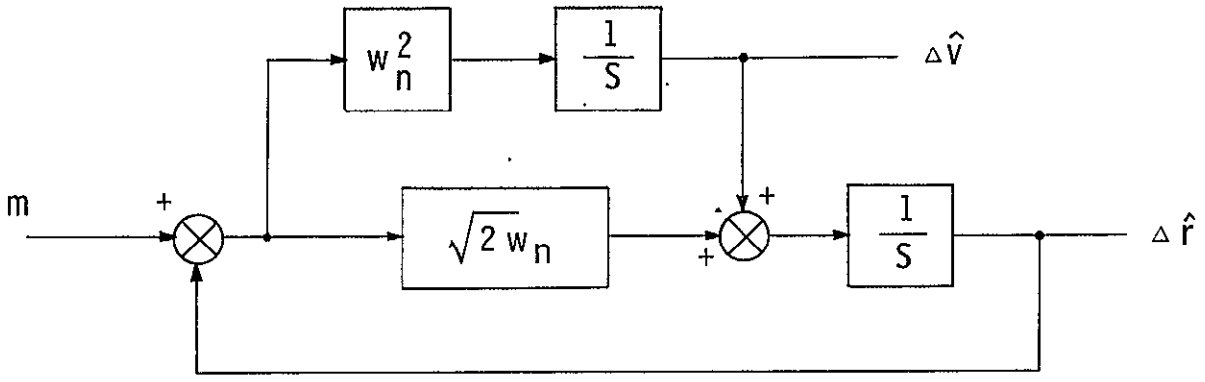

Fig. 2.3-1 Optimum Steady-State Filter for Position and Velocity Errors

The wind velocity, $\underline{W}$, can be expressed as the difference between the ground velocity ($\underline{V}$) and the velocity of the aircraft relative to the air mass ($\underline{V}_a$). Thus

$$W_x = V_x - V_{ax} \tag{2.4-1}$$

$$W_y = V_y - V_{ay} \tag{2.4-2}$$

where

$$\underline{V}_a = \begin{bmatrix} V_{ax} \\ V_{ay} \\ V_{az} \end{bmatrix} = \begin{bmatrix} |V_a| \cos\theta \cos\psi \\ |V_a| \cos\theta \sin\psi \\ |V_a| \sin\theta \end{bmatrix} \tag{2.4-3}$$

and

θ = pitch attitude of the aircraft

ψ = heading of the aircraft relative to the runway centerline (as measured by the inertial system)

It is assumed in this analysis that the sideslip angle, β, is small and that the deviation of the angle of attack, $\Delta\alpha$, from the trim angle of attack is also small. If these assumptions are not valid, then α and β could be measured by appropriate sensors, or estimates of α and β could be obtained from measurements of vertical and side forces acting on the vehicle. For this approach the model relating the aerodynamic forces to the angles α and β would have to be included in the navigation equations.

In order to construct an estimator for the wind velocity, the true airspeed, V_{as}, (as measured by the air data computer) must be provided to the navigation computer. It is assumed that the error in the airspeed measurements can be modeled as correlated noise, thus

$$|V_a| = V_{as} + \epsilon_{as} \tag{2.4-4}$$

$$\dot{\epsilon}_{as} = -\frac{1}{\tau_{as}} \epsilon_{as} + w_{as} \tag{2.4-5}$$

Considering the accuracy of the ground velocity data provided by the complemented inertial system, it would appear unnecessary to augment the state to include a model for the wind. Instead it would be better (and simpler) to model the wind separately and treat the inertially derived velocity as an independent measurement. Thus we can define the measurements for this filter as

$$\underline{m} = \begin{bmatrix} \hat{V}_x - V_{as} \cos\theta \cos\psi \\ \hat{V}_y - V_{as} \cos\theta \sin\psi \end{bmatrix} \tag{2.4-6}$$

where $\hat{V}_x$, $\hat{V}_y$ are the estimated components of ground velocity from the output of the complemented inertial systems.

Thus

$$\underline{m} = \begin{bmatrix} V_x - |V_a| \cos\theta \cos\psi + \epsilon_{as} \cos\theta \cos\psi \\ V_y - |V_a| \cos\theta \cos\psi + \epsilon_{as} \cos\theta \sin\psi \end{bmatrix} + \begin{bmatrix} \epsilon_{\hat{V}_x} \\ \epsilon_{\hat{V}_y} \end{bmatrix} \tag{2.4-7}$$

or in terms of the standard notation

$$\underline{m} = H\underline{x} + \underline{\nu}$$

where

$$H = \begin{bmatrix} 1 & 0 & \cos\theta \cos\psi \\ 0 & 1 & \cos\theta \sin\psi \end{bmatrix} \tag{2.4-8}$$

$$x = \begin{bmatrix} W_x \\ W_y \\ \epsilon_{as} \end{bmatrix} \tag{2.4-9}$$

If the wind can properly be modeled as a random walk process, then

$$\dot{W}_x = w_{wx} \tag{2.4-10}$$

$$\dot{W}_y = w_{wy} \tag{2.4-11}$$

The optimal filter for this system can then be deduced using the techniques presented in Section 2.3.

Estimation of wind shear (s_x, s_y) could be accomplished by adding the terms

$\hat{V}_z \; s_x$
$\hat{V}_z \; s_y$

V_z = inertially derived vertical velocity

to the right hand side of Eq. 2.4-10 and 2.4-11, and augmenting the state variables to include the following shear model

$$\dot{s}_x = w_{sx} \tag{2.4-12}$$

$$\dot{s}_y = w_{sy} \tag{2.4-13}$$

However, it would be undesirable to complicate the wind model unless it could be shown that the estimates of wind shear would significantly increase the dynamic response of the system.

Chapter 2 References

1. Hollister, W.M. and Brayard, M.C., Optimum Mixing of Inertial Navigator and Position Fix Data, M.I.T. Measurement Systems Laboratory Report, RE-62, August, 1969.

2. Kalman, R.E., and Bucy, R.S.,"New Results in Linear Filtering and Prediction Theory," Transactions of the ASME, Journal of Basic Engineering, March 1961.

CHAPTER 3

OPTIMAL TRAJECTORY MANAGEMENT FOR THE SPACE SHUTTLE

by

Mukund Desai

3.1 Introduction

Since the weight of the fuel required for post-reentry subsonic cruise is directly deductable from the orbited payload and increases the energy requirements during reentry, attention is focused on the determination of post-reentry flight paths which minimize fuel requirements. The delineation of the subsonic-range capabilities of the shuttle, subject to fuel restrictions ranging from zero to amounts sufficient for extended cruise, is an essential design and operational consideration. Solution to the range-fuel problem must be obtained to

1. Ensure the capability of the shuttle to meet design specifications.
2. Determine the operational utility of an existing shuttle.

Such problems are particularly suitable for formulation within the framework of Optimal Control Theory. Optimization problems of this nature often require extensive numerical computation.

The amount of difficulty and expense involved in the performance optimization of shuttle flight paths depends upon the complexity of the model used. In this chapter an energy-state model approximation is used which yields useful optimal trajectory information. The computational simplicity of the solutions makes the energy-state approach particularly attractive for onboard trajectory management.

Section 3.2 derives the energy-state model of the shuttle. The results of this derivation are then applied to a class of shuttle-trajectory optimization problems in Section 3.3. We shall here consider mainly the flights in a vertical plane (ie, longitudinal flight).

Detailed considerations for performance problems involving lateral-flight considerations have been limited in the past[23,24] to special cases, such as lateral flight in a horizontal plane, which reduce the order of the flight dynamics. With

the energy-state approximation, it is possible to consider, with no great added complexity, a broader spectrum of performance problems involving lateral-flight considerations.

3.2 An Energy State Model for the Space Shuttle

Aerodynamic vehicle models range from a simple point-mass quasi-steady representation to models that include the deflections of the airframe. It is usually adequate to consider the aircraft as a point-mass, because the motion of the vehicle around the center of mass and the airframe deflections have little effect on the flight path.

The nomenclature commonly used for a point-mass model is given in Fig. 3.2-1. For the most part we shall consider only paths contained in a vertical plane.

The following approximations are also made:

1) The curvature and the rotation of earth are neglected, since their effect on short flight paths at sub-orbital speeds is negligible.
2) The variation of gravity with altitude is negligible.

The equations of motion for the point-mass model are as follows:

$$\dot{V} = \frac{T \cos(\alpha+\epsilon) - D}{m} - g \sin\gamma \tag{3.2-1}$$

$$V\dot{\gamma} = \frac{T \sin(\alpha+\epsilon) + L}{m} - g \cos\gamma \tag{3.2-2}$$

$$\dot{h} = V \sin\gamma \tag{3.2-3}$$

$$\dot{x} = V \cos\gamma \tag{3.2-4}$$

$$\dot{m} = -f \tag{3.2-5}$$

where

$$L = L(h, V, \alpha) = \text{lift}$$

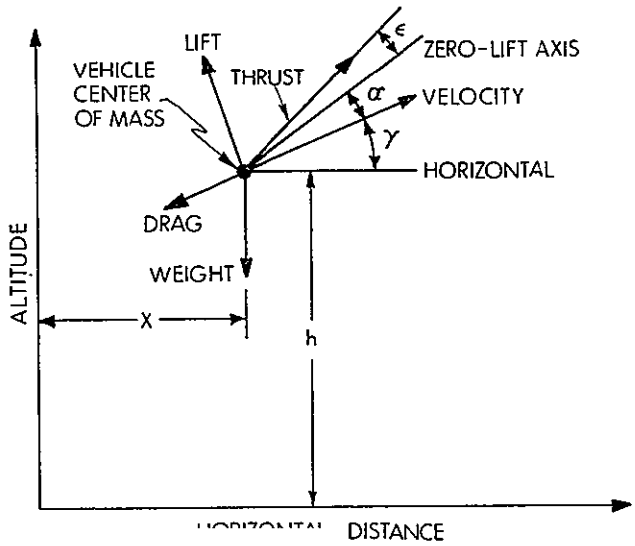

Figure Used for a Vehicle Flying in a Vertical Plane

V = velocity

γ = flight path angle

h = altitude

x = horizontal range

m = mass

T = $T(V,h)$ = thrust at maximum throttle

D = $D(V,h,\alpha)$ = drag

α = angle of attack

g = accleration of gravity

f = $f(V,h)$ = fuel flow rate at maximum throttle

ϵ = angle between thrust axis and zero-lift axis (assumed given)

Since both α and ϵ are small, Eq. 3.2-1 and 3.2-2 can be simplified by using the small-angle approximation $\sin(\alpha+\epsilon) \cong \alpha+\epsilon$, $\cos(\alpha+\epsilon) \cong 1$. The tangential and normal accelerations to the flight path are given by Eq. 3.2-1 and 3.2-2, respectively. Equations 3.2-3 and 3.2-4 represent the kinematical relationships in vertical and horizontal directions. Equations 3.2-5 is the definition of the fuel-flow rate. Except for Eq. 3.2-4, equations of motion do not depend on x, the horizontal range. However, x may enter into the performance index or into an isoperimetric constraint since

$$x(t_f) - x(t_0) = \int_{t_0}^{t_f} V \sin r \, dt.$$

Thus, we may eliminate Eq 3.2-4 for the determination of many flight paths. This leaves us with a point-mass model with four state variables, V, γ, h, and m; and one control variable α.

The flight paths have to be considered subject to some inflight and terminal constraints. The experience of various investigators indicates the difficulty and complexity involved in the numerical solution of the optimization problem, in dealing with such a model involving higher-order dynamics, and in the handling of the constraints. We shall briefly consider approximations to the point-mass model equations, that may be used in the performance optimization of shuttle flight-paths. We shall investigate the energy-state approximation in detail and shall see that vehicle-energy is an important and adequate variable in the consideration of flight paths. The comparison of the results for an aircraft, considered in Ref. 18, 20,

and 21, obtained by using energy-state approximation with the results for "exact" (4-state variable) model shows that the energy-state approximation, properly interpreted, is adequate for the performance optimization of shuttle flight paths.

3.2.1 Point Mass Approximations

For flights confined to subsonic speeds, it is usually adequate to use the quasi-steady point-mass model in which both the components of the accleration are neglected.[1] This approximation is quite good for slow-moving vehicles where $\frac{1}{2} V^2_{max} << gh_{max}$. The omission of the acceleration terms obviously simplifies the equations of motion and the performance- optimization problem becomes amenable to ordinary calculus procedures (theory of maxima and minima). However, the neglect of tangential acceleration leads to the neglect of the change in kinetic energy ($\frac{1}{2}mV^2$) so that only the change in potential energy (mgh) is considered during the flight. With the advent of supersonic aircraft, it was recognized that the change in kinetic energy in accelerating to supersonic speeds was comparable to the change in potential energy when climbing from sea level to altitudes above 50,000 feet. It was also realized, since these aircrafts were capable of rapid climb and dive maneuvers, that kinetic energy and potential energy are readily interchangable. Kaiser[2] used the concept of energy-height ($h + V^2/2g$) in discussing aircraft flight paths. This concept leads to a simple way of taking into account the acceleration of the aircraft. Energy-height can be used as a state variable in place of h or V in the equations of motion 3.2-1 to 3.2-4.

Next in the heirarchy of point-mass approximations is the energy-state approximation. In this model, the tangential acceleration is neglected. If nearly horizontal flight is assumed (with small flight path angle, γ), energy (henceforth, we shall refer to energy per unit mass or energy-height as simply energy) and mass are the only two relevant state variables. If the variation of the mass of the aircraft during flight is considered negligible, then energy remains the only relevant variable for flight-path considerations in this approximation. The energy-state approximation has been used by a number of investigators[3,4,6,7,8] in considering minimum time or minimum fuel climbs to given altitudes and velocities. In Ref. 4,9,10, the optimal-climb problem has been investigated, using similar approximations to the equations of motion 3.1-1 to 3.1-4 as in energy-state approximation and without using energy as one of the states. It may be noted that, on the flight path, energy remains a continuous variable whereas sudden changes in h and V, leading to rapid dives or climbs in the flight path, are possible.

An improvement to the above approximation is to remove the assumption of nearly horizontal flight paths and consider the flight path angle γ as a control variable,

with velocity and altitude as state variables. The angle of attack is determined from the normal equillibrium equation, viz, $L = mg \cos\gamma$, which results from neglecting the normal acceleration. The only substantial difference between this approximation and the energy-state approximation is that zoom dives and climbs require finite time instead of zero time.

The next step in the improvement is to drop the assumption of negligible normal acceleration. The mass of the aircraft may be approximated as constant or as a known function of time. Thus V, h, γ are the state variables and α is the control variable in this approximation.

The most accurate point-mass model is to treat V, h, γ, and $\dot{m}$ as state variables and α as the control variable. The optimization problem using this model with gravity, thrust and aerodynamic forces and inflight and terminal constraints has been investigated in Ref. 12, 13, 14, 15, 16. The experience of the investigators[14, 15, 17, 18, 19] indicates some of the difficulties involved in the numerical solution of a problem of this order (four state variables). In most cases the method employed was the Bryson-Kelley steepest-ascent method.[14,18]. Slow convergence was sometimes reported, especially with the maximum range problems. The "indirect" method of making initial guesses on the missing boundary conditions was employed in Ref. 15, 17, 19. The flight paths were reported to be highly sensitive to the initial guesses, making it difficult to guess the missing boundary conditions so that terminal conditions were met.

Therefore, any reduction in the difficulty of the numerical solution, either by improved numerical methods or by making use of the special properties of the problem, would be very welcome. With an eye on the latter proposition, we shall investigate the approximations to the "exact" model, especially the energy-state approximation.

3.2.2 The Quasi-Steady Approximation

Here both components of the acceleration are neglected. We can rewrite the equations of motion 3.2-1 to 3.2-4:

$$0 = T(h,V) - D(h,V,\alpha) - mg \sin\gamma \tag{3.2-6}$$

$$0 = L(h,V,\alpha) - mg \cos\gamma \tag{3.2-7}$$

$$\dot{h} = V \sin\gamma \tag{3.2-8}$$

$$\dot{x} = V \cos \gamma \tag{3.2-9}$$

$$\dot{m} = - f(h,V) \tag{3.2-10}$$

To minimize the time to reach a given altitude, we maximize

$$\frac{dh}{dt} = V \sin \gamma$$

with respect to α at a given altitude, subject to the constraints 3.2-6 and 3.2-7 which determine V and γ in terms of h and α.

From Eq. 3.2-6 and 3.2-8

$$\frac{dh}{dt} = \frac{V[T(h,V) - D(h,V,\alpha)]}{m\,g}, \tag{3.2-11}$$

Assuming $\cos \gamma \approx 1$, Eq 3.2-7 may be used to determine $\alpha(v,h)$; and, for a given altitude, find V to maximize the excess power, V(T - D) and, consequently, the rate of climb.

Similarly, to minimize the fuel spent to reach a given altitude, we minimize

$$-\frac{dh}{dm} = v \sin \gamma / f(h,V)$$

With respect to α, at a given altitude, subject to constraints 3.2-6 and 3.2-7.

3.2.3 The Energy-State Approximation

In quasi-steady optimal-climb problems, only final altitude can be specified. However, for high-performance aircraft, it is more meaningful to consider optimal climb to a given altitude and velocity. The energy derived from the expenditure of fuel raises the aircraft's altitude as well as its velocity. The interchangeability of the kinetic and the potential energy makes it possible to spend energy to reach a given altitude and velocity by accelerating to higher speeds at lower altitudes, then trade the excess kinetic energy to reach the given higher altitude. Thus, it seems meaningful to view the climb of an aircraft in "energy" space, and to specify the energy to be reached in place of altitude and velocity.

Energy per unit mass, E, can be considered as a state variable and is related to h and V by

$$E = V^2/2 + gh \tag{3.2-12}$$

The time rate of change of E is given by

$$\dot{E} = V\dot{V} + g\dot{h}$$

Substituting for $\dot{V}$ and $\dot{h}$, from Eq 3.2-1 and 3.2-3, in the above relation yields

$$\dot{E} = V[T(E,V) - D(E,V,\alpha)]/m \tag{3.2-13}$$

To maximize the rate of energy change, it is necessary to determine V and α in conjunction with the other equations of motion, viz, $\dot{\gamma}$, $\dot{h}$, and $\dot{m}$ equations. However, considerable simplification occurs if the α dependence in Eq. 3.2-13 is removed.

If we assume small normal accelerations and nearly horizontal flight paths, then Eq. 3.2-7 becomes simply

$$L(\alpha, E, V) \approx mg \tag{3.2-15}$$

From Eq. 3.2-15, we can express α in terms of E and V, i.e.,

$$\alpha = \alpha(V,E) \tag{3.2-16}$$

Under the above assumptions, we can write down the energy-state approximation equations as follows:

$$\dot{E} = \frac{V[T(V,E) - D(V,E)]}{m} \tag{3.2-17}$$

$$\dot{m} = -f(V,E) \tag{3.2-18}$$

with h and α determined in terms of V and E by Eq. 3.2-12 and 3.2-16, respectively.

3.2.4 Mimimum Time to Climb

To minimize the time required to go from a given initial altitude and velocity to a final altitude and velocity (equivalently, energy), the time rate of change of energy must be maximized, ie,

$$\underset{V}{\text{maximize}} \quad \left\{ \frac{V(T - D)}{m} \right\} \text{ for a given } E.^{*} \tag{3.2-19}$$

We have assumed for simplicity that m = constant; m may also be approximated as a known function of time. Equation 3.2-19 yields a unique V for a given E (except where we have two equal maxima for two different velocities for a given E, in which case there will be a constant-energy velocity change on the flight path), resulting in a feedback law V(E).

Constant-energy contours may be plotted in the h,V plane as shown in Fig. 3.2-2. In the energy-state approximation, it is possible to move anywhere on a constant-energy contour in zero time. ABCDF is a typical minimum-time energy-climb path, as determined by Eq. 3.2-19, starting from energy position A and climbing to a given energy position F. Note that the segment AB is a path constrained to move along the constraint $h \geq 0$ (a state-control constraint $\dot{E} = -\frac{V^2}{2} \geq 0$), and the segment CD corresponds to the situation referred to above, $\dot{E}$ having two equal maxima for two different velocities for a given E. In practical situations, a minimum-time path is desired from an initial V,h to a desired V, h. In such situations, in general, the optimal path has constant-energy climbs or dives as the initial and final phases of the flight. A'B' and FG represent the zoom dive and climb for such a flight path. It may be noted that such rapid dive and climb paths violate the assumption that $\cos\gamma \approx 1$. However, the comparison between the "exact" path (obtained by using 4-variable point-mass model) and the "energy-climb" path in Ref. 19 and 20 shows that the "exact" path is very close to the "energy-climb" path, with the sharp corners at the beginning and the end of constant-energy zoom paths rounded off. The predicted flight times are also comparable.

The data on lift, drag, maximum thrust, and fuel consumption at maximum thrust (which has been approximated here as proportional to thrust) for the aircraft, investigated in Ref. 18, 20, and 21, are given in Tables 3.2-I and 3.2-II. We shall use this aircraft for the sake of illustration of the usefulness of energy-state approximation. The initial conditions that will be investigated are as follows.

$h(0) = 500$ ft
$V(0) = 800$ ft per sec
$gm(0) = 36000$ lb

*The only difference from the quasi-steady approximation is in holding E = constant instead of h = constant in the maximization of V(T - D).

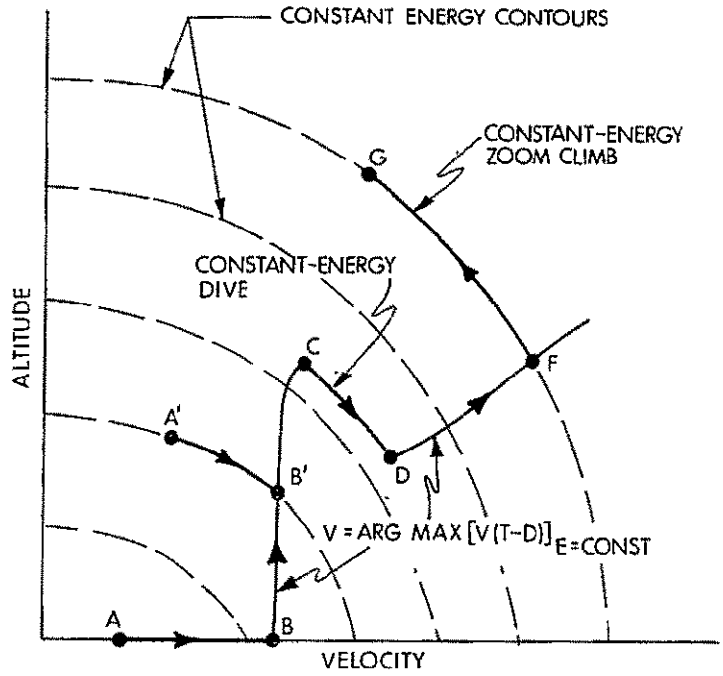

Fig. 3.2-2 Sketch of a Typical Minimum-Time Energy-Climb Path

Table 3.2-I

Maximum Thrust and Fuel Consumption at Maximum Throttle as a Function of Altitude and Mach Number

Thrust, T (thousands of pounds)

Mach No., M	Altitude, h (thousands of feet) 0	5	15	25	35	45	55	65	75	85	95	105
0	23.3	20.6	15.4	9.9	5.8	2.9	1.3	0.7	0.3	0.1	0.1	0.0
0.4	22.8	19.8	14.4	9.9	6.2	3.4	1.7	1.0	0.5	0.3	0.1	0.1
0.8	24.5	22.0	16.5	12.0	7.9	4.9	2.8	1.6	0.9	0.5	0.3	0.2
1.2	29.4	27.3	21.0	15.8	11.4	7.2	3.8	2.7	1.6	0.9	0.6	0.4
1.6	29.7	29.0	27.5	21.8	15.7	10.5	6.5	3.8	2.3	1.4	0.8	0.5
2.0	29.9	29.4	28.4	26.6	21.2	14.0	8.7	5.1	3.3	1.9	1.0	0.5
2.4	29.9	29.2	28.4	27.1	25.6	17.2	10.7	6.5	4.1	2.3	1.2	0.5
2.8	29.8	29.1	28.2	26.8	25.6	20.0	12.2	7.6	4.7	2.8	1.4	0.5
3.2	29.7	28.9	27.5	26.1	24.9	20.3	13.0	8.0	4.9	2.8	1.4	0.5

Fuel Consumption: $f = \frac{T}{cg}$ slugs/sec, where c = 2800 sec

Table 3.2-11

Lift and Drag Coefficients as a Function of Angle of Attack and Mach Number

M	0	0.4	0.8	1.2	1.6	2.0	2.4	2.8	3.2
C_{L_α}	2.240	2.325	2.350	2.290	2.160	1.950	1.700	1.435	1.250
C_{D_0}	0.0065	0.0055	0.0060	0.0118	0.0110	0.0086	0.0074	0.0069	0.0068

$C_L = C_{L_\alpha}{}^{\alpha}$ $\quad L = C_L \frac{1}{2} \rho V^2 S$ $\quad S = 500\ ft^2$

$C_D = C_{D_0} + \eta C_{L_\alpha}{}^{\alpha^2}$ $\quad D = C_D \frac{1}{2} \rho V^2 S$ $\quad \eta = 1.0$

with

$$g = 32.178 \text{ ft per sec}^2.$$

Figure 3.2-3 shows the contours of constant excess power, V(T - D), and of constant energy on an h,V plane, for the aircraft under investigation. The minimum-time path follows the ridge of the excess-power contours, except when against the constraint h = 0.

3.2.5 Minimum Fuel-to-Climb

We can replace the independent variable "t" by "m". Dividing Eq. 3.2-17 by Eq. 3.2-18, we have,

$$\frac{dE}{dm} = -\frac{V(T - D)}{mf} \tag{3.2-23}$$

It is clear from Eq. 3.2-23 that, to minimize the amount of fuel burned for a given change in energy, we have to minimize, dE/dm, i.e.,

$$\underset{V}{\text{maximize}} \quad \left\{ \frac{V(T - D)}{f} \right\} \quad \text{for a given E.} \tag{3.2-24}$$

Figure 3.2-4 shows the contours of constant energy-increase per unit of fuel burned, $\frac{V(T - D)}{-\dot{m}g}$. The minimum-fuel climb-path is also shown.

3.2.6 Drag Dependence on Load Factor

As remarked earlier, comparision of a minimum-time path obtained by the energy-state approximation with the path obtained by the "exact" four-variable model has shown that[19,20] the maximum V(T - D) curve forms a basic path that the "exact" paths follow closely, only deviating to meet initial and terminal conditions. The deviations follow closely the zoom-climb or zoom-dive paths of the energy-state path but sharp corners are rounded off.

Figure 3.2-5 shows the variation of drag with mach number, at a given altitude, for several different load factors. The variation of drag for different load factors is very small for Mach numbers > 1.2. Thus, with the assumption of unity load factor (ie, L = mg), errors will be small in the computation of drag for M > 1.2., and we expect that the "exact" paths at larger speeds, where $D \approx D_0(E, V)$ would follow closely the energy-state paths.

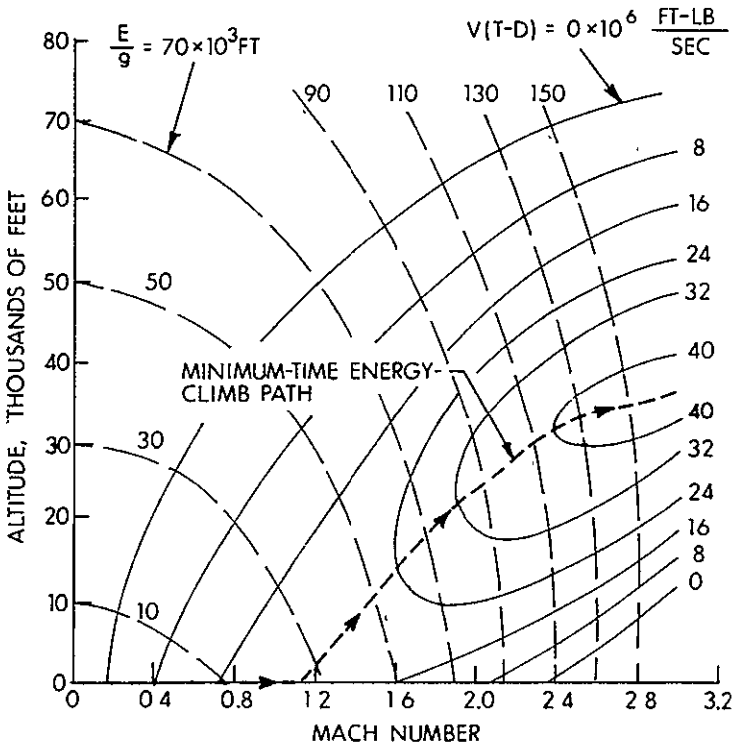

Fig. 3.2-3 Contours of Constant Excess Power and Minimum-Time Energy-Climb Path

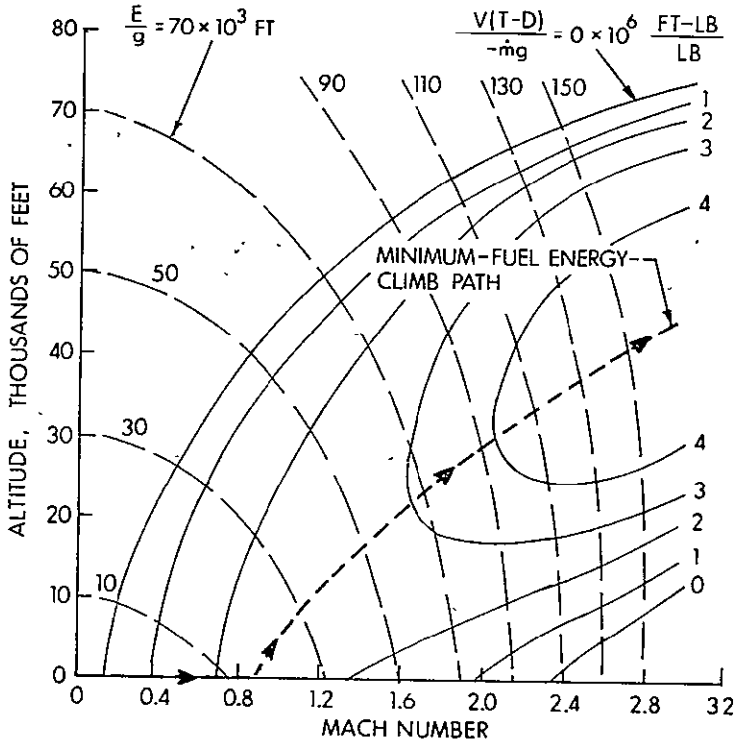

Fig. 3.2-4 Contours of Constant Energy Increase Per Pound of Fuel Burned and Minimum-Fuel Energy-Climb Path

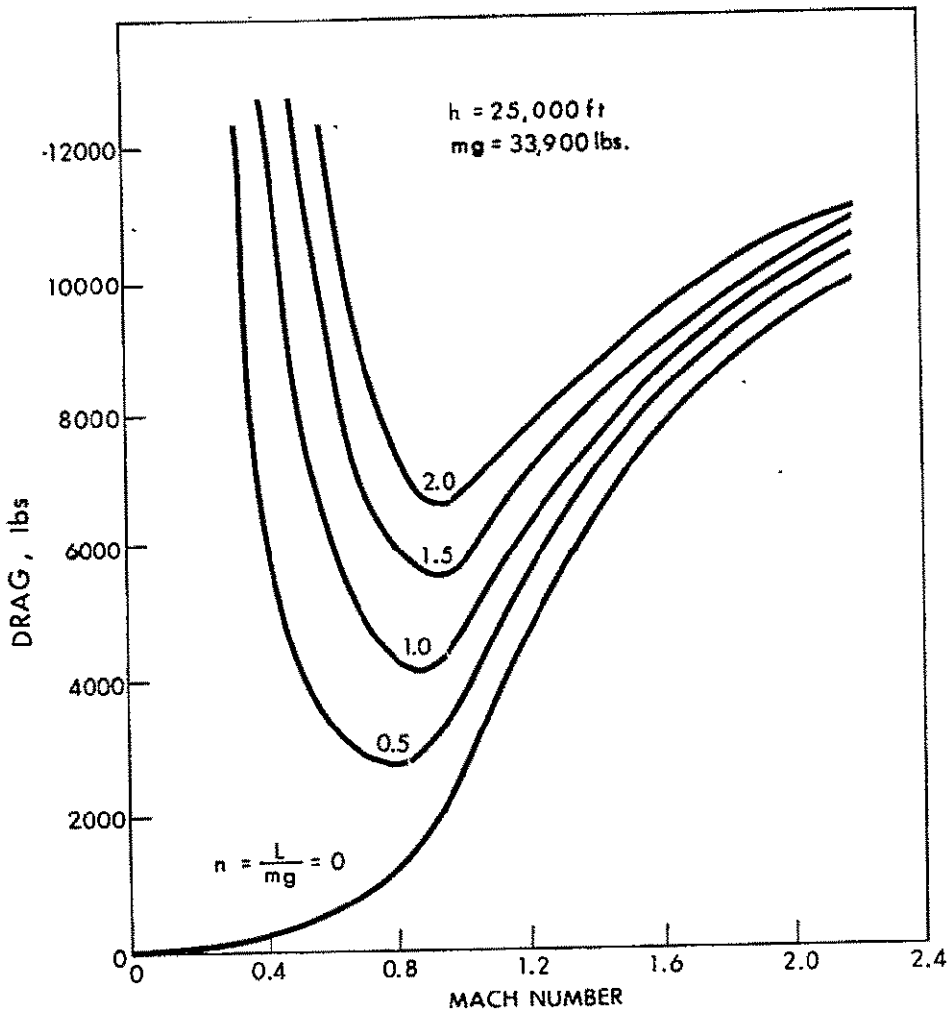

Fig. 3.2-5 Drag Versus Mach Number for Various Load Factors

3.3 Optimal Subsonic Trajectory Management for the Space Shuttle

The estimation of the range capability of the shuttle is important from both the design and operational aspects. As a result of the precious nature of the fuel reserved for the post-reentry phases of flight, subsonic trajectory management will be guided by minimal-fuel and maximum-range criteria.

In this section two versions of the maximum-range problem are considered separately for the sake of clarity.

1. Maximum range for a gliding flight*
2. Maximum range for a given amount of fuel**

Application of energy-state concepts results in solutions which are illustrated by application to the high-performance aircraft, referred to in Section 3.2.5.

3.3.1 Maximum Range for Gliding Flight

The equations of motion for an unpowered flight (T = f = 0) are:

$$\frac{dE}{dt} = -\frac{VD}{m} \tag{3.3-1}$$

and

$$\frac{dx}{dt} = V \tag{3.3-2}$$

Dividing Eq. 3.3-2 by Eq. 3.3-1, we get

$$\frac{dx}{dE} = \frac{-m}{D}$$

and the range covered over an energy drop from an initial energy E_o to a final energy E_f is given by

---

* (T = f = 0)

** Minimum fuel for a given range is an equivalent problem. Problem 1 is a special case of problem 2.

$$R = \int_{E_f}^{E_0} \frac{m}{D}\, dE \tag{3.3-3}$$

Clearly, to maximize the range R, we have to minimize $D(E,\dot{V})$ with respect to V for a given E. In the quasi-steady approximation, the minimization of D(h,V) is performed with respect to V at a given altitude h and the range is given by

$$R = \int_{h_f}^{h_0} \frac{mV}{D}\, dV \tag{3.3-4}$$

Figure 3.3-1 shows a typical maximum-range glide path. Glide path BCD can be reached by a zoom-climb or a zoom-dive from starting points which are off BCD. Path CD is constrained to level flight, just above the ground until the stalling speed is reached at D. For the optimal glide path, ABCD, the range R is given by

$$R = \int_{E_1}^{E_0} \frac{m\,dE}{D_{min}(E)} + \int_{E_s}^{E_1} \frac{mV}{D(V)}_{h=0}\, dV \tag{3.3-5}$$

where

E_o = initial energy,

E_1 = energy at h = 0 at minimum drag for L = mg,

E_s = energy at stalling speed and L = mg.

Using a parabolic drag polar, with L = mg, we have

$$D = D_o + D_I. \tag{3.3-6}$$

where

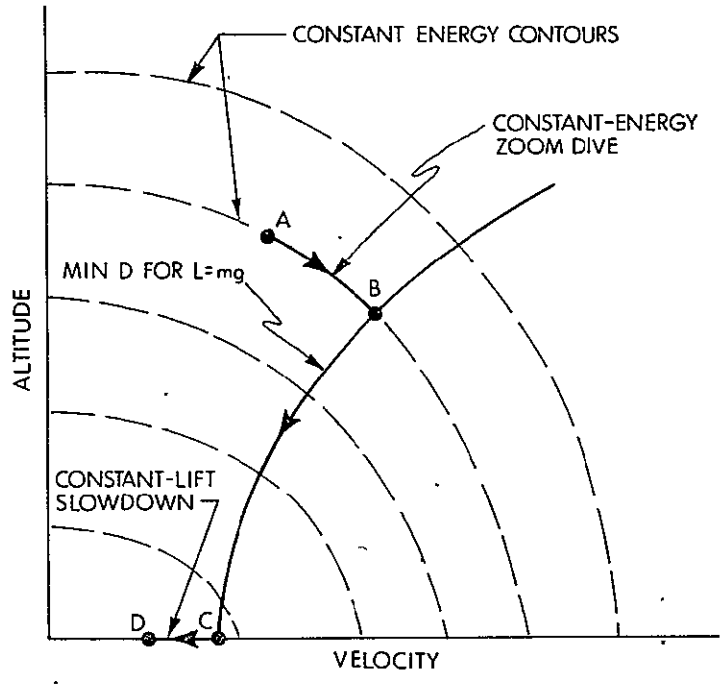

Fig. 3.3-1 A Typical Maximum Gliding Range Trajectory in the Altitude-Velocity Plane

$$D_o = C_{D_o} qS$$

$$D_L = \frac{(mg)^2}{C_{L\alpha} qS} \tag{3.3-7}$$

$$q = \frac{1}{2}\rho(h)V^2$$

If the variation of the coefficients C_{D_o} and $C_{L\alpha}$ with M is small, the minimum of D with respect to V for a given E or given h occurs at

$$D_o = D_L \tag{3.3-8}$$

with

$$\frac{q}{mg} = \frac{1}{S\sqrt{C_{L\alpha} C_{D_o}}} \tag{3.3-9}$$

Using Eq. 3.3-8 and 3.3-9 in Eq. 3.3-6, we have

$$D = 2\, C_{D_o} qS = D(mg) \tag{3.3-10}$$

Thus, under the simplifying assumption of constant C_{D_o} and $C_{L\alpha}$, the glide paths given by the energy-state approximation and the quasi-steady approximation are the same and correspond to constant drag and constant dynamic pressure q. However, the ranges given by the two approximations are different. The range using the quasi-steady approximation is given by

$$\int_o^{h_o} \frac{mg}{D_{min}}\, dh = \frac{mg}{D_{min}}\, h_o \tag{3.3-11}$$

whereas the range using the energy-state approximation is given by

$$\int_{E_1}^{E_o} \frac{m}{D_{min}}\, dE = \frac{m}{D_{min}} (gh_o + V_o^2 - V_1^2) \tag{3.3-12}$$

that is

$$R(E_0) = \frac{L}{D_{min}} \frac{}{g} (E_o - E_1)$$

$$= \frac{1}{2g} \sqrt{\frac{C_{L\alpha}}{C_{D_o}}} (E_o - E_1) \qquad (3.3\text{-}12)$$

It may be noted from Eq. 3.3-12 that, under the assumptions of constant C_{D_o} and $C_{L\alpha}$, range achieved during the glide is

1) independent of the weight of the shuttle, and
2) proportional to the energy lost over this glide path.

The difference between Eq. 3.3-11 and 3.3-12 arises because, in the quasi-steady approximation, the changes in kinetic energy during the flight are neglected in comparison with the changes in potential energy.

Under the assumption of constant C_{D_o} and $C_{L\alpha}$, q is constant, and thus

$$V \frac{dV}{dh} = \frac{V^2}{2} \beta(h) \approx \frac{V^2}{2} \beta \qquad (3.3\text{-}13)$$

where

$$\beta(h) = -\frac{1}{\rho} \frac{d\rho}{dh} . \qquad (3.3\text{-}14)$$

For an exponential model for atmospheric density $\beta(h)$ = constant and $\beta \approx 1/23{,}800$ ft.$^{-1}$

The relative variation in the kinetic energy and the potential energy of the vehicle during the glide is given by

$$\frac{VdV/dt}{gdh/dt} = \frac{VdV}{gdh} \approx \frac{V^2\beta}{2g} \qquad (3.3\text{-}15)$$

by using Eq. 3.3-13.

This ratio is nearly equal to one for M = 1.1. Thus, for a glide starting with mach no. M >> 1.1, the vehicle initially dissipates mostly kinetic energy against drag while maintaining almost constant potential energy (ie, constant altitude). Only towards the end of the glide does the vehicle dissipate its potential energy.

In most cases, the variation in the coefficients C_{D_0} and $C_{L\alpha}$ with respect to M is not negligible. Hence, the maximum-range glide path differs from the constant dynamic-pressure path. Figure 3.2-2 shows contours of constant drag for L = mg on an h, V plane, for the airplane under consideration here. It also shows the "energy-state" optimal glide path determined by the locus of the points where constant-energy contours are tangent to constant-drag contours. A four-state-variable optimal glide path for the same airplane[18] is also shown for a starting position that lies above the $\left(\frac{L}{D}\right)_{max}\Big|_E$ path. The "exact" path follows above and under the $\left(\frac{L}{D}\right)_{max}$ path, moving closer to it at subsonic speeds and flaring out near the ground.

3.3.3 Maximum Range for a Given Amount of Fuel

In equations of motion 3.2-1 to 3.2-4, we considered thrust and fuel flow at maximum throttle setting. If there is no constraint on throttle setting, it is obvious that maximum range for a given amount of fuel will be achieved by operating at less than maximum throttle settings over at least part of the flight. Thrust and fuel flow can be expressed as a function of E, V, and η, where η is a variable defining the throttle setting with the following constraints on thrust.

$$0 \leq T(E,V,\eta) \leq T_{max}(E,V) \tag{3.3-16}$$

In order to maximize range for a given amount of fuel, we have to choose V(t) and $\eta(t)$, so as to maximize

$$R = \int_{t_o}^{t_f} V dt \tag{3.3-17}$$

subject to the following flight equations:

$$\frac{dE}{dt} = \frac{V}{m}[T(E,V,\eta) - D(E,V)] \tag{3.3-18}$$

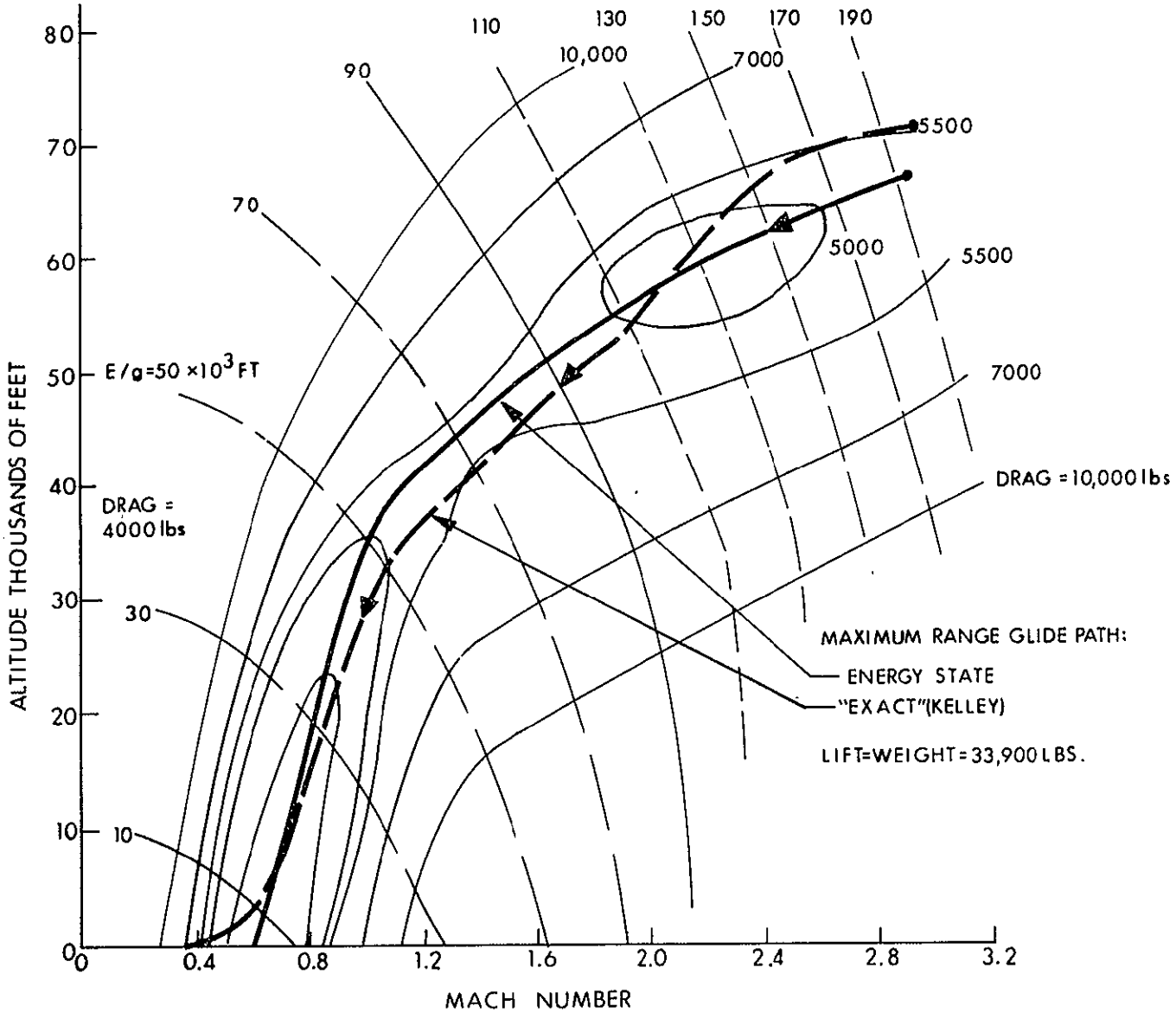

Fig. 3.3-2 Contours of Constant Drag for Lift = Weight and Maximum Range Glide Paths

$E(t_o)$ specified, $E(t_f) = E_s$ where E_s = energy at stalling speed and L = mg.

$$\frac{dm}{dt} = -f(E, V, \eta) \tag{3.3-19}$$

$m(t_o)$ and $m(t_f)$ specified.
t_o given, t_f free.

The above problem can be solved using the calculus of variations. The variational Hamiltonian is

$$H = V + \lambda_E \frac{V(T - D)}{m} - \lambda_m f \tag{3.3-20}$$

The influence functions λ_E and λ_m must satisfy

$$\frac{d\lambda_E}{dt} = -\frac{\partial H}{\partial E} \tag{3.3-21}$$

and

$$\frac{d\lambda_m}{dt} = -\frac{\partial H}{\partial m} \tag{3.3-22}$$

with the boundary conditions at both ends open. We have H = 0 as a first integral on the optimal path, ie,

$$V + \lambda_E \frac{V(T - D)}{m} - \lambda_m f = 0 \tag{3.3-23}$$

V and η for a given E, λ_E, and λ_m are given by the following optimality conditions:

$$V = \arg \max_V H(E, \lambda_E, \lambda_m, V, \eta) \tag{3.3-24}$$

subject to the following constraints:

$$c_1(E,V) = V_s(E) - V \leq 0 \tag{3.3-24a}$$

$$c_2(E,V) = V - \sqrt{2E} \leq 0 \tag{3.3-24b}$$

The first constraint corresponds to the stalling speed and the second one corresponds to the constraint $h \geq 0$, and

$$\eta = \arg \max_{\eta} H(E, \lambda_E, \lambda_m, V, \eta) \tag{3.3-25}$$

subject to the constraints 3.3-16.

To determine the optimal value of η, it is useful to evaluate

$$\frac{\partial H}{\partial \eta} = \lambda_E \frac{V}{m} \frac{\partial T}{\partial \eta} - \lambda_m \frac{\partial f}{\partial \eta} \tag{3.3-26}$$

Now, from Eq. 3.3-23, provided $f \neq 0$,

$$\lambda_m = \frac{1}{f}\left[V + \lambda_E \frac{V(T-D)}{m}\right] \tag{3.3-27}$$

using Eq. 3.3-27 in Eq. 3.3-26, we have

$$\begin{aligned} \frac{\partial H}{\partial \eta} &= \lambda_E \frac{V}{m} \frac{\partial T}{\partial \eta} - \frac{1}{f}\left[V + \lambda_E \frac{V(T-D)}{m}\right] \frac{\partial f}{\partial \eta} \\ &= \lambda_E \frac{V}{m} \frac{1}{f} \frac{\partial f}{\partial \eta}\left[D + \Delta - \frac{m}{\lambda_E}\right] \qquad f \neq 0 \end{aligned} \tag{3.3-26a}$$

where

$$\Delta = -T + f \frac{\partial T/\partial \eta}{\partial f/\partial \eta}$$

Since $\lambda_E > 0$ and $\frac{\partial f}{\partial \eta} > 0$,

$$\operatorname{sgn} \frac{\partial H}{\partial \eta} = \operatorname{sgn}\left\{D + \Delta - \frac{m}{\lambda E}\right\}, \qquad f \neq 0 \tag{3.3-26b}$$

Now

$$\frac{\partial T/\partial \eta \Big|_{V,E}}{\partial f/\partial \eta \Big|_{V,E}} = \frac{\partial T}{\partial f}\Big|_{V,E}$$

and

$$\Delta = -T + f\,\frac{\partial T}{\partial f}$$

The sign and magnitude of Δ depend on the variation of T with respect to f. For example, for the curve labelled c in Fig. 3.3-3, we have

$$\frac{T}{f} < \frac{\partial T}{\partial f}$$

and consequently $\Delta > 0$.

If the variation of T is linear with f as shown by curve b in above sketch, then $\Delta = 0$.

We shall first consider the case of $\Delta > 0$.

In Fig. 3.3-4, BC represents a maximum-range flight path with full throttle and DD'E represents a maximum-range glide path. AB is a constant-energy zoom dive from starting position A to the maximum range path with full throttle. From Section 3.2.2, on a maximum range glide path (T = 0),

$$\lambda_E = \frac{m}{D_{min}}\Big|_E \qquad (3.3\text{-}28)$$

and

$$\frac{\partial D}{\partial V}\Big|_E = 0.$$

On a maximum total range path, initially $\lambda_E >> m/D$, so that $\partial H/\partial \eta > 0$. Thus $T = T_{max}$ until a point C on the flight path is reached where λ_E has decreased to such a value that

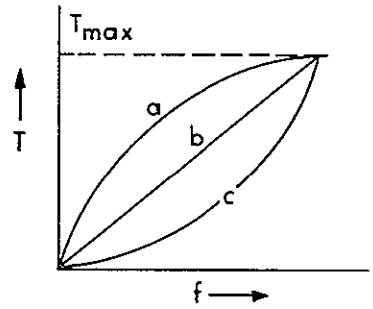

Fig. 3. 3-3 Thrust Versus Fuel Flow at Different Throttle Settings, for Given E and h

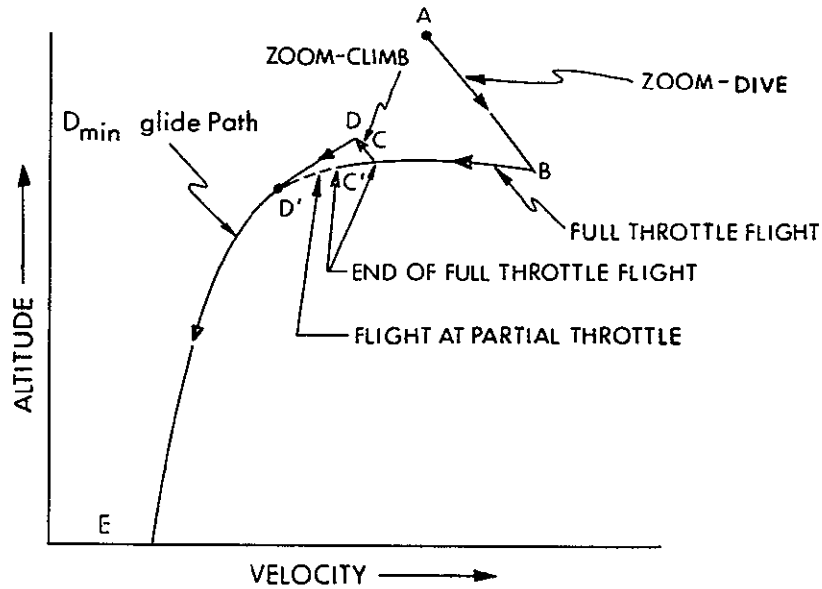

Fig. 3. 3-4 Maximum Range Path for a Given Amount of Fuel

$$\frac{\lambda_E}{m} = \left.\frac{1}{D_{min}}\right|_E$$

At this stage, two possible modes of operation must be considered. The first alternative is to move to a point D (on the glide path), where $\partial H/\partial \eta < 0$ (note, for f=0, $\partial H/\partial \eta$ is given by Eq. 3.3-26, with $\lambda_E = m/D_{min}$ and λ_m given by Eq. 3.3-27 evaluated at point C) and consequently T = 0 and $\delta D/\delta V\big|_E = 0$. Once we are on the glide path, the rest of the flight path is the same as the maximum-range glide path since, on the glide path, $\partial H/\partial \eta < 0$ for all V for a given E. Since $\partial H/\partial \eta > 0$ at C, the second alternative at C is to continue the flight with $T = T_{max}$, to a point C', where λ_E has decreased to such a value that

$$\frac{\lambda_E}{m} = \frac{1}{D + \Delta}$$

where $\Delta > 0$, and is evaluated at $T = T_{max}$. For the first time on the flight path, $\partial H/\partial \eta = 0$ and the possibility exists of operating at intermediate throttle settings,

$$0 \leq T(E, V, \eta) < T_{max}(E, V).$$

In such a case V and η are determined from $\partial H/\partial \eta = 0$ and $\delta H/\delta V = 0$. If this intermediate-thrust path leads to the glide path (ie, to T = 0), we have to choose that mode of operation that gives us better range for a given amount of fuel. If, however, the intermediate-thrust path does not lead to the glide path, then the possibility of operating at intermediate throttle settings is ruled out and the total maximum range path will be a full-throttle flight followed by a glide, as shown by the path ABCDE.

Now let us consider the case of $\Delta < 0$. If the magnitude of Δ is large enough, then we may have $\lambda_E/m = 1/(D + \Delta)$ satisfied at some point on the flight path before point C is reached. In this case, we have to rule out the possiblity of an optimal path with full throttle followed by a glide; since, to reach a point where $\lambda_E = m/D_{min}$, we have to operate at full throttle and this is non-optimal since $\lambda_E/m < 1/(D + \Delta)$ on this section of the path. Thus we are left with the only alternative of operating at intermediate throttle settings with $\partial H/\partial \eta = 0$ and $\partial H/\partial V = 0$, until either $\lambda_E = m/D_{min}$ at $T > 0$ (in which case the thrust takes a jump to T = 0) or we reach the glide path with T = 0. The magnitude of Δ may not be large, in which case λ_E may reach a value equal to m/D_{min} with $\lambda_E/m < 1/(D + \Delta)$. In this case, the comments for the case $\Delta \geq 0$ obtain.

For the aircraft under investigation here, data on fuel consumption at partial throttle was not available. So, a linear variation in thrust with η was assumed, ie,

$$T(E,V,\eta) = \eta T_{max}(E,V)$$

and

$$f(E,V,\eta) = \frac{\eta T_{max}(E,V)}{c} \tag{3.3-29}$$

where c = specific fuel consumption (c is assumed to be constant over the portions of h,V plane of interest).

Under assumption 3.3-29, we have from Eq.3.3-26.

$$\frac{\partial H}{\partial \eta} = \frac{VD}{\eta}\left(\frac{\lambda_E}{m} - \frac{1}{D}\right), \qquad \eta \neq 0. \tag{3.3-30}$$

From the optimality condition 3.3-25, we have for $\frac{\partial H}{\partial \eta} > 0$, $T = T_{max}$; for $\frac{\partial H}{\partial \eta} < 0$, $T = 0$; and for $\frac{\partial H}{\partial \eta} = 0$, we have the possibility of operating for some time at intermediate throttle settings, between $T = 0$ and $T = T_{max}$.

For the case when $\frac{\partial H}{\partial \eta} = 0$, from Eq. 3.3-30 we have

$$\lambda_E/m = 1/D \tag{3.3-31}$$

Also the optimality condition 3.3-24 gives us

$$T = V\frac{\partial D}{\partial V}, \tag{3.3-32}$$

when constraints 3.3-24a, 3.3-24b, and 3.3-16 are not effective.

On a path that satisfies Eq. 3.3-31 and 3.3-32, we should have

$$\frac{d}{dt}(\lambda_E D - m) = 0 \tag{3.3-33}$$

or

$$D\frac{d\lambda_E}{dt} + \lambda_E\left(\frac{\delta D}{\delta E}\frac{dE}{dt} + \frac{\delta D}{\delta V}\frac{dv}{dt}\right) + \frac{T}{c} = 0$$

Using in the above, Eq. 3.3-18, 3.3-21, 3.3-23, 3.3-31, and 3.3-32, we get

$$\frac{dV}{dt} = -\frac{V}{mc}\left(D + cV\frac{\partial D}{\partial E}\right) \tag{3.3-34}$$

For the aircraft under investigation, it was found that the path, as given by Eq. 3.3-33, starting from a point on the full-throttle path, where $\lambda_E/m = 1/D$, does not lead to the glide path. Thus, the operation at partial throttle is ruled out under the assumption 3.3-29.

If we assume the variation of C_{D_o} and C_L with respect to M to be small, we can reach the same conclusion in another way. On a full-throttle path, the value of λ_E at the point where $\partial H/\partial \eta = 0$, is smaller than the value of λ_E on the glide path. As seen in Section 3.3.1, λ_E remains constant ($= m/D_{min}$) on the glide path. Thus, if a path, operating at intermediate-throttle settings with $\partial H/\partial \eta = 0$ and $\partial H/\partial V = 0$, is to take us from the maximum-range full-throttle path to the maximum-range glide path, we should have on this path,

$$\frac{d\lambda_E}{dt} > 0 \tag{3.3-35}$$

Now, on this path

$$\begin{aligned}
\frac{d\lambda_E}{dt} &= -\frac{\partial H}{\partial E} \\
&= -\frac{\partial}{\partial E}\left(V + \lambda_E \frac{V(T - D)}{m} - \lambda_m \frac{T}{c}\right) \\
&= \frac{\lambda E}{m} V \frac{\partial D}{\partial E} \\
&= \frac{V}{gD} \left.\frac{\partial D}{\partial h}\right|_v \\
&= -\frac{\beta V}{Dg}(D_0 - D_L)
\end{aligned} \tag{3.3-36}$$

where

$$\beta = -\frac{1}{\rho}\frac{\partial \rho}{\partial h}$$

As seen in Section 3.3.1, $D_0 = D_L$ on a glide path, and $D_0 > D_L$ below the glide path in an h,M space. In view of this, we find from Eq. 3.3-36 that $d\lambda_E/dt < 0$ at all points on the path operating at parial-throttle settings with $\partial H/\partial \eta = 0$ and $\partial H/\partial V = 0$. Thus, in view of the contradiction with Eq. 3.3-35, we find that the operation at partial throttle is ruled out, under the assumption of constant C_{D_0} and C_{L_α}. Thus, the maximum-range path consits of a full-throttle path followed by a glide.

Since the amount of fuel is specified, it is often convenient to use the amount of fuel expended as the independent variable for the full-throttle portion of the path. Let

$$\mu = m_0 - m \tag{3.3-37}$$

represent the amount of fuel mass used. Dividing Eq. 3.2-17 by Eq. 3.2-18 and using Eq. 3.3-37, we get

$$\frac{dE}{d\mu} = \frac{V(T - D)}{mf} \tag{3.3-38}$$

$$E(0) \quad \text{specified} \tag{3.3-39}$$

The range can be expressed as

$$R = \int_0^{\mu_f} \frac{V}{f} \, d\mu \tag{3.3-40}$$

where μ_f = amount of fuel-mass to be used in the flight.

The maximization problem can be solved by using the calculus of variations approach. The variational Hamiltonian for this problem is

$$H = \frac{V}{f} + \lambda_E \frac{V(T - D)}{mf} \tag{3.3-41}$$

The optimality condition is

$$V = \arg \underset{V}{\text{Max}} \, H(E, V, \lambda_E, \mu) \tag{3.3-42}$$

where V is subject to the constraints 3.3-24a and 3.3-24b.

The influence function, λ_E, is determined by the following equations, when the path is not on either of the constraint boundaries:

$$\frac{d\lambda_E}{dt} = -\frac{\partial H}{\partial E} \tag{3.3-43}$$

When the path is against one of the constraints,

$$\frac{d\lambda_E}{dt} = -\frac{\partial H^*}{\partial E} \tag{3.3-44}$$

where

$$H^* = H + \nu_1 c_1 + \nu_2 c_2 \tag{3.3-45}$$

In Eq. 3.3-45, $\nu_i = 0$ for $C_i(E, V) < 0$, i = 1 or 2; and for $C_i(E, V) = 0$, i = 1 or 2, corresponding ν_i is given by

$$\frac{\partial H^*}{\partial V}(E, V, \lambda_E, \mu, \nu_i) = 0$$

The boundary condition for λ_E at $\mu = \mu_f$ is

$$\lambda_E(\mu_f) = \frac{m_f}{D_{min}(\mu_f)} \tag{3.3-46}$$

where D_{min} represents the minimum drag with respect to V for a given E. The glide path starting from $E(\mu_f)$ is the maximum-range glide path.

Thus we have to solve a two-point boundary value problem which involves solving simultaneously two differential Equations 3.3-38 and either 3.3-43 or 3.3-44, with boundary condition 3.3-39 and 3.3-46 and V determined by the optimality condition 3.3-42. The boundary-value problem can be easily solved, for example, by guessing the missing boundary condition $\lambda_E(\mu = 0)$. Each value of $\lambda_E(\mu = 0)$ corresponds to a certain amount of total fuel-mass, μ_f, used, and thus it is possible to sweep out maximum-range paths for different amounts of fuel by selecting different values of $\lambda_E(\mu = 0)$ and solving differential Eq. 3.3-38 and 3.3-43 (or 3.3-44) forward until boundary condition 3.3-46 is satisfied and determining V at each stage by the optimality condition 3.3-42.

Figure 3.3-5 shows the Mach no./altitude path for maximum total range using 2100 lb of fuel, obtained by using the energy-state approximation. Initially, the maximum total-range path starts out closer to the minimum-fuel energy-climb path. (This is apparent from Eq. 3.3-41, and also, since initially $\lambda_E(\mu)$ is larger and decreases as the flight progresses.) As the flight progresses, the path starts diverging away from the minimum-fuel path, but still progressing towards higher-energy levels to take advantage of the greater glide range that can be obtained by starting the glide from higher-energy levels. At the end of the powered flight, there is a short constant-energy zoom-climb to the maximum-range glide path. A Mach no./altitude path obtained by using the four-variable model[18] under similar conditions is also shown in Fig. 3.3-5. The "exact" path is close to the "energy-state" path, but lies above it throughout the h,M space. The maximum-range glide paths are the same as those shown in Fig. 3.3-4. The ranges shown on the figure have been calculated for flight ending at h = o in both cases. However, the "exact" path flares out near the ground to use up the kinetic energy for gaining extra range, and the path terminates on the ground at lower velocity. For the energy-state path, if we consider a constant-lift slow-down path near h = 0 ending at the same velocity

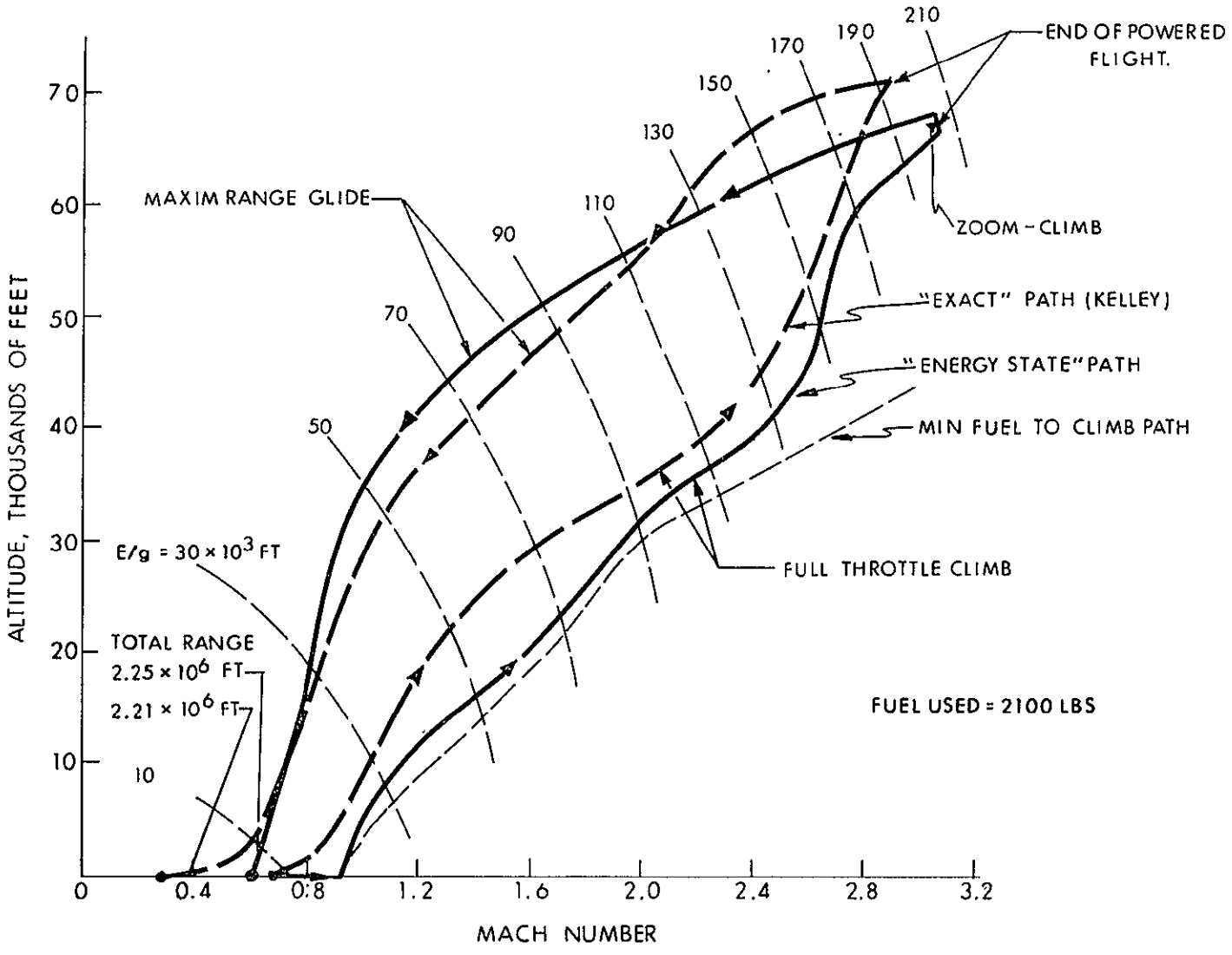

Fig. 3. 3-5 Maximum Total Range Path for Given Amounts of Fuel

as that for the "exact" path, then the total range equals 2.30×10^6 ft. This value is within 4% of the range obtained on the "exact" path.

Figure 3.3-6 shows the fuel, λ_E, and the range histories during the flight for the maximum total range "energy-state" path of Fig. 3.3-5. Only about one-third of the total range is gained on the powered flight. Note that λ_E is relatively insensitive to the starting point of the glide path. Figure 3.3-7 shows the range vs altitude profiles for the maximum-range path corresponding to that in Fig. 3.3-5.

Figure 3.3-8 shows the Mach no./altitude paths for maximum total-range paths for 1800 lb and 2400 lb of fuel. Only one maximum-range glide path using 2400 lb of fuel is shown. The glide path using 1800 lb of fuel is very close to that of 2400 lb. Figure 3.3-9 shows the total range vs fuel used for the maximum-range paths shown in Fig. 3.3-5 and 3.3-8.

3.3.4 Conclusions

We have seen that energy of the vehicle is an important variable to describe the state of the flight. The reduction in the order of the flight dynamics in energy-state approximation leads to considerable ease in the solution of optimal-flight paths and also to valuable insight into their nature. Flight-path constraints are particularly easy to handle using the energy-state approximation. Most of the flight constraints, which may arise due to structural, propulsive, aerodynamic, flight-path, and other considerations, are in the state-control inequality constraint category.* In the energy-state formulation such constraints are relatively easy to handle numerically; whereas, in the "exact" (4-variable) model, these limitations are mainly on the state-variables and these are rather difficult to handle numerically.

Besides optimal-climb problems, the following maximum-range problems applicable to the shuttle have been investigated using energy-state methods.

1) Maximum range for a gliding flight
2) Maximum range for a given amount of fuel.

We have seen that the maximum-range paths for the aircraft (which have been used in this chapter for illustrative purposes), using energy-state model and "exact" model (4-variable), compare very well.

For a gliding flight, we find that the maximum-range glide-path follows a

*(ie, involving both the state and control variables.)

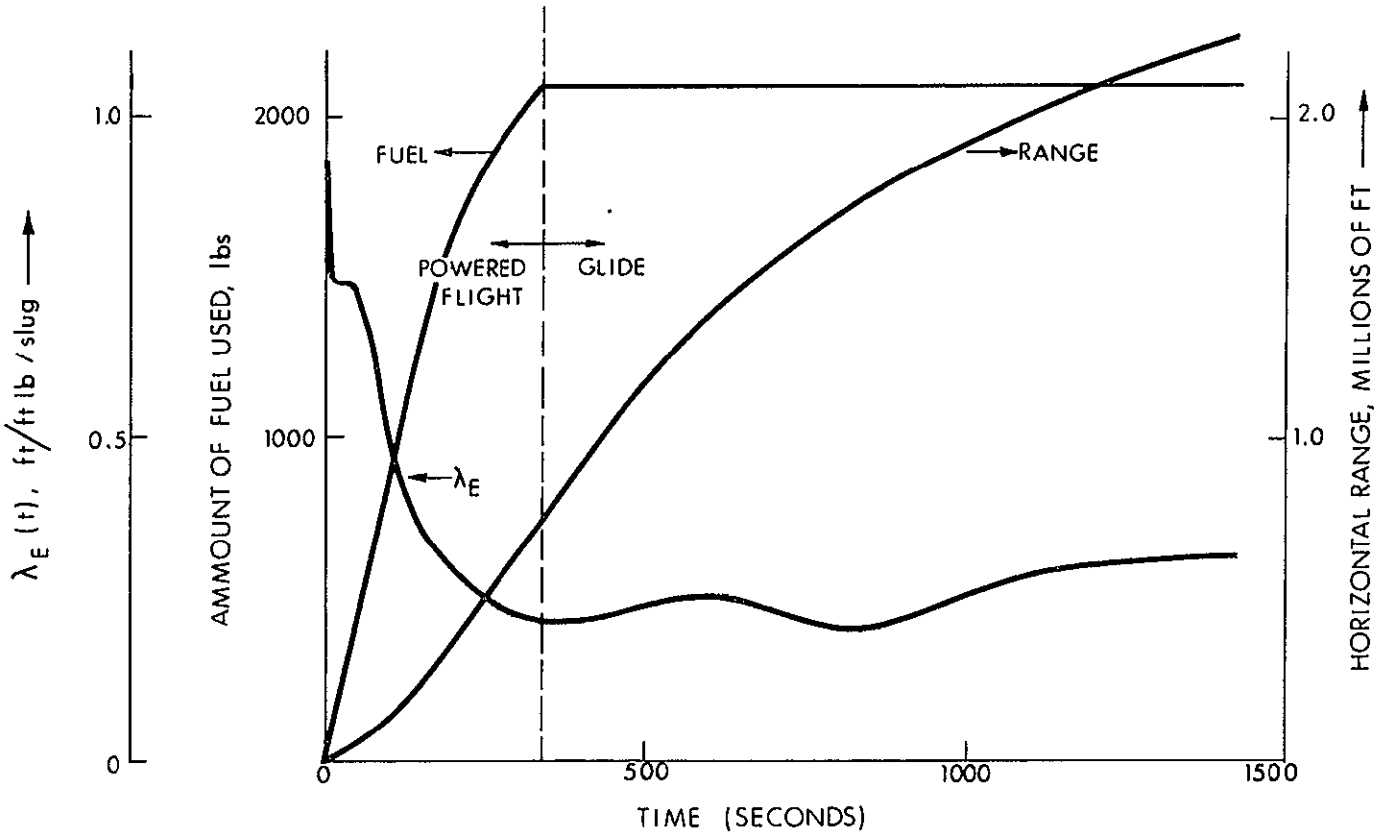

Fig. 3. 3-6 Fuel, λ_E and Range Histories for a Maximum Total Range Path for a Given Amount of Fuel

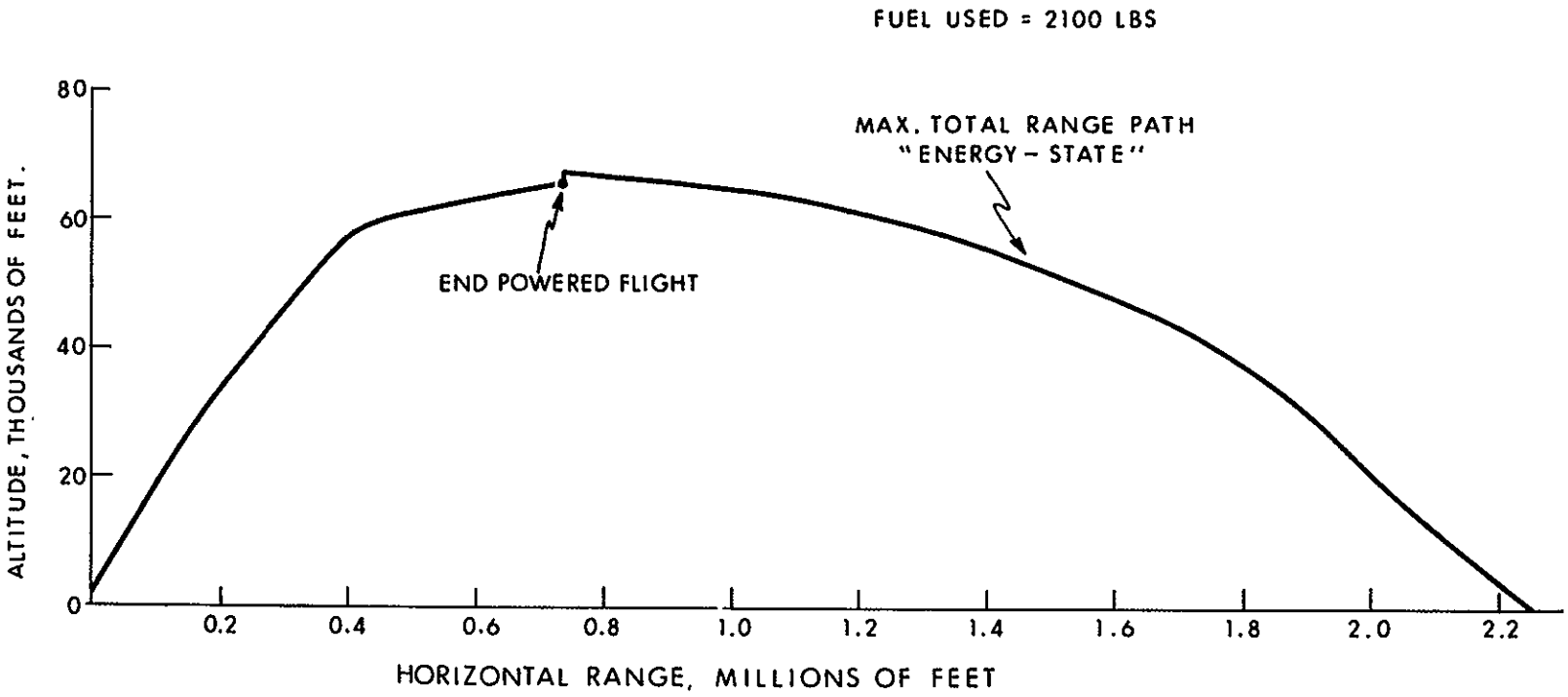

Fig. 3.3-7 Maximum Range Profiles for a Given Amount of Fuel

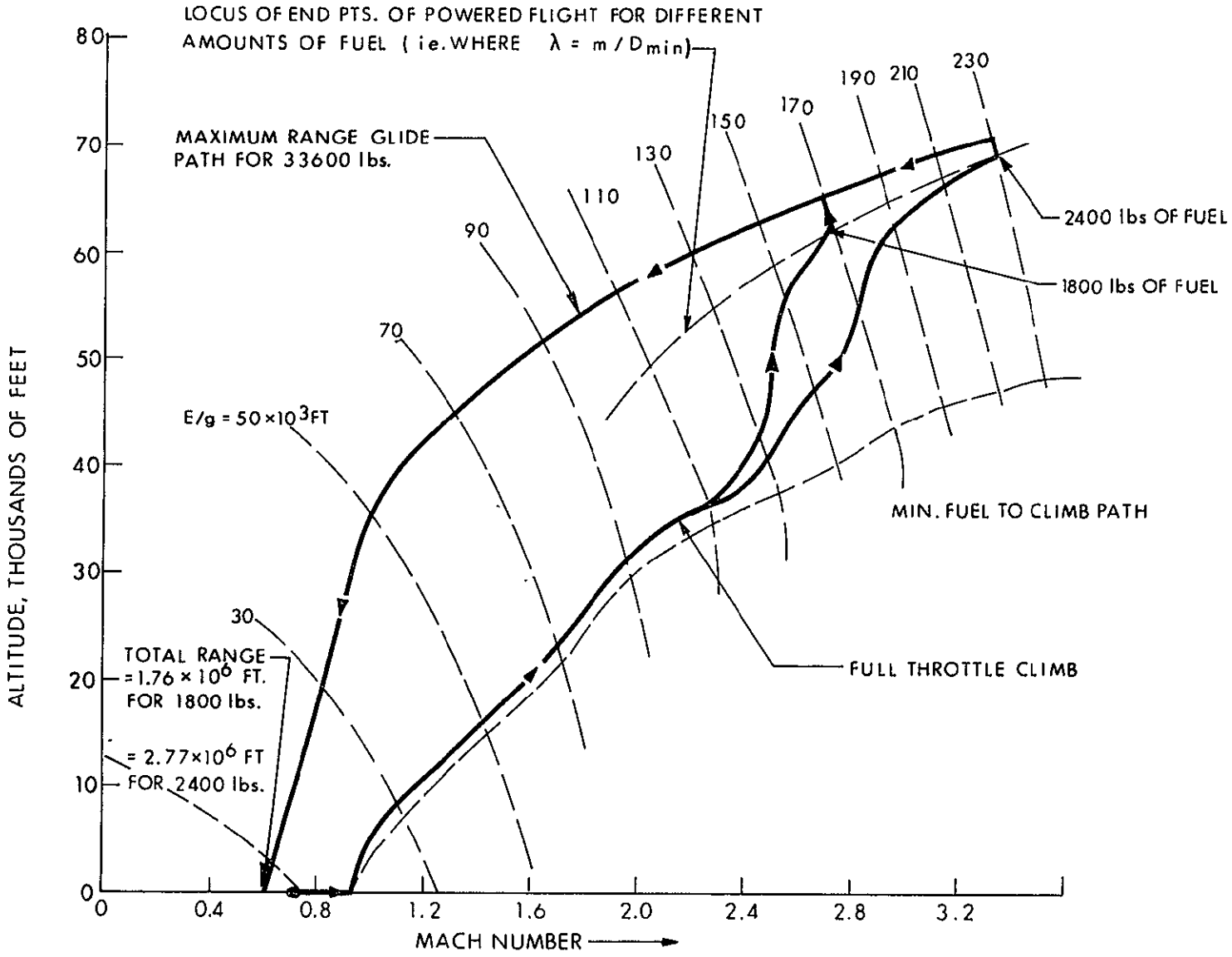

Fig. 3.3-8 Maximum Total Range Paths for a Given Amount of Fuel

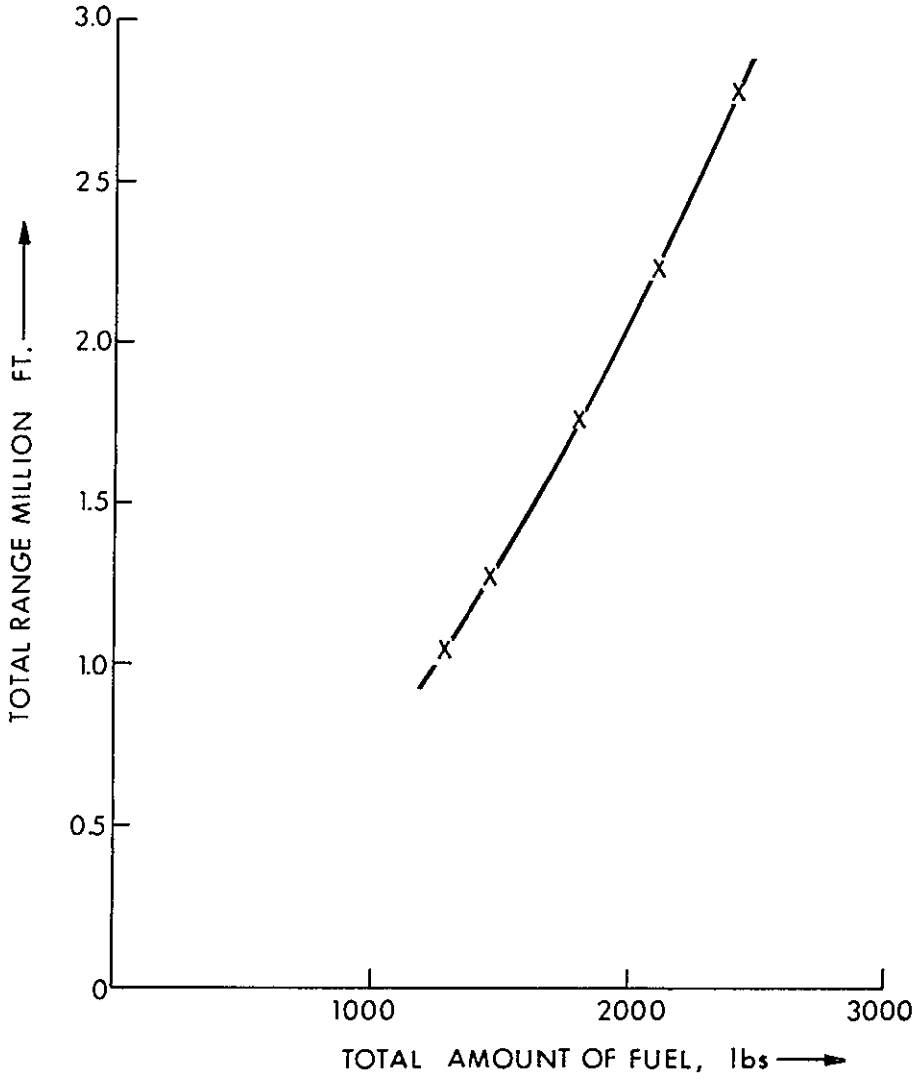

Fig. 3.3-9 Range Versus Total Amount of Fuel, for Maximum Total Range Paths for Given Amounts of Fuel

minimum drag path. In the case of the space shuttle, the range achievable by a gliding flight merits important consideration, in view of the direct trade-off between the deliverable orbital payload and the amount of fuel reserved for subsonic flight. The energy of the vehicle at the start of the glide and the L/D_{min} ratio of the vehicle are the important factors affecting the maximum-glide range. The effect of the weight of the vehicle is relatively unimportant.

In the case of the maximum-range problem for a given amount of fuel, the optimal trajectory consists of a powered flight followed by a glide. The initial phase of the flight is powered, operating at full throttle except towards the end when operation at intermediate throttle may occur. The gliding flight forms the final phase. Figure 3.3-10 indicates the maximum-range capability that we may expect for a subsonic shuttle flight, for flights starting from two different initial energy positions. It may be seen that the range capability of the shuttle not only depends on the amount of fuel available, but also on the energy of the shuttle at the beginning of the subsonic phase. We may expect that most of the range would be achieved over the glide phase of the maximum-range path, in view of the small amount of fuel and little excess-power capability (which requires $T - D > 0$) of the shuttle over most of the flight path.

For a given $E(t = 0)$, the maximum-range capability can be investigated by solving the Euler-Lagrange equations of Section 3.3.3 for different values of $\lambda_E(t = 0)$. Minimum amount of fuel necessary for the range capability that may be required for a given subsonic shuttle-flight can be determined easily by iterating on $\lambda_E(t = 0)$, until the required range is achieved. Earlier experience[25] indicates that the functional dependence of $\lambda_E(t = 0)$ on total range, x_f, is usually smooth and thus the number of iterations required would be small. Thus, the optimal path can be determined with considerable computational simplicity, and on-board computation may be feasible.

To conclude, the energy-state approximation, properly interpreted, is adequate for determining optimal trajectories for the Space Shuttle for various operating conditions during its subsonic flight. By reducing the order of the flight dynamics, a computationally simple formulation is achieved which readily incorporates flight-path constraints. This simplicity raises the possibility of on-board computation.

In addition to its operational role in trajectory definition, the energy-state approach is invaluable during the early stages in shuttle design to determine the effect of various design parameters on the operational capability of the shuttle.

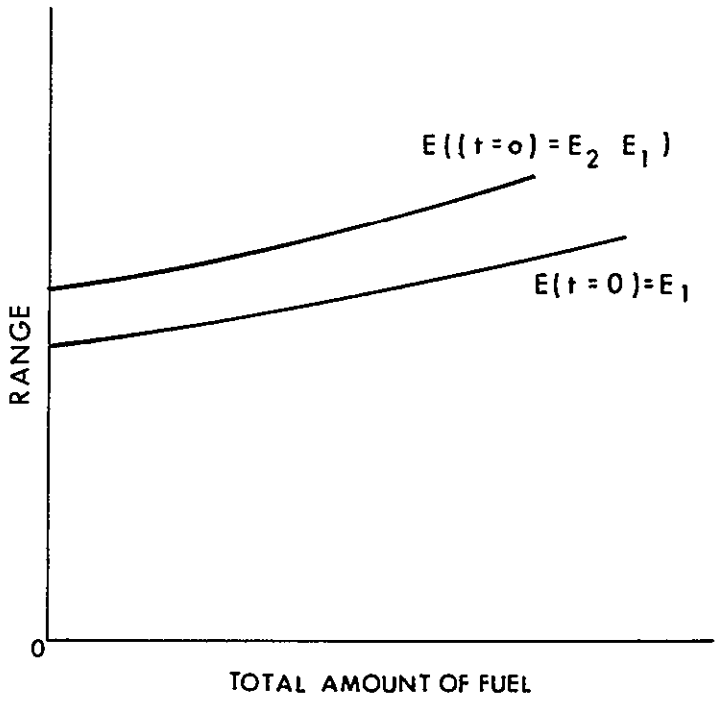

Fig. 3.3-10. Range Capability of Shuttle for Different Amounts of Fuel

Chapter 3 References

1. Perkins, C.D., Hage, R.E., "Airplane Performance Stability and Control", Wiley, N.Y., 1949, pp. 175-182.
2. Kaisero, F., "The Climb of Jet-Propelled Aircraft Part I - Speed Along the Path in Optimum Climb", RTP/TIB translation No. GDC/15/148T, British Ministry of Supply, April, 1944.
3. Lush, K.J., "A Review of the Problem of Choosing a Climb Technique with Proposals for a New Climb Technique for High Performance Aircraft", British Aero. Research Council, R&M 2557, 1951.
4. MIELE, A., "General Solutions of Optimum Problems in Nonstationary Flight", NACA, TM 1388, Oct., 1955.
5. Kelly, L., "Optimum Climbing Techniques' for a Jet-Propelled Aircraft", The College of Aeronautics, Cranfield, April, 1952.
6. Garbell, M.A., "Optimum Climbing Techniques for High Performance Aircraft", Garbell Aeronautical Series No. 8, 1953.
7. Rutkowski, E.S., "Energy Approach to the General Aircraft Performance Problem", Jour. Aero. Sci., Mar., 1954, Vol. 21, No. 3, pp. 187-195.
8. Lush, K.J., Davy, B., Dommasch, D.O., Renaudie, J.F., "Total Energy Methods", Ch. 7, Vol. I, AGARD Flight Test Manual, 1952.
9. Cartaino, J. F., Dreyfus, S.E., "Application of Dynamic Programming to the Airplane Minimum Time-to-Climb Problem", Rep. p-834 (revised), The Rand Corporation, Jan., 1957.
10. Cicala, P., Miele, A., "Brachistocronic Maneuvers of a Constant Mass Aircraft in a Vertical Plane", Jour. of Aeronautical Sciences, Vol. 22, No. 4, April.
12. Hestenes, M.R., "A General Problem in the Calculus of Variations with Application to Paths of Least Time", Rand R-M 100, March, 1950.
13. Miele, A., "Minimal Maneuvers of High Performance Aircraft in a Vertical Plane", NASA TND-155, Sept., 1959.
14. Bryson, A.E., Denham, W.F., "A Steepest-Ascent Method for Solving Optimal Programming Problems", Jour. Appl. Mech., Vol. 29, June, 1962.
15. Kelley, H.J., "An Investigation of Optimal Zoom-Climb Techniques", Jour. of the Aerospace Sciences, Vol. 26, 1959, pp. 794-802, 824.
16. Breakwell, J.V., "The Optimization of Trajectories", Jour. of the Soc. of Industrial and Appl. Maths., Vol. 7, June 1959, pp. 215-247.
17. Mengel, A.S., "Optimum Trajectories", Rand Report, p-199, 1951.

18. Kelley, H.J., Falco, M., Ball, D.J., "Air Vehicle Trajectory Optimization", Symposium on Multivariable System Theory, Fall Meeting of Soc. Ind. Appl. Math, Cambridge, Mass., 1962.
19. Heermann, H., Kretsinger, P., "The Minimum Time Problem", The Jour. of the Astronautical Sciences, Vol. XI, No. 4, 1964, pp. 93-107.
20. Bryson, A.E., Desai, M.N., Hoffman, W.C., "The Energy-State Approximation in Performance Optimization of Supersonic Aircraft", Journal of Aircraft, Vol. 6, No. 6, Nov-Dec., 1969, pp. 481-488.
21. Denham, W.F., "Steepest-Ascent Solution of Optimal Progr amming Problems", Ph. D. Dissentation, Div. Engr. and Appl. Physics, Harvard Univ., 1963, Chapter 6.
22. Miele, A., "Flight Mechanics Vol. 1, Theory of Flight Paths", Addison-Wesley, Reading, Mass:, 1962, pp. 143-145.
23. Bryson, A.E., Lele, M.M., "Minimum Fuel Lateral Turns at Constant Altitude", AIAA Journal, Vol. 7, No. 3, March 1969, pp. 559-560.
24. Connor, M.A., "Optimization of a Lateral Turn at Constant Height", AIAA Journal, Vol. 58, No. 2, Feb., 1967, pp. 335-338.
25. Desai, M.N., "Energy-State Approximation in Performance Optimization of Supersonic Aircraft", Ph. D. Thesis, Harvard University.
26. Kelley, H.J., Edelbaum, T.N., "Energy-Climbs, Energy-Turns and Asymptotic Expansions", J. of Aircraft, Vol. 7, No. 1, Jan-Feb., 1970, pp. 93-95.

SECTION 4

SPACE SHUTTLE GUIDANCE DURING APPROACH AND LANDING

by
George W. Cherry
and
Barton DeWolf

The function of the space-shuttle guidance system in the approach and landing phase is to generate control-system signals that will cause the vehicle upon entering the ILS coverage volume to acquire the localizer and glide planes, flare, decrab, touchdown, and finally roll out along the runway.

In this section we outline certain guidance concepts which should enable the system to serve this function. Approach trajectories are discussed in subsection 4.1, and guidance laws for following specified trajectories are discussed in subsection 4.2. Guidance concepts for flare, are discussed in subsection 4.3.

4.1 Planning The Approach Trajectory

Approach trajectories must satisfy initial and final boundary conditions and must not require maneuvers, maneuver rates, or engine performance beyond the vehicle's capabilities; but otherwise the trajectories may be selected to secure some specified advantage (for example, the saving of fuel). This section describes the philosophy of trajectory planning by working out a scheme for ground-track planning. It is necessary to control ground track because the final ground track must be coincident with the extended runway center-line. (A later section will deal with ground-track following, a control process which should take the steady-state winds explicitly into account.)

4.1.1 Constraints on the Ground Track

This section describes some of the constraints on ground-track planning.

Figure 4.1-1 illustrates an idealized approach to the runway center-line. The shuttle flies a straight line between A and B. At point B, in anticipation of intercepting the final approach course, the shuttle is instantaneously (ideally) rolled to a bank angle, ϕ, which causes the shuttle to turn about X with radius-of-curvature R. If the point B, the point X, and the radius of curvature R are properly chosen, the shuttle can roll (instantaneously) to the wings-level orientation at point C and proceed perfectly along the final approach course to landing, touch-down, and roll-out. There are physical limitations on the location of X and B, however. This section describes these limitations.

Ground-track planning involves lateral-acceleration profile planning or the allocation of some part of the lift vector to the horizontal plane. On straight-line ground tracks, no part of the lift vector is allocated to the horizontal plane, but when the ground track is curved, as during the transistion between two intersecting straight-line ground tracks, some part of the lift vector is allocated to the horizontal plane and the vehicle is banked more or less away from wings-level flight.

If the turn is coordinated (no side-slip and no skid), the radius of curvature of the turn, the airspeed, and the angle-of-bank, are related as follows.

$$\tan \phi = \frac{v^2}{gR} \tag{4.1-1}$$

This equation is easily derived by reference to Fig. 4.1-2, which depicts the lift vector (tilted away from the vertical) of an aircraft flying away from the reader and turning to his left. If the vehicle turns without slipping or skidding, the lift vector must be anti-parallel to the resultant of the centrifugal and gravitation forces.

$$\text{centrifugal force} = Mv^2/R$$
$$\text{gravitational force} = Mg$$

$$\tan \phi = \text{centrifugal force/gravitational force}$$
$$= v^2/gR \tag{4.1-1}$$

If the aircraft is to maintain altitude during the turn, there is a constraint on the magnitude of the lift vector also.

$$L \cos\phi = Mg = W \tag{4.1-2}$$

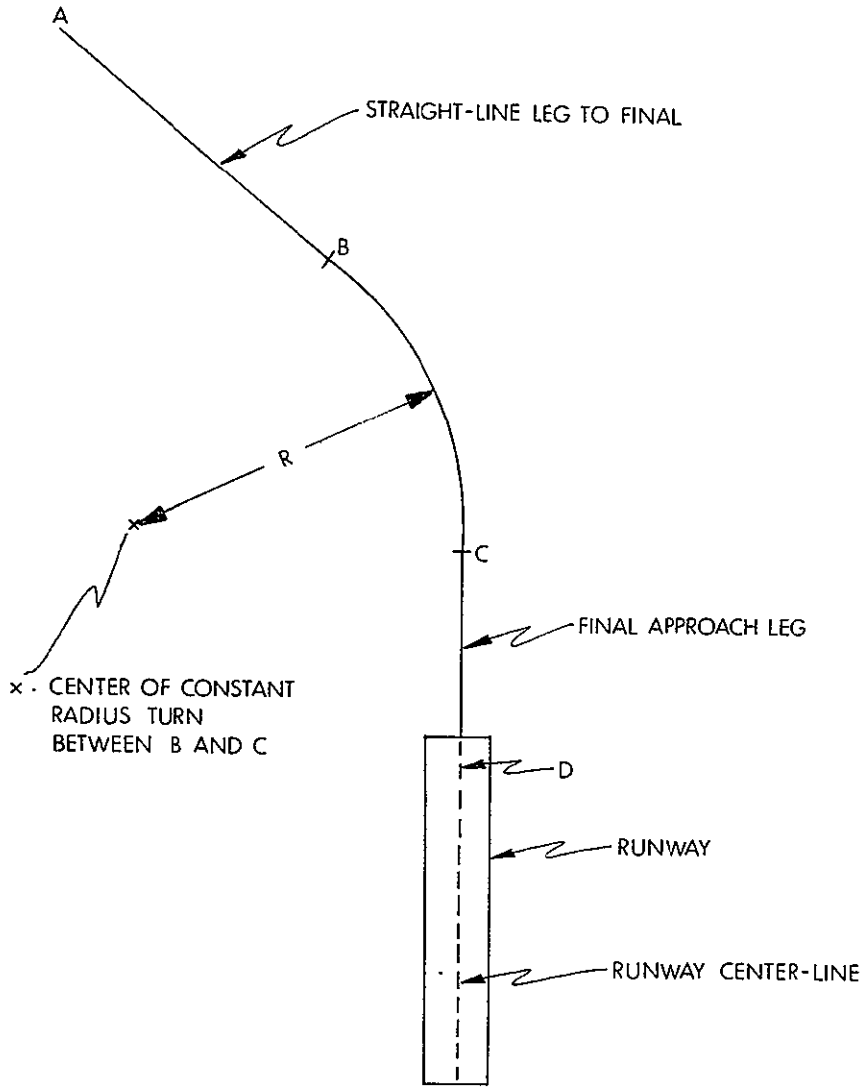

Fig. 4.1-1 Ground Track for Runway Approach

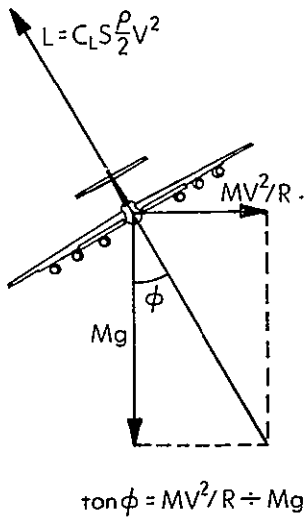

Fig. 4.1-2 Bank Angle in a Coordinated Turn

or

$$L = \sqrt{W^2 + (Mv^2/R)^2} \tag{4.1-3}$$

If the aircraft were maintaining altitude before the turn,

$$L = W \quad \text{(before turn)} \tag{4.1-4}$$

it must generate more lift during the turn in order to continue to maintain altitude.

$$L = W/\cos \phi \quad \text{(during turn)} \tag{4.1-5}$$

The additional lift can be calculated by subtracting Eq. 4.1-4 from Eq. 4.1-5.

$$\Delta L = W(\sec \phi - 1) \tag{4.1-6}$$

Since

$$L = C_L S \frac{\rho}{2} v^2 \tag{4.1-7}$$

the additional lift must be provided by increasing C_L or v or both. In order to increase v, power must be added (thrust must be increased). In order to increase C_L, the angle of attack must be increased. But, increasing the angle of attack increases C_D and D and, therefore, requires an increase in thrust and power. A power limitation therefore precludes an arbitrarily small R (unless it is permissible to lose altitude during the turn). It is sometimes possible to negotiate a gentle turn, without losing altitude and without increasing power, by continually increasing the angle-of-attack and accepting the loss in airspeed. For moderate bank angles, up to 20 degrees, say, this strategy can be adopted with no or little loss in altitude. If the aircraft is flying near the stall speed, this strategy would not be acceptable.

Finally, if the landing is dead-stick (engine throttles back or off), the flight path angle must be depressed. The tangent of the flight path angle is

$$\tan \phi = C_D/C_L \tag{4.1-8}$$

Since C_D and C_L are functions of angle-of-attack, we can plot angle of glide versus angle of attack. This function (shown for the Orbiter 245 configuration) is illustrated in Fig. 4.1-3. If the aircraft is flying the minimum flight-path angle on a straight

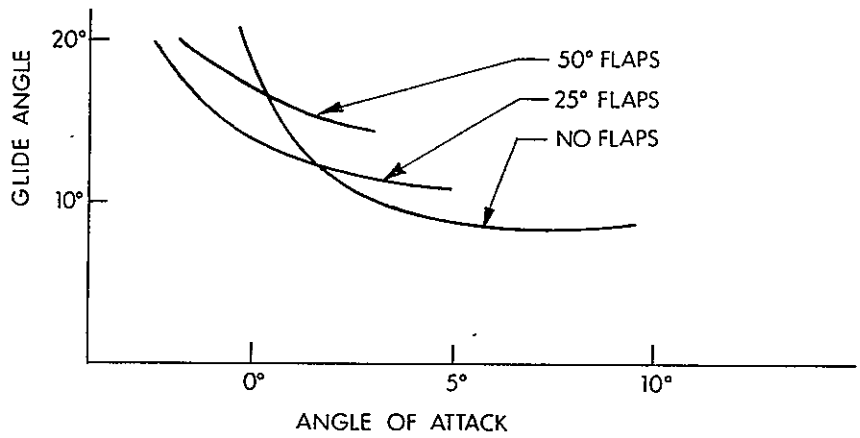

Fig. 4.1-3 Glide Angle Versus Angle of Attack for Unpowered Shuttl

leg, it must steepen its flight path during a turn. The greater loss of altitude per unit time during a turn must be considered in trajectory planning.

Figure 4.1-4 illustrates a family of constant-radius transition turns between the leg of heading ψ_i and the final approach leg of heading ψ_f. Transition turn A is undesirable because the aircraft does not return to the wings-level orientation and fly straight until reaching the runway threshold. Transition turns like D and sharper turns (like E) may be undesirable because of several reasons

1. Too great a bank angle may be required.
2. If it is a powered landing and if it is desired to maintain altitude, too much power may be required.
3. If it is a dead-stick landing, too large a sink rate may develop.
4. If the aircraft is flying slowly, the stall margin may be violated.

The range of permissible radii of curvature may be computed. Consider Fig. 4.1-5. Suppose that λ is the minimum acceptable straight-in final approach to the runway.

Then $$\ell = \Lambda - \lambda \tag{4.1-9}$$

and a maximum radius of turn can be computed as shown in the figure. This leads to the following inequality statement for R

$$R < \ell \tan \left(\left| \psi_f - \psi_i \right| / 2 \right) \tag{4.1-10}$$

An equation for minimum radius of curvature can be computed from Eq. 4.1-1 if the maximum bank angle is limited.

$$R > v^2 / g \tan \phi_{max} \tag{4.1-11}$$

combining Eq. 4.1-10 and 4.1-11 yields the permissible interval for R

$$v^2 / g \tan \phi_{max} < R < \ell \tan \left(\left| \psi_f - \psi_i \right| / 2 \right) \tag{4.1-12}$$

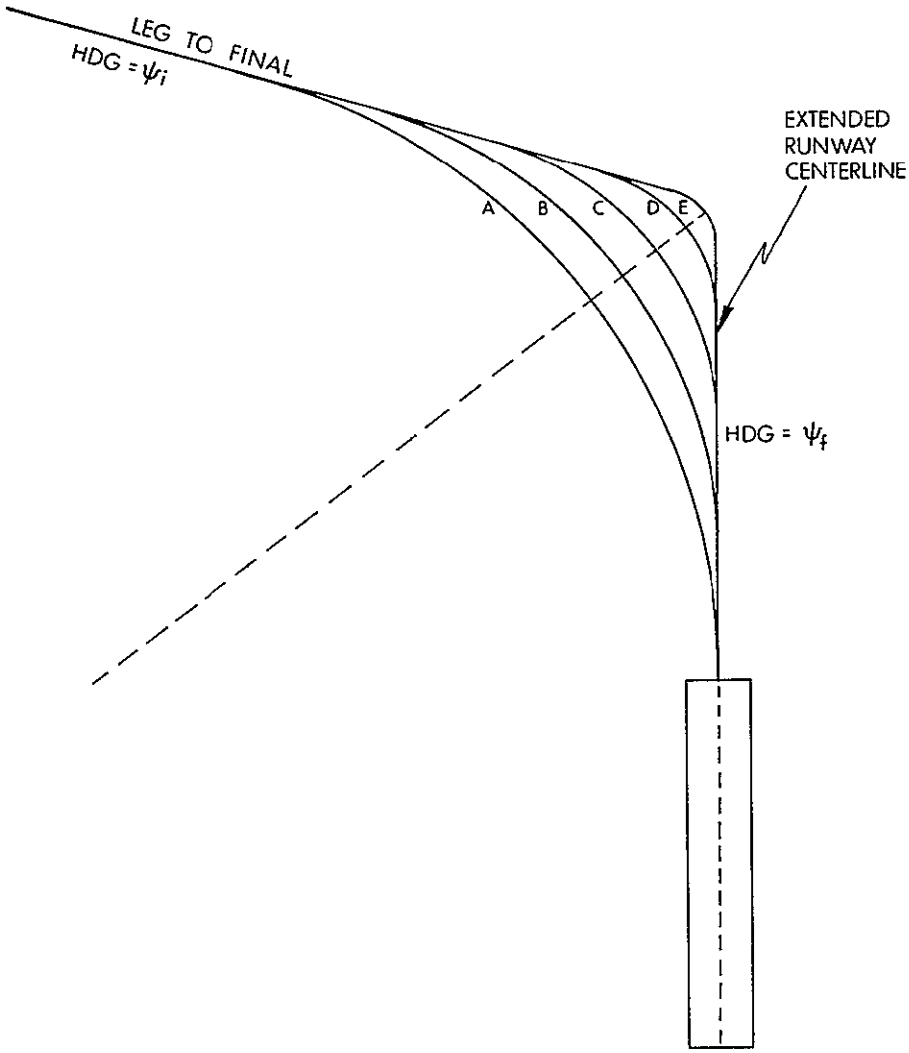

Fig. 4.1-4 Family of Transition Turns

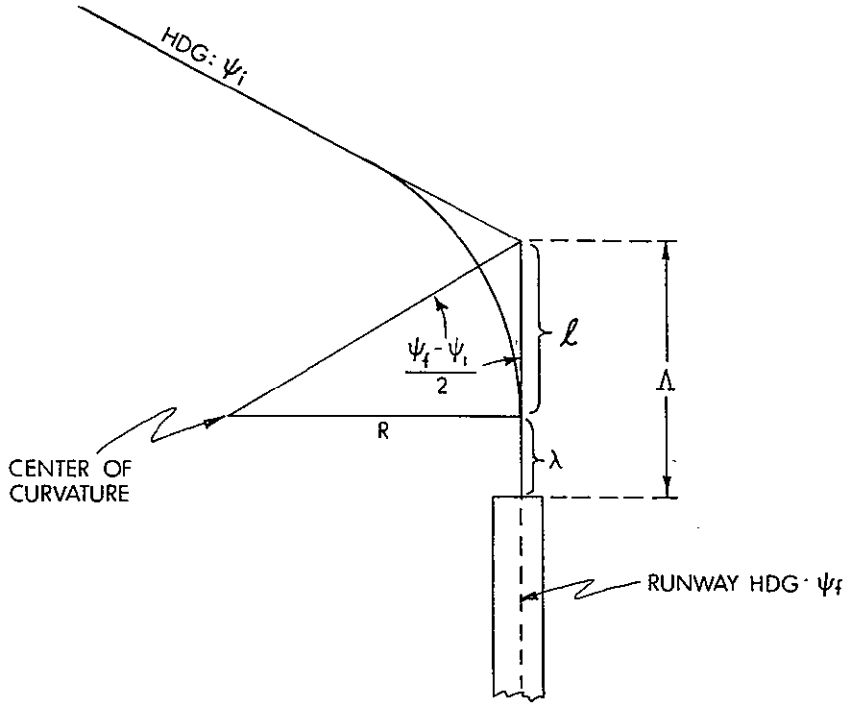

$$\ell = \Lambda - \lambda$$

$$\tan\left(\frac{|\psi_f - \psi_i|}{2}\right) = \frac{R}{\ell}$$

NOTE: λ is the minimum acceptable straight-in leg of the final approach path.

Fig. 4.1-5 Transition Turn of Largest Permissible Radius

Equation 4.1.12 does not take explicitly into account factors 2, 3, and 4 alluded to above in setting a minimum radius of curvature. As a practical matter, since approach speed is usually fairly consistent, these constraints can be translated into a maximum permissible bank angle.

The equation of constraint on R, Eq. 4.1-12, allows a value of R to be chosen from the permissible interval which secures some specified advantage. Some examples of payoff functions that might be optimized are

1. Minimize fuel.
2. Minimize altitude lost in the dead-stick case.

Criterion 1 is discussed in Reference 1.

Other criteria may be used for choosing R from the interval. Some examples are

1. Use a standard bank angle, say 30 degrees.
2. Control time-of-arrival at the runway threshold. (This criterion may be useful for increasing the capacity of a heavily used runway — but it is not very applicable to the Space Shuttle landing)
3. Help solve the vertical-control problem by losing a specified amount of altitude during the turn.

This section has described some of the considerations for ground-track trajectory planning. Additional research on ground-track planning and vertical-trajectory planning is under way.

4.1.2 Designing A Flyable Approach Trajectory

A key concept in this chapter is the design of reference trajectories which are realistically flyable; i.e., trajectories whose curvature,* rate of change of curvature, and second derivative of curvature, take into account the Space Shuttle's maneuver, maneuver-rate, and maneuver-acceleration limitations. In Section 4.1.1 we discussed the bank-angle limitations on vehicle maneuvers and how these limitations constrain the radius of curvature of the nominal transition turn onto the final approach course. We must also take into account the roll-angle dynamics of the Space Shuttle, and design reference transition turns which do not require too large a rate-of-change of the radius of curvature. The ground-track traces shown

* The curvature of a path is defined as the reciprocal of the radius of curvature of the path; therefore, the tangent of the bank angle, Eq. 4.1-1, is directly proportional to the curvature of the path.

in Fig. 4.1-1 and 4.1-4 are examples of trajectories which are essentially "unflyable" because they violate this consideration. Consider the trajectory in Fig. 4.1-1. Between B and C the "aircraft" flies a finite-radius-of-curvature path, of radius R; at C, the "aircraft" instantaneously rolls out to wings-level flight and flies the infinite-radius-of-curvature path from C to touchdown at D. The real vehicle, unable to roll to wings-level flight instantaneously at C, would not acquire the final approach course accurately. The trouble is that the "trajectory design" in Fig. 4.1-1 did not take into account the roll dynamics of the vehicle, which may reasonably accurately be described as

$$\ddot{\phi}(t) + 2\zeta\omega\dot{\phi}(t) + \omega^2\phi(t) = \omega^2\phi_c(t) \tag{4.1-13}$$

where ω, the undamped natural frequency, and ζ, the damping ratio, are determined from the autopilot-vehicle-dynamics combination of the Space Shuttle system. If the roll dynamics are critically damped ($\zeta = 1$) and $\phi_c(t)$ is a unit step command, the roll-angle response to $\phi_c(t)$ (the solution to Eq. 4.1-13) is

$$\phi(t) = 1 - e^{-\omega t}(1 + \omega t) \tag{4.1-14}$$

We will take account of the roll dynamics and the limitations of the autopilot-vehicle system by insisting in our trajectory design that the required lateral acceleration vary between that required for straight-line flight and that required for curvilinear flight in the manner described in Eq. 4.1-14. To be conservative and to ensure that the vehicle can follow the trajectory so designed, we will take care to use a value of ω in our trajectory design which is lower than that of the Space Shuttle design.

Consider Fig. 4.1-1 again. An instant before reaching point B, the "aircraft" is flying straight and undergoing a net centrifugal acceleration of v^2/R with respect to the reference centers for the turn, the point X (X_c, Y_c). Upon reaching point B, the "aircraft" is expected to roll instantaneously to a new bank angle; to project a component of its lift vector into the horizontal plane, and by this abrupt maneuver generate enough centrifugal acceleration in the horizontal plane to cancel v^2/R. The idealized profile of total lateral acceleration (computed with respect to X in the rotating frame) is depicted in Fig. 4.1-6. Also depicted in Fig. 4.1.6 is a realizable acceleration profile (based on a critically damped second-order response to a step-change command).

In order to formulate the realizable total acceleration profile in mathematical terms which permit a complete specification of the trajectory, we propose the following model

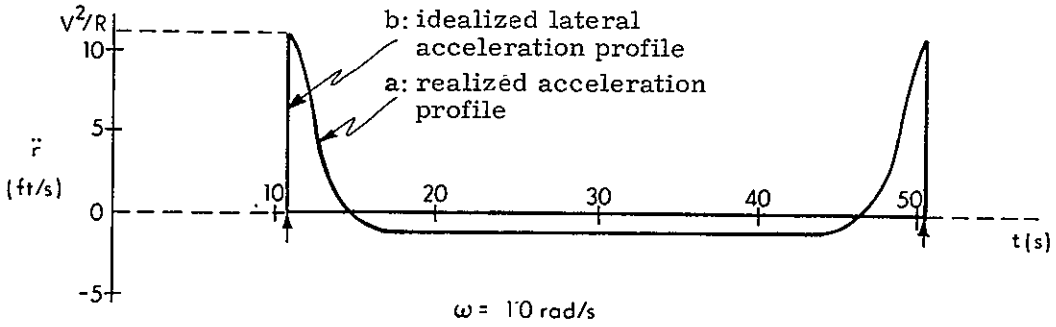

Figure 4.1-6 Idealized and Realizable Lateral Acceleration Profiles

$$\ddot{r}(t) = A\left[e^{-\omega(t-t_1)} + \omega(t - t_1)e^{-\omega(t-t_1)}\right] + B + D\left[e^{-\omega(t_2-t)} + \omega(t_2 - t)e^{-\omega(t_2-t)}\right] \quad (4.1\text{-}15)$$

It is simple to determine the values of A, B, and D which satisfy the following boundary conditions

$$\ddot{r}(t_1) = v_1^2/r_1 \qquad \text{continuity of acceleration at } t_1 \quad (4.1\text{-}16)$$

$$\dot{r}(t_2) = 0 \qquad \text{course constraint} \quad (4.1\text{-}17)$$

$$\ddot{r}(t_2) = v_2^2/r_2 \qquad \text{continuity of acceleration at } t_2 \quad (4.1\text{-}18)$$

where

$$t_1 = t_B \quad (4.1\text{-}19)$$

$$t_2 = t_C \quad (4.1\text{-}20)$$

$$r_1 = r(t_1) \quad (4.1\text{-}21)$$

$$r_2 = r(t_2) \quad (4.1\text{-}22)$$

It is Eq. 4.1-15, with A, B and D appropriately chosen, which is plotted (curve a) in Fig. 4.1-6. However, with only three degrees of freedom (the parameters A, B, and D), Eq. 4.1-15 cannot, in general, satsify

$$r(t_2) = r_D = R \quad (4.1\text{-}23)$$

as well as Eq. 4. 1-16, -17, and -18. Therefore, we add a linear term to Eq. 4. 1-15 with an additional degree of freedom, the multiplier C. The new equation (defining $T = t_2 - t_1$ and $E = e^{-\omega(t_2 - t_1)}$ for convenience) and its first and second integrals are:

$$\ddot{r}(t) = A\left[e^{-\omega(t-t_1)} + \omega(t - t_1)\, e^{-\omega(t-t_1)}\right] + B + C(t - t_1) + D\left[e^{-\omega(t_2-t)} + \omega(t_2 - t)\, e^{-\omega(t_2-t)}\right] \quad (4.1\text{-}24)$$

$$\dot{r}(t) = \dot{r}_1 + A\left\{2\left[1 - e^{-\omega(t-t_1)}\right]/\omega - (t - t_1)e^{-\omega(t-t_1)}\right\} + B(t - t_1) + C(t - t_1)^2/2 + D\left\{2\left[e^{-\omega(t_2-t)} - E\right]/\omega - ET + (t_2 - t)e^{-\omega(t_2-t)}\right\} \quad (4.1\text{-}25)$$

$$r(t) = r_1 + \dot{r}_1(t - t_1) + A\left\{(t - t_1)\left[2 + e^{-\omega(t-t_1)}\right]/\omega - 3\left[1 - e^{-\omega(t-t_1)}\right]/\omega^2\right\} + B(t - t_1)^2/2 + C(t - t_1)^3/6 + D\left\{3\left[e^{-\omega(t_2-t)} - E\right]/\omega^2 - ET/\omega - E(t - t_1)(2/\omega + T) + (t_2 - t)e^{-\omega(t_2-t)}/\omega\right\} \quad (4.1\text{-}26)$$

We can now develop four linear equations of constraint for the four parameters A, B, C, and D.

Combining Eq. 4.1-16 and 4.1-24 yields

$$v_1^2/r_1 = \ddot{r}(t_1) = A + B + D(E + \omega TE) \quad (4.1\text{-}27)$$

Combining Eq. 4.1-17 and Eq. 4.1-25 yields

$$0 = \dot{r}_2 - \dot{r}_1 = A\left[2(1 - E)/\omega - TE\right] + BT + CT^2/2 + D\left[2(1 - E)/\omega - ET\right] \quad (4.1\text{-}28)$$

Combining Eq. 4.1-23 and 4.1-26 yields

$$r_2 - (r_1 + T\dot{r}_1) = A\left[T(2 + E)/\omega - 3(1 - E)/\omega^2\right] + BT^2/2 \; CT^3/6 + D\left[3(1 - E)/\omega^2 - 3ET/\omega - ET^2\right] \quad (4.1\text{-}29)$$

and, finally, combining Eq. 4.1-18 and 4.1-24 yields

$$v_2^2/r_2 = \ddot{r}(t_2) = A(E + \omega TE) + B + CT + D \quad (4.1\text{-}30)$$

The solution to Eq. 4.1-27, -28, -29, and -30 is

$$\begin{bmatrix} A \\ B \\ C \\ D \end{bmatrix} = T^{-1} \begin{bmatrix} \ddot{r}_1 \\ \dot{r}_2 - \dot{r}_1 \\ r_2 - (r_1 + T\dot{r}_1) \\ \ddot{r}_2 \end{bmatrix} \tag{4.1-31}$$

where

$$T = \begin{bmatrix} 1 & 1 & 0 & E + \omega TE \\ 2(1 - E)/\omega - TE & T & T^2/2 & 2(1 - E)/\omega - ET \\ T(2 + E)/\omega \\ -3(1 - E)/\omega^2 & T^2/2 & T^3/6 & 3(1 - E)/\omega^2 \\ & & & -3ET/\omega - ET^2 \\ E + \omega TE & 1 & T & 1 \end{bmatrix} \tag{4.1-32}$$

Trajectory planning proceeds, first, by choosing the radius and center of curvature for making a reference transition turn; second, by computing A, B, C, and D from the reference boundary conditions at $t = t_1$ and t_2; and third, by generating the reference trajectory $\ddot{r}(t)$ and $\dot{r}(t)$ from Eq. 4.1-24 and 4.1-25 for feed-forward commands and r(t) from Eq. 4.1-26 for position feedback commands.

In Chapter 2 of this report, a state estimator is described which obtains estimates in a runway Cartesian coordinate system. In Section 4.2 of this chapter the equations for computing feed-forward and feedback commands for the autopilot are described; they are also based on a runway Cartesian coordinate system. In order to generate the Cartesian coordinates of the reference ground track we must generate the polar coordinates of the ground track, adding a $\theta(t)$ specification to the r(t) specification. The same kind of analysis which we have just applied to r(t) can be applied to $\theta(t)$. The result is

$$\begin{bmatrix} A \\ B \\ C \\ D \end{bmatrix} = T^{-1} \begin{bmatrix} \ddot{\theta}_1 \\ \dot{\theta}_2 - \dot{\theta}_1 \\ \theta_2 - (\theta_1 + \dot{\theta}_1 T) \\ \ddot{\theta}_2 \end{bmatrix} \tag{4.1-33}$$

and $\ddot{\theta}(t)$, $\dot{\theta}(t)$, and $\theta(t)$ are generated from equations with the same form as those in Eq. 4.1-24, -25, and -26 respectively, using, of course, the A, B, C, and D from Eq. 4.1-33.

The equations which convert from polar coordinates to the runway Cartesian coordinates are straight forward. (See Fig. 4.1-7.)

$$x = x_c + r\cos\theta \tag{4.1-34}$$

$$y = y_c + r\sin\theta \tag{4.1-35}$$

$$\dot{x} = \dot{r}\cos\theta - r\dot{\theta}\sin\theta \tag{4.1-36}$$

$$\dot{y} = \dot{r}\sin\theta + r\dot{\theta}\cos\theta \tag{4.1-37}$$

$$\ddot{x} = (\ddot{r} - r\dot{\theta}^2)\cos\theta - (2\dot{r}\dot{\theta} + r\ddot{\theta})\sin\theta \tag{4.1-38}$$

$$\ddot{y} = (\ddot{r} - r\dot{\theta}^2)\sin\theta + (2\dot{r}\dot{\theta} + r\ddot{\theta})\cos\theta \tag{4.1-39}$$

The boundary conditions for Eq. 4.1-25 and Eq. 4.1-26 are chosen as follows.

$$\ddot{r}_1 = v_1^2/r_1 \tag{4.1-40}$$

$$\dot{r}_2 = 0 \tag{4.1-41}$$

$$\ddot{r}_2 = v_2^2/r_1 \tag{4.1-42}$$

$$v_1 = \underline{T}_1 \cdot \underline{w} + \left[(\underline{T}_1 \cdot \underline{w})^2 - w^2 + v_a^2\right]^{1/2} \tag{4.1-43}$$

$$v_2 = \underline{T}_2 \cdot \underline{w} + \left[(\underline{T}_2 \cdot \underline{w})^2 - w^2 - v_a^2\right]^{1/2} \tag{4.1-44}$$

$$\ddot{\theta}_1 = 0 \tag{4.1-45}$$

$$\dot{\theta}_1 = v_1/r_1 \tag{4.1-46}$$

$$\dot{\theta}_2 = v_2/r_2 \tag{4.1-47}$$

$$\ddot{\theta}_2 = 0 \tag{4.1-48}$$

and (r_1, θ_1), (r_2, θ_2) are specified by the ground-track planning program. Equations 4.1-43 and 4.1-44 require some explanation. The vector $\underline{T}_1$ is a unit vector in the direction of the straight-line course approaching the transition turn; it is the direction of segment A-B in Fig. 4.1-1. The vector $\underline{T}_2$ is the analogous vector for segment C-D in Fig. 4.1-1. Since we do not want to constrain ground speed (there is a constraint on ground track but not on the rate of progress along that track), v_1 and v_2, the ground speeds along the tracks $\underline{T}_1$ and $\underline{T}_2$, are computed from the estimated wind velocity, $\underline{w}$, and the desired airspeed, v_a. Equations 4.1-43 and 4.1-44 are derived in Section 4.2.

We have in this section described ground-track trajectory planning and reference-trajectory generation for accurate course following and course acquisition. We have deferred the discussion of wind compensation to the next section, 4.2.

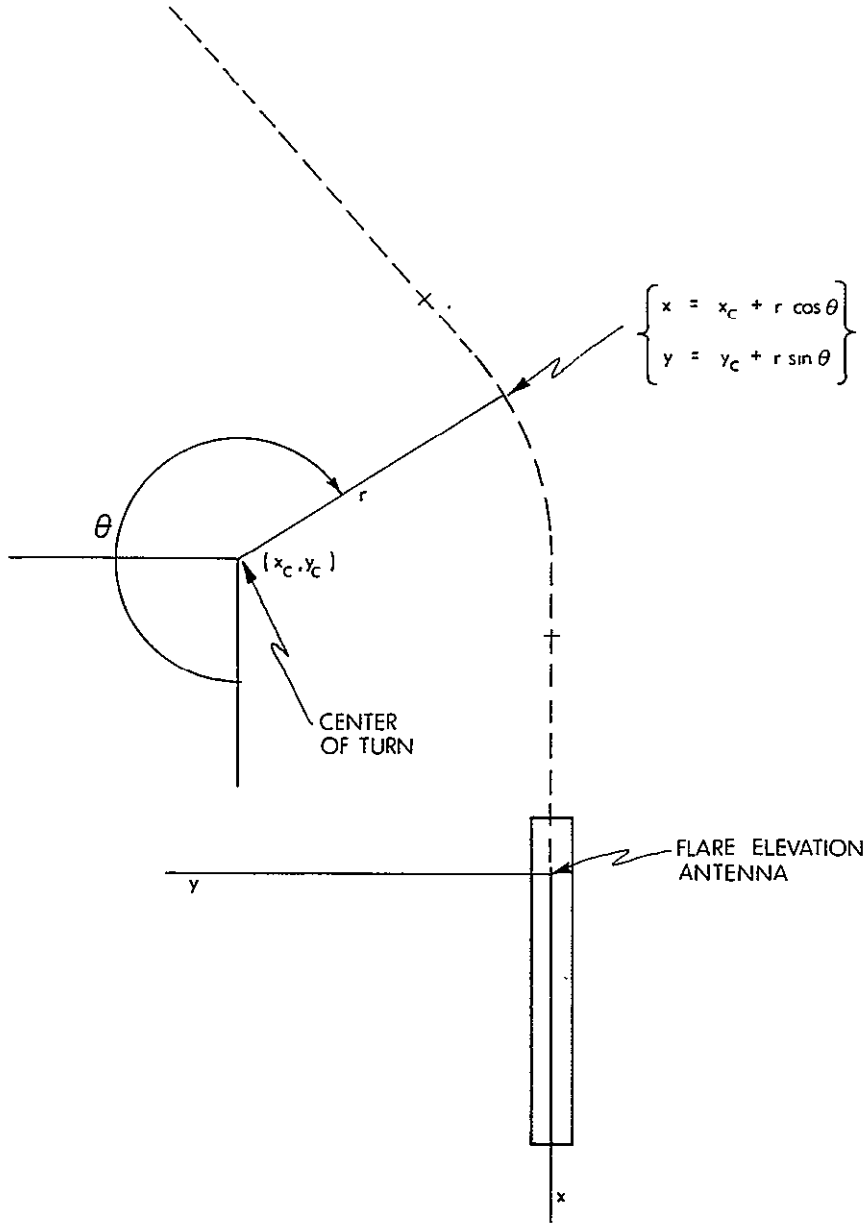

Fig. 4.1-7 Converting Polar Coordinates of the Transition Turn to the Runway Coordinate System

4.2 Guidance along the Approach Trajectory

In this subsection we attempt to define guidance laws that will enable the space shuttle vehicle to follow a specified approach trajectory. In the preceeding subsection, a way of defining approach ground-track trajectories in terms of straight-line segments and curvilinear transitions was presented. Inasmuch as other types of approach trajectories might be ultimately selected as best suited for the orbiter vehicle, we shall seek guidance laws that would be applicable to any type of trajectory, assuming only that the trajectory has been selected so as to not require unreasonable or unrealizable control actions. It will be more convenient in this subsection to consider trajectories specified in terms of arc length as a parameter rather than time. Control in time along the trajectory will not ordinarily be of interest, although it might be advisable during turning maneuvers in order to simplify the guidance problem. We shall consider in particular the powered-flight case, although several of the results would be applicable to the engines-off approach problem.

Both feed-forward or open-loop guidance and feedback are required if the specified approach trajectories are to be followed accurately. Feed-forward guidance is required so that the vehicle will begin maneuvers at the proper time without waiting for position errors to develop. Feedback is required to correct for wind gusts and wind shear, errors in the estimated mean wind and vehicle state, and inaccuracies in modeling the control system and vehicle response to open-loop commands.

4.2.1 Feed-forward Guidance

In developing feed-forward guidance laws one tries to answer the question: Given a desired flyable trajectory, given that the vehicle is initially positioned on the trajectory with the proper velocity, acceleration, roll, pitch, and yaw, and given estimates of the current wind components as one proceeds, what should the control-system signals be in order to enable the vehicle to fly along the trajectory as accurately as possible in the absence of any further information about the vehicle state? If accurate wind estimates are available and if satisfactory feed-forward guidance laws can be developed, then the feedback system should have to correct only for relatively small errors.

One method for developing feed-forward guidance laws is suggested by the fact that, at any given point along the trajectory, the required velocity and acceleration with respect to a ground-fixed coordinate frame for remaining on the trajectory is completely determined by the trajectory direction cosines and curvature and by the

vehicle's speed with respect to the ground. The required heading and pitch angle of the velocity vector as measured with respect to the ground can be easily calculated. Furthermore, if a steady wind is present which translates the vehicle at a constant known velocity, it is easy to calculate the required heading and pitch angle of the velocity vector as measured with respect to the moving air mass. This information together with some assumptions about the vehicle's sideslip angle and angle of attack is sufficient to determine the relevant state parameters. Certain of the state parameters (e.g., roll, roll rate) for this imaginary vehicle could then be fed forward into the actual-vehicle control system as explicitly commanded quantities.

In an actual case, of course, the wind is neither steady nor known, and the procedure must be modified. We assume that the translational velocity of the aircraft due to wind can be modeled as a nonstationary, vector random process with a mean value that varies slowly in time. Furthermore, we assume that the navigation filter will be able to provide reasonably accurate estimates of the components of the mean translational velocity due to wind. Open-loop control system signals can then be derived by solving for the state of an imaginary vehicle which moves along the given trajectory in a constant wind equivalent to the estimated mean wind at that time.

We shall refer to this hypothetical vehicle which moves along the given trajectory exactly as the reference vehicle. In addition to providing a reference for calculating feed-forward guidance commands, it will serve as a reference for the feedback system as we shall see in subsection 4.2.2 below.

Let us suppose that we would like to utilize wind estimates to obtain feed-forward control-system commands which will enable the vehicle to fly with given airspeed v_a along a given trajectory as accurately as possible. In order to implement the above strategy, we must first obtain equations for the velocity, acceleration, and attitude of a reference vehicle at some arbitrary point along the trajectory in a constant wind field.

The velocity and acceleration of the reference vehicle can be expressed as functions of the vehicle velocity due to wind $\underline{w}$, the airspeed v_a, and quantities describing the curve at the arbitrary point. Let us suppose that the curve is given in terms of the arc-length parameter s as measured from some origin. Any point along the curve may then be specified by the vector $\underline{r}(s)$:

$$\underline{r}(s) = x(s)\underline{i} + y(s)\underline{j} + z(s)\underline{k} \tag{4.2-1}$$

where $\underline{i}$, $\underline{j}$, and $\underline{k}$ are unit vectors in the ground-fixed x, y, and z directions, respectively. The velocity and acceleration are found by differentiating:

$$\underline{v} = \dot{s}\left[\frac{dx}{ds}\underline{i} + \frac{dy}{ds}\underline{j} + \frac{dz}{ds}\underline{k}\right] \tag{4.2-2}$$

$$\underline{a} = \ddot{s}\left[\frac{dx}{ds}\underline{i} + \frac{dy}{ds}\underline{j} + \frac{dz}{ds}\underline{k}\right] + \dot{s}^2\left[\frac{d^2x}{ds^2}\underline{i} + \frac{d^2y}{ds^2}\underline{j} + \frac{d^2z}{ds^2}\underline{k}\right] \tag{4.2-3}$$

One can express these equations in a somewhat more compact form by making use of some notation commonly used in differential geometry.[2] The partial derivatives dx/ds, dy/ds, and dz/ds will be recognized as the direction cosines of the curve, and the bracketed factor in Eq. 4.2-2 is a unit vector $\underline{T}$, tangent to the curve. In Eq. 4.2-3, the bracketed quantity in the second term can be shown to be directed along a unit vector $\underline{N}$, the principal normal to the curve, and to have magnitude equal to the curvature κ. Making these substitutions and noting that $\dot{s} = v$, we obtain

$$\underline{v} = v\underline{T} \tag{4.2-4}$$

$$\underline{a} = \dot{v}\,\underline{T} + v^2\kappa\underline{N} \tag{4.2-5}$$

It remains to find an expression for v and $\dot{v}$ in terms of the vehicle velocity due to wind $\underline{w}$, the airspeed v_a, and its rate of change $\dot{v}_a$. This can be accomplished by noting that the total velocity of the vehicle is the sum of the velocity due to the wind $\underline{w}$ and the velocity vector relative to the moving air mass $\underline{v}_a$. Thus

$$\underline{v} - \underline{w} = \underline{v}_a \tag{4.2-6}$$

which can be squared to obtain

$$v^2 - 2\underline{T}\cdot\underline{w}\,v + w^2 = v_a^2 \tag{4.2-7}$$

The solution is

$$v = \underline{T}\cdot\underline{w} + \left[(\underline{T}\cdot\underline{w})^2 - w^2 + v_a^2\right]^{1/2} \tag{4.2-8}$$

where the plus sign is chosen for the radical so that v approaches $+v_a$ when the wind vanishes. This equation simply states that the total velocity along the trajectory is the sum of the projection of $\underline{w}$ along the trajectory and the projection of $\underline{v}_a$ along the trajectory. An equation for $\dot{v}$ can be obtained by differentiating (note that $\dot{\underline{T}} = \kappa v\underline{N}$):

$$\dot{v} = \kappa v\underline{N}\cdot\underline{w} + \frac{\kappa v(\underline{N}\cdot\underline{w})(\underline{T}\cdot\underline{w}) + v_a\dot{v}_a}{\left[(\underline{T}\cdot\underline{w})^2 - w^2 + v_a^2\right]^{1/2}} \tag{4.2-9}$$

The velocity and acceleration of the reference vehicle moving along the trajectory at any specified airspeed in a constant wind field can now be found by substituting Eq. 4.2-8 and 4.2-9 into Eq. 4.2-4 and 4.2-5.

Alternatively, the airspeed v_a and its rate of change $\dot{v}_a$ can be written as a function of the velocity measured with respect to the ground. In some situations it is more convenient to specify a ground-track velocity and vary the airspeed accordingly. For reference, let us include these expressions.

$$v_a = \left[v^2 - 2v\underline{T}\cdot\underline{w} + w^2 \right]^{1/2} \tag{4.2-10}$$

$$\dot{v}_a = \frac{v\dot{v} - \dot{v}\underline{T}\cdot\underline{w} - \kappa v^2 \underline{N}\cdot\underline{w}}{\left[v^2 - 2v\underline{T}\cdot\underline{w} + w^2 \right]^{1/2}} \tag{4.2-11}$$

Next we seek expressions for the attitude of the reference vehicle, given the trajectory and some assumptions about the sideslip angle and the angle of attack. We assume that vehicle turns are coordinated such that the sideslip angle is always zero. Let us assume for the time being that the angle of attack is also zero. We can then determine not only the pitch and yaw angles of the vehicle, but also the roll angle.

The pitch angle θ and yaw angle ψ for this case are shown in Fig. 4.2-1. Since sideslip angle and angle of attack are zero, the vehicle is aligned along the airspeed vector $\underline{v}_a$. One has

$$\tan \psi = \frac{v_y - w_y}{v_x - w_x} \tag{4.2-12}$$

$$\sin \theta = - \frac{v_z - w_z}{v_a} \tag{4.2-13}$$

where v_i and w_i indicate the i^{th} component of the vectors $\underline{v}$ and $\underline{w}$.

These equations express the well-known fact that, in order to follow a given path in space, vehicle heading and pitch must be adjusted to compensate for the wind.

An expression for the roll angle ϕ can be obtained as a result of the requirement that turns be coordinated. The lateral equation of motion in body coordinates is in general

$$\dot{V} + rU - pW - g \sin\phi \cos\theta = \sum Y/m \tag{4.2-14}$$

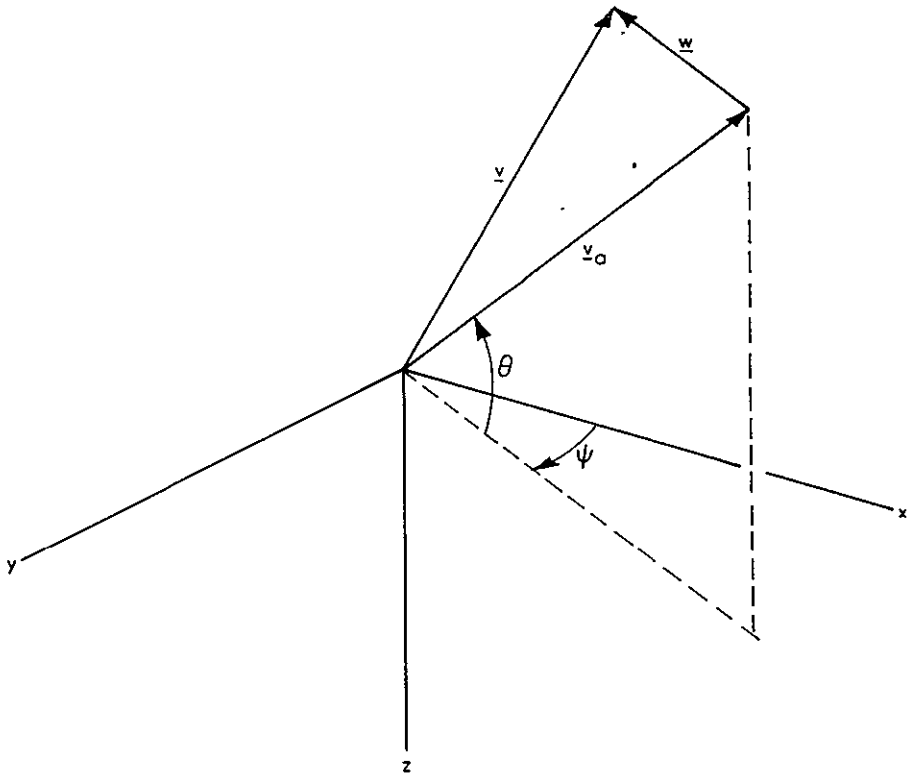

Fig. 4.2-1 Geometry for Zero Angle of Attack

'here U, V, and W are the components of the airspeed in the x, y and z body axes, espectively, p is the x-component of the angular-velocity vector, r is the z-component f the angular velocity vector, Y represents assorted forces acting on the vehicle ı the y-direction (except gravity which has been explicitly included) and m is the ıass. As a result of the above assumptions concerning sideslip angle and angle of ttack, $\dot{V}$ and W are zero. Since the wind field is constant and since there are no erodynamic or thrust forces acting laterally, the right-hand side of Eq. 4.2-14 ıust vanish. As a result one has

$$rv_a - g \sin\phi \cos\theta = 0 \tag{4.2-15}$$

3ut it is also true that

$$r = -\dot{\theta} \sin\phi + \dot{\psi} \cos\phi \cos\theta \tag{4.2-16}$$

:liminating r, one finds

$$\tan\phi = \frac{v_a \dot{\psi} \cos\theta}{g \cos\theta + v_a \dot{\theta}} \tag{4.2-17}$$

'or horizontal flight this reduces to the familiar coordinated-turn expression

$$\tan\phi = \frac{v_a \dot{\psi}}{g} \tag{4.2-18}$$

:he required roll angle can thus be calculated from θ, $\dot{\psi}$, and $\dot{\theta}$. The latter two [uantities can be obtained by differentiating Eq. 4.2-12 and 4.2-13:

$$\dot{\psi} = \frac{(v_x - w_x)a_y - (v_y - w_y)a_x}{(v_x - w_x)^2 + (v_y - w_y)^2} \tag{4.2-19}$$

$$\dot{\theta} = \frac{(v_z - w_z)\dot{v}_a - v_a a_z}{v_a\left[(v_x - w_x)^2 + (v_y - w_y)^2\right]^{1/2}} \tag{4.2-20}$$

The attitude of a vehicle moving along the trajectory at constant airspeed in constant-wind field with zero sideslip angle and zero angle of attack is thus given)y Eq. 4.2-12, 4.2-13 and 4.2-17, with the use of Eq. 4.2-19 and 4.2-20.

Feed-forward control-system commands can now be obtained in real time by ıdvancing the reference vehicle along the desired trajectory with a velocity given)y Eq. 4.2-8, and then calculating the reference-vehicle state using the above

equations. Whenever components of wind are required in the equations, the estimated wind components are used. Certain of the reference-vehicle state parameters (for example, roll angle, vertical velocity) are then fed into the actual-vehicle control system as explicitly commanded quantities. The actual quantities fed forward will depend on the control-system configuration.

The problem with the above procedure is that no account has been taken of the actual-vehicle response characteristics. A commanded quantity is not obtained instantaneously as required for accurate trajectory following. Considerable position errors can develop even when the trajectory has been carefully designed to be flyable.

This difficulty can be resolved if the vehicle response characteristics are known and can be modeled. The combined autopilot-aircraft response to a commanded roll angle ϕ_c, for example, is often assumed to be given by the second-order transfer function

$$\frac{\phi}{\phi_c} = \frac{\omega_\phi^2}{s^2 + 2\omega_\phi \zeta_\phi s + \omega_\phi^2} \tag{4.2-21}$$

or the equivalent differential equation

$$\ddot{\phi} + 2\omega_\phi \zeta_\phi \dot{\phi} + \omega_\phi^2(\phi - \phi_c) = 0 \tag{4.2-22}$$

If the desired response is $\phi(t)$ as calculated from Eq. 4.2-17, then the command to control system which compensates for the vehicle lag is just

$$\phi_c = \phi + \frac{2\zeta_\phi}{\omega_\phi}\dot{\phi} + \frac{1}{\omega_\phi^2}\ddot{\phi} \tag{4.2-23}$$

The required derivations $\dot{\phi}(t)$ and $\ddot{\phi}(t)$ can be obtained by numerically differentiating the desired roll-angle profile $\phi(t)$.

Let us give some examples to illustrate the use of these equations.

Some plots of roll angle calculated from Eq. 4.2-17 for level flight at constant airspeed on a constant-radius turn with various wind speeds are shown in Fig. 4.2-2. These plots give an indication of the increment in roll angle required to compensate for the wind. Trajectories must be planned so that the roll angle will not exceed design limits, even under extreme wind conditions, as mentioned in subsection 4.1 above.

Some plots of roll angle for the same turn calculated for flight along a curvilinear transition of the type discussed in the previous subsection (with ω = 1 rad/sec) are

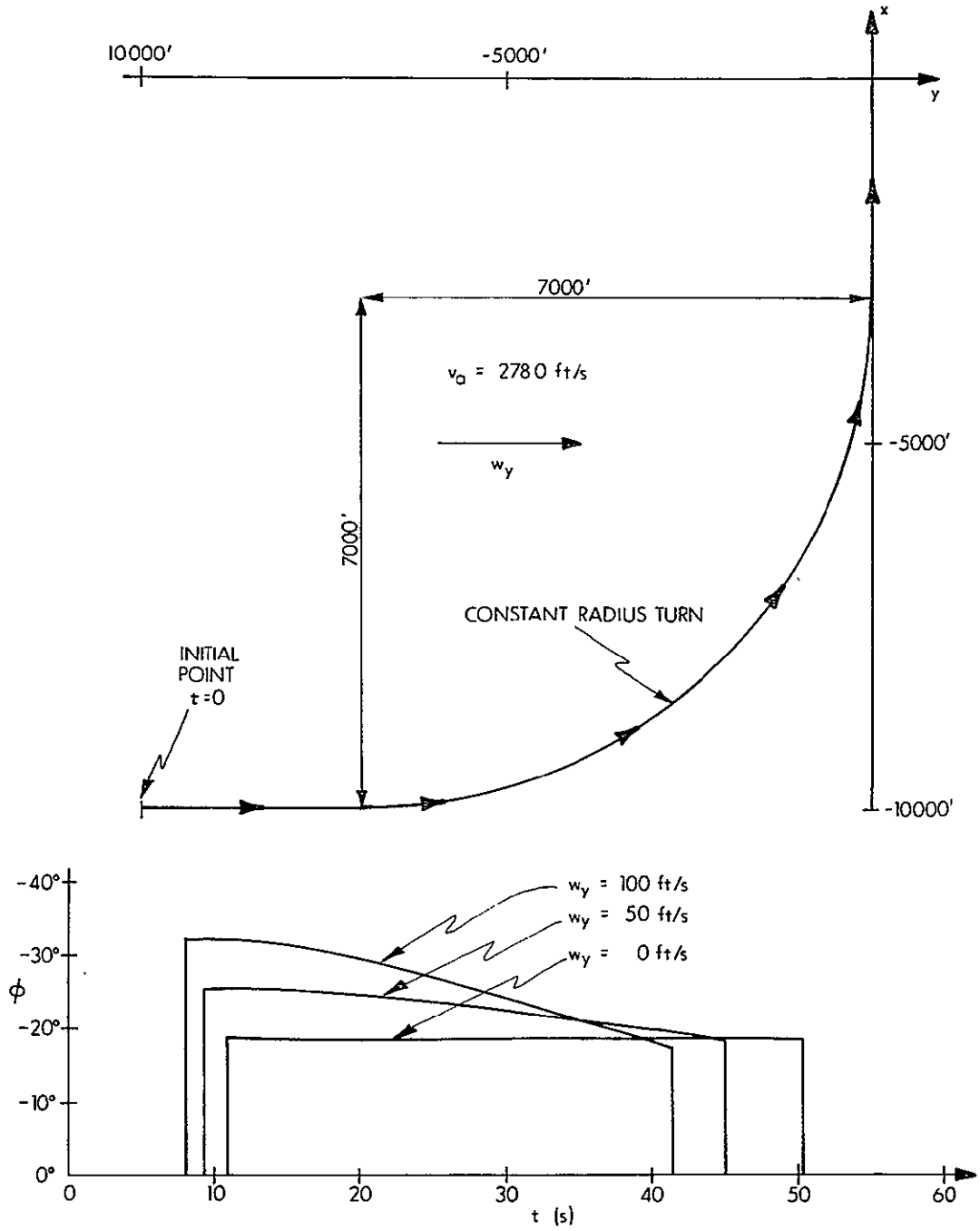

Fig. 4.2-2 Above, Plan View of Constant Radius Turn. Below, Explicit Bank Angle Required as a Function of Wind Velocity

shown in Fig. 4.2-3c. The difference in radial distance between these trajectories and the constant radius trajectory is shown in Fig. 4.2-3a. The airspeed is constant before and after the turn, but is allowed to vary during the turn as shown in Fig. 4.2-3b. The boundary conditions are met and the required roll angle varies smoothly through the turn as desired.

The ability of equations like Eq. 4.3-23 to compensate for actual-vehicle response characteristics was investigated by simulating on the computer (an XDS 9300) the flight of a model vehicle through a right-angle turn. The model vehicle has second-order roll-command characteristics as given by Eq. 4.2-21 and 4.2-22 with $\zeta_\phi = 1.2$ and $\omega_\phi = 1.8$ rad/s, and first-order airspeed-command characteristics with a time constant of 1.0 s. A first-order equation corresponding to Eq. 4.2-23 was used to calculate the commanded airspeed. Limits were imposed on the ability of the model vehicle to follow roll-angle commands as follows

$$|\phi| \text{ model} \leq 40 \text{ deg}$$
$$|\dot{\phi}| \text{ model} \leq 10 \text{ deg/s}$$
$$|\ddot{\phi}| \text{ model} \leq 10 \text{ deg/s}^2$$

Three types of trajectories were then used to make the right-angle turn:

1. A constant-radius trajectory with a 7000-ft radius of curvature and 278-ft/s airspeed as shown in Fig. 4.2-2.
2. A curvilinear transition trajectory such as that illustrated in Fig. 4.2-3 with $\omega = 1$ rad/s.
3. A similar curvilinear transition trajectory with $\omega = 0.5$ rad/s.

Three different constant wind conditions were investigated (w_y = 0, 50, and 100 ft/s, respectively). Position error was defined to be the difference between the reference-vehicle and model-vehicle positions. Trajectory-following accuracy was evaluated by calculating both the rms three-dimensional position error e_{rms} through the turn, and the lateral position error e_y at the completion of the turn.

The results are shown in Table 4.2-I. Large errors develop when the constant-radius trajectory is flown because of the limits imposed on vehicle response. The transition-type trajectory with $\omega = 1$ rad/s works well in the absence of wind, but otherwise requires maneuvers in excess of vehicle limits; and objectionable errors develop. By increasing the time constant on this type of trajectory ($\omega = 0.5$ rad/s), a situation is reached in which the trajectory-following ability of the guidance laws is quite satisfactory. The results presented in this table indicate that guidance

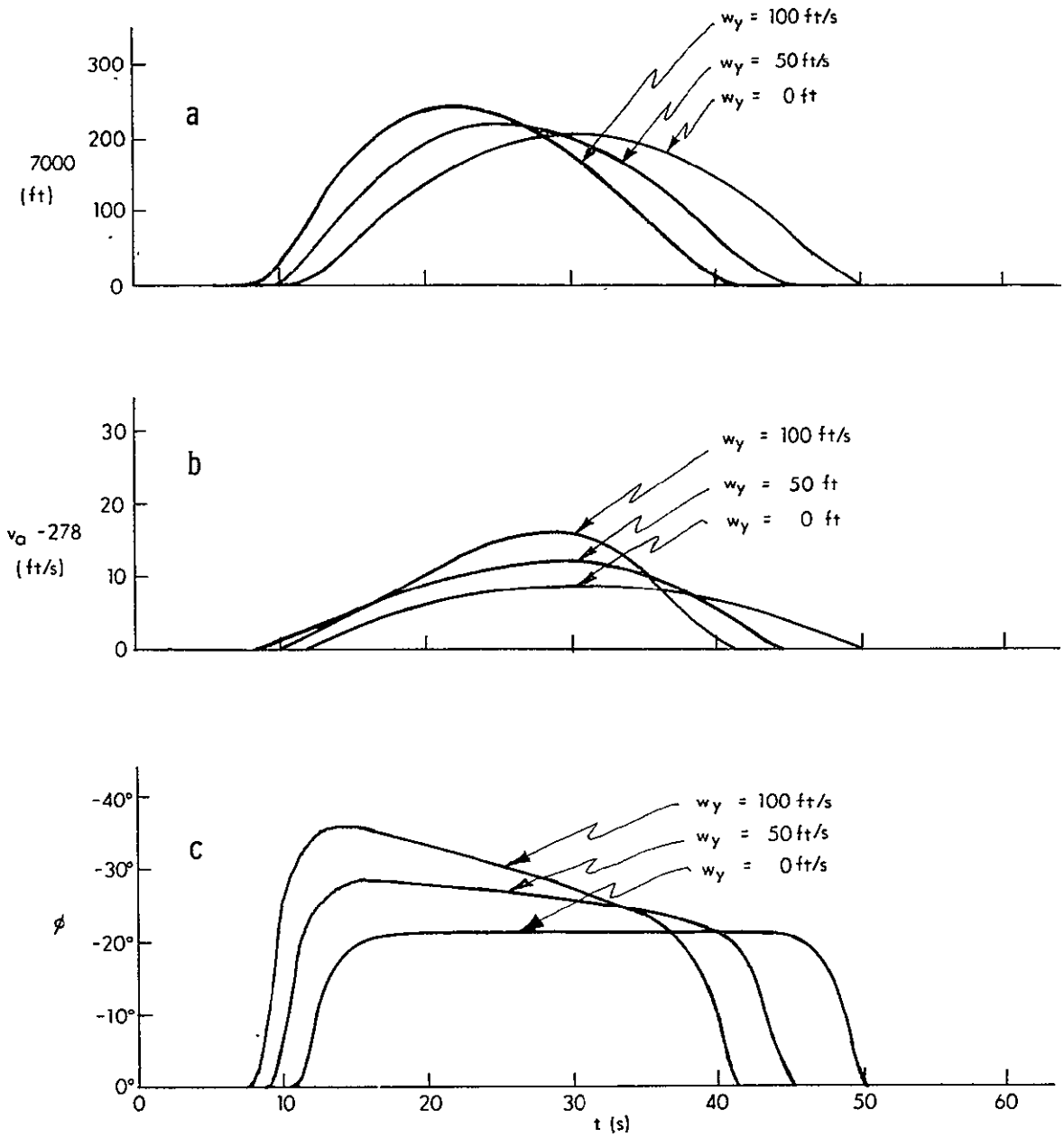

Fig. 4.2-3 Flight Path Radius, Airspeed, and Bank Angle for Flight Along a Curvilinear Transition Trajectory

Table 4.2-I

Position Errors as a Function of Wind and Type of Trajectory; 90^{o} Turn

Type of Trajectory	Wind (ft/s)	e_{rms} (ft)	Terminal e_y (ft)
Constant Radius	0.	359.7	-488.3
	50.	520.2	-697.5
	100.	717.3	-980.0
Transition Type ω = 1 rad/s	0.	3.2	0.6
	50.	78.7	-107.6
	100.	242.1	-334.5
Transition Type ω = 0.5 rad/s	0.	3.4	8.5
	50.	6.2	6.1
	100.	6.9	16.3

laws of the type presented in this section are able to ensure accurate trajectory following as long as the trajectory does not require maneuvers beyond vehicle limits, and as long as the winds and vehicle response characteristics are known.

Some modifications to the above equations should be made when the angle of attack is nonzero. The situation is shown in Fig. 4.2-4 with a negative roll angle. When the angle of attack α is small, the modified heading and pitch angle can be written:

$$\psi^* = \psi + \alpha \sin \phi \tag{4.2-24}$$

$$\theta^* = \theta + \alpha \cos \varphi \tag{4.2-25}$$

Modifications to the roll-angle calculation can also be made, but Eq. 4.2-17 is probably accurate enough for our purpose.

Reference-vehicle state parameters other than those calculated above can be obtained in like fashion if required by the control system. For example, in negotiating a turn at constant airspeed, the angle of attack must be increased to increase the lift and prevent the vehicle from losing altitude. The thrust must be increased to balance the drag caused by the increased angle of attack. If the lift and drag coefficients are known explicitly as functions of the angle of attack, then the required increase in angle of attack and thrust can be calculated and fed forward into the vehicle control system.

Two advantageous features of the type of feed-forward guidance discussed in this section should be pointed out. First, the equations are applicable to any type of trajectory providing only that the derivatives of the trajectory as required in Eq. 4.2-2 and 4.2-3 exist and can be calculated. Mode switching is not required in the guidance laws, although it may occur in the course of defining the trajectory. Second, the compensation for the wind takes place in a uniform fashion throughout the course of the trajectory. For example, the same procedure is used during curved portions of the trajectory as on straight portions.

4.2.2 Feedback

The purpose of feedback in the guidance equations is to correct for position errors that develop due to inaccuracies in the feed-forward guidance commands, wind gusts, navigation errors, and so forth. Position errors with respect to the reference vehicle must be kept small if the feed-forward guidance is to function properly.

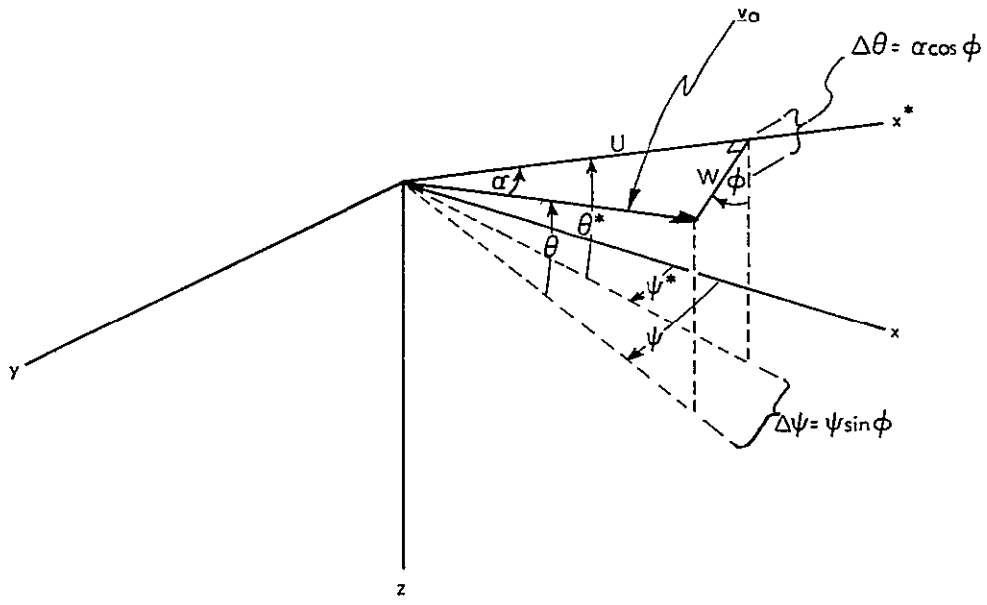

Fig. 4.2-4 Geometry for Non-Zero Angle of Attack α

Closed-loop control-system signals are obtained by adding to the open-loop signals terms proportional to the difference between reference-vehicle position and estimated actual-vehicle position, resolved in a suitable set of coordinate axes. One logical choice for the axes would be the actual-vehicle coordinate system, since the maneuvers required to correct the errors are separable in a convenient fashion. Errors in y-position are corrected by adding a feedback term to the commanded roll angle. Errors in z-position are corrected by adding a feedback term to the commanded pitch angle, or vertical velocity. Errors in x-position are best corrected by adding a feedback term to the reference-vehicle airspeed, inasmuch as it is likely that only lateral tracking accuracy with respect to the desired trajectory will be required for the orbiter vehicle. This avoids the need for any throttle variations in the actual vehicle due to longitudinal position errors.

The use of lateral position-error signals in the actual-vehicle control system will be discussed further in Chapter 5.

4.3 Flare Guidance Laws

A variety of flare-guidance laws have been proposed and a fair percentage of these have been flight-tested. One commonly used flare law programs descent rate as an exponential function of altitude (the descent rate decays exponentially to zero at an altitude reference plane below the runway plane). The Air Force has flight-tested a law which commands a small (about 1 degree) flight-path angle at the flare-initiation altitude. Reference 3 gives a law presently being simulated at NASA/MSC. This section gives a guidance law derived at MIT/DL which allows an arbitrary amount of shaping of a flare reference trajectory which satisfies the boundary conditions of matching the vehicle's state at the flare-initiation altitude and matching the desired terminal boundary conditions. Furthermore, this law limits the value of the terminal total acceleration which results in constraining the terminal attitude and crab angle of the aircraft. Because it is desirable to have the aircraft touch down before passing the flare-antenna location, the intersection of the flare path with the runway should be constrained thus

$$\underline{r}_2 = 500\,\underline{i} + 0\,\underline{j} + 0\,\underline{k} \qquad \text{(ft)} \qquad (4.3\text{-}1)$$

$$\underline{v}_2 = 160\,\underline{i} + 0\,\underline{j} + 2\,\underline{k} \qquad \text{(ft/s)} \qquad (4.3\text{-}2)$$

might represent a reasonable touchdown boundary condition (located 500 feet before the flare antenna).

These equations are derived very much in the spirit of Reference 4. However, they are used to generate a reference trajectory for position feedback and the derivatives of the reference trajectory for position feed-forward signals. Unlike the application of Reference 4 to Apollo, the reference trajectory will not be periodically re-computed.

The boundary-value statement of the flare problem is

Given: $\underline{r}(t_1)$, $\underline{v}(t_1)$, $T = t_2 - t_1$

Find $\ddot{\underline{r}}(t)$ such that

$$\underline{r}(t_2) = \underline{r}_d \text{ (for example, Eq. 4.3.1)}$$

$$\underline{v}(t_2) = \underline{v}_d \text{ (for example, Eq. 4.3.2)}$$

$$\ddot{\underline{r}}(t_2) = \ddot{\underline{r}}_d$$

A solution to this problem is

$$\ddot{\underline{r}}(t) = \underline{a} + \underline{b}(t_2 - t) + \sum_{n=1}^{k} \underline{c}_n f_n(t) \tag{4.3-3}$$

where

$$\underline{a} = 4(\underline{v}_2 - \underline{v}_1)/T - 6(\underline{r}_2 - \underline{r}_1 - T\underline{v}_1)/T^2 \tag{4.3-4}$$

$$\underline{b} = 6(\underline{v}_2 - \underline{v}_1)/T^2 + 12(\underline{r}_2 - \underline{r}_1 - T\underline{v}_1)/T^3 \tag{4.3-5}$$

$$f_n(t) = (t_2 - t)^{n-1} - 2(n+2)(t_2 - t)^n/nT + (n+2)(n+3)(t_2 - t)^{n+1}/n(n+1)T^2 \tag{4.3-6}$$

The $f_n(t)$ are interesting because

$$\int_{t_1}^{t_2} f_n(t)\, dt = 0 \tag{4.3-7}$$

$$\int_{t_1}^{t_2} \left[\int_{t_1}^{t} f_n(s)\, ds \right] dt = 0 \tag{4.3-8}$$

and, therefore, the $\underline{c}_i$ in Eq. 4.3-3 are arbitrary (they have no effect on the achievement of the terminal boundary conditions) and may be used to shape and optimize the flare trajectory. The reference trajectory generated by Eq. 4.3-3, -4, and -5 is

$$\underline{r}(t) = \underline{r}_1 + (t - t_1)\underline{v}_1 + \underline{a}(t - t_1)^2/2 + \underline{b}\left[T^2(t - t_1)/2 - T^3/6 + (t_2 - t)^3/6\right] + \sum_{n=1}^{k} \underline{c}_n\left[(t_2 - t)^{n+1}/n(n+1) - 2(t_2 - t)^{n+2}/n(n+1)T + (t_2 - t)^{n+3}/n(n+1)T^2\right] \quad (4.3\text{-}9)$$

$$\underline{v}(t) = \underline{v}_1 + \underline{a}(t - t_1) + \underline{b}\left[T^2/2 - (t_2 - t)^2/2\right] + \sum_{n=1}^{k} \underline{c}_n\left[-(t_2 - t)^n/n + 2(n+2)(t_2 - t)^{n+1}/n(n+1)T - (n+3)(t_2 - t)^{n+2}/n(n+1)T^2\right] \quad (4.3\text{-}10)$$

Since all the $f_i(t)$ except $f_1(t)$ are zero for $t = t_2$, we have

$$\ddot{\underline{r}}(t_2) = \underline{a} + \underline{c}_1$$

Hence, if

$$\underline{c}_1 = \ddot{\underline{r}}(t_2) - \underline{a}$$

we can specify the terminal acceleration

$$\ddot{\underline{r}}(t_2) = \ddot{\underline{r}}_d$$

As a practical matter, the higher-order $f_i(t)$ will not be used. It is interesting to note, however, that <u>any</u> trajectory that satisfies the boundary conditions can be developed by the expressions given here; in other words, the $f_i(t)$, if a sufficient number of them are used, can span function space.

In resolving the errors in following the reference trajectory, the error along the path can be ignored and time-of-touchdown not constrained.

Chapter 4 References

1. Bryson, A.E., Lele, M.M., "Minimum Fuel Lateral Turns at Constant Altitude", Technical Note, AIAA Journal, Vol. 7, March, 1969.
2. Struik, D.J., "Lectures on Classical Differential Geometry", 2nd Ed., Reading, Mass., Addison-Wesley Pub. Co., 1961.
3. Suddath, J.H., "Guidance Equations for Automatic Shuttle Landings", Informal NASA/MSC memorandum dated 9 February, 1970.
4. Cherry, G.W., "E Guidance—A General, Explicit, Optimizing Guidance Law for Rocket-Propelled Spacecraft", R-456, August, 1964, MIT Instrumentation Laboratory, Cambridge, Mass.

CHAPTER 5

APPLICATIONS OF OPTIMIZATION THEORY TO SPACE SHUTTLE TRAJECTORY CONTROL IN THE SUBSONIC REGIME

by

Duncan MacKinnon

and

Paul Madden

5.1 Introduction

During the subsonic phase of the return to earth, the Space Shuttle will be guided with respect to a trajectory which returns it to the terminal area and, ultimately, to the runway. Guidance relative to the reference trajectory presents the system analyst with problems quite distinct from trajectory synthesis. A control system is required which operates on the position, velocity, and acceleration errors between the simplified vehicle model and the actual shuttle, producing effector commands which tend to minimize the error magnitudes. Such a control system is generally a linear transformation, which may include dynamics. This chapter discusses energy and accuracy considerations associated with the design of the feedback path control system and computer-oriented synthesis procedures based on parameter optimization theory.

The design procedures are illustrated by application to the vertical and lateral position control system of a transport aircraft, the Convair 880 described in Appendixes B and C.

5.1.1 Trajectory Control System Requirements for Subsonic Flight

The requirements for trajectory control in the subsonic flight regime are outlined in Table 5.1-I. At Mach numbers between 1.0 and 0.3, the vehicle is guided relative to a trajectory which satisfies minimal fuel and maximum range considerations discussed in Section 3.1. At lower velocities the shuttle is assumed to be in the approach-and-landing configuration.

Sensitivity analyses provide the basis for path control system accuracy requirements for both flight velocity regimes. Accuracy requirements between Mach 1.0 and 0.3 will undoubtedly be less stringent than the trajectory precision necessary during final approach and automatic landing.

Table 5.1-I
Control System Requirements for Subsonic Flight Regimes

Velocity (Mach No.)	Desirable Qualities
1.0-0.3	Moderate precision guidance relative to range optimal trajectories Minimization of control energy a prime consideration
0.3-0.0 (approach and landing)	High precision guidance All-weather approach and landing capability Control energy minimization a secondary consideration

What is the price of accurate guidance? Accurate guidance demands higher feedback gains. As a result, effector response to disturbing atmospheric phenomena and sensor noise is increased. This results in increased expenditures of fuel, an expensive shuttle commodity. It seems reasonable, therefore, to perform a study that will lead to the minimization of effector control energy while still satisfying path accuracy requirements in a worst-case environment. The study should result in the description of the required vehicle effectors and the control laws associating the effector commands with the trajectory errors.

5.2 Stochastic Control System Design Using Parameter Optimization

An outstanding problem associated with the design of aerodynamic vehicle control systems is the large number of parameters which commonly define the control law. This complexity is a result of the number of available feedback variables and a variety of effectors. Such multiplicity results in an extremely tedious design process if conventional cut-and-try procedures are applied. To circumvent this difficulty, systematic parameter optimization techniques are utilized. The solutions generated by parameter optimization are optimal with respect to the selected performance index. By suitably scanning the performance index basic performance limitations associated with the selected control law structure, effector size and type, and control energy limits may be identified. Such information is extremely valuable at this stage of the space shuttle program since it can lead to vehicle modifications which will improve overall performance.

The following sections will introduce methods for determining the behavior of a physical system subject to stochastic disturbances, formulate a parameter optimization problem, and investigate the necessary conditions for the existence of an optimal solution.

Unlike the linear optimal control approach,[1, 2, 3] the parameter optimization techniques will not require the measurement or estimation of all the elements of the state vector of the vehicle and its control system, nor precise knowledge of the time history of environmental disturbances.

5.2.1 Response of a Linear System to Stochastic Inputs

In order to facilitate this analysis, the characteristics of the response of a linear system to stochastic inputs must be delineated mathematically. Consider the system of linear differential equations

$$\dot{x} = Fx + Gu \tag{5.2-1}$$

where x is a vector describing the state of the system, and u is a vector of Gaussian white noise inputs; u is assumed to be uncorrelated with the state x. The matrix F describes the structure of the system, while the matrix G indicates the manner in which the distrubances act on the system.

The covariance matrix X of x is defined by the relationship

$$X = E(xx') \tag{5.2-2}$$

where E is the mathematical expectation operator. It is apparent that X is a symmetric matrix, a property which may be used advantageously in computations.

The value of X satisfies the matrix differential equation

$$\dot{X} = FX + XF' + GQG' \tag{5.2-3}$$

subject to the boundary condition

$$X(0) = X_0 \tag{5.2-4}$$

where X_0 is the value of X at t = 0.

Of prime interest in control system investigations are time-invariant or stationary systems.* A linear system of the form (Eq. 5.2-1) is time-invariant if the matrices F and G are constant. If the system is time-invariant and asymptotically stable, and if the correlation matrix Q is also constant, the matrix X will approach a constant as $t \to \infty$. This implies that the derivative $\dot{X}$ of X vanishes as $t \to \infty$ or that the final value of X satisfies the set of linear algebraic equations.(4)

$$FX + XF' + GQG' = 0 \tag{5.2-5}$$

The process is then said to be statistically stationary in the limit $t \to \infty$.

The solution of 5.2-5 is conveniently obtained by transformation to a set of ordinary linear algebraic equations which are then solved using any one of a multitude of standard techniques.

Since the diagonal terms of X represent the mean-square values of the state elements responding to the stochastic disturbance, X provides the basis for formulating an optimization problem which leads to the minimization of system response to stochastic inputs subject to penalties on the expended control energy.

5.2.2 Problem Formulation for Stochastic Response Minimization

Let the performance index, J, be defined as a linear combination of the diagonal elements of the covariance matrix, X. Such a performance index may be expressed in the form

$$J = \sum_{i=1}^{n} \alpha_i x_{ii} \tag{5.2-6}$$

where

$$\alpha_i > 0 \qquad i = 1,n \tag{5.2-7}$$

The elements of α are selected to reflect the control goal. For example, the association of nonzero values of α_i with the trajectory error and the effector output results in a solution which minimizes the mean-square value of the trajectory error subject to a penalty on effector activity.

---

*Such an assumption is valid over a small range of vehicle velocities. Each speed regime must be investigated separately and control system parameter values suitably scheduled.

For analytical purposes 5.2-6 is conveniently expressed in the equivalent form

$$J = \text{trace } CX \tag{5.2-8}$$

where

$$\text{trace } CX = \sum_{i=1}^{n} (CX)_{ii} \tag{5.2-9}$$

and

$$c_{ij} = \begin{cases} 0 & i \neq j \\ \alpha_i & i = j \end{cases} \tag{5.2-10}$$

If it is assumed that the system of Eq. 5.2-1 are stationary so that X is the solution of 5.2-5, the optimization problem may be described

Definition of the Problem:

Find a set of parameters, p, which minimizes the performance index

$$J = \text{trace } CX \tag{5.2-11}$$

subject to the constraint

$$FX + XF' + GQG' = 0 \tag{5.2-12}$$

where

- p is vector of adjustable parameters
- F is a matrix which is a function of the parameter vector, p
- X is the covariance matrix of the system state vector x
- Q is the covariance matrix of the white noise process, u
- G is a matrix specifying the coupling between the system and the stochastic disturbance vector, u.

5.2.3 The First Necessary Condition for the Existence of a Weak Relative Minimum

In the calculus of functions of a single variable, the necessary condition for a weak relative minimum is the vanishing of the first derivative of the function with respect to the variable. In the case of functionals such as

$$J = \text{trace } CX \tag{5.2-13}$$

the general concept of a derivative can be extended using the Calculus of Variations.

A parameter value p_{opt} is said to produce a weak relative minimum if the change in J for small perturbations, δp, in p_{opt} satisfies the following inequality:

$$J(p_{opt} + \delta p) \geq J(p_{opt}) \tag{5.2-14}$$

The necessary condition for the existence of a weak relative minimum in J may be deduced by expanding the perturbation δJ due to δp in a Taylor's series.

$$\delta J = \delta p' J_p + \text{higher-order terms in } \delta p \tag{5.2-15}$$

The notation J_p signifies the gradient of J with respect to the ℓ elements of p.

$$J_p = \begin{bmatrix} \frac{\partial J}{\partial p} \\ \vdots \\ \frac{\partial J}{\partial p_\ell} \end{bmatrix} \tag{5.2-16}$$

If δp is sufficiently small, the higher-order terms in δp may be neglected and δJ approximated by

$$\delta J = \delta p' J_p. \tag{5.2-17}$$

In order to satisfy the inequality it is apparent that J_p must vanish for $p = p_{opt}$.

$$J_p(p_{opt}) = 0 \tag{5.2-18}$$

This condition is called the First Necessary Condition of the Calculus of Variations.

5.2.4 The Canonical Equations of the First Variation

In the problem defined in Section 5.2.2 the minimization of the performance index is carried out subject to the constraint imposed by the system dynamics in Section 5.2.1. These restrictions may be introduced by adjoining the constraints to the performance index through the artifice of a Lagrange Multiplier Matrix, P.[5] The performance index is then written

$$J = \text{trace}\left[CX + P\left[FX + XF' + GQG'\right]\right] \tag{5.2-19}$$

The first variation in the performance index may then be written by considering perturbations in P, X, and p.

$$\begin{aligned}\delta J = &\text{ trace } \delta P \left[FX + XF' + GQG'\right] \\ &+ \text{trace } \delta X\left[C + PF + F'P\right] \\ &+ \text{trace } \sum_{i=1}^{\ell} 2\delta p_i PX \frac{\partial}{\partial p_i} F'\end{aligned} \tag{5.2-20}$$

The last term may be identified as

$$\delta p' J_p = \text{trace } \sum_{i=1}^{\ell} 2\delta p_i PX \frac{\partial}{\partial p_i} F' \tag{5.2-21}$$

where each element of the vector J is defined

$$J_{p_i} = \frac{\partial}{\partial p_i} J \tag{5.2-22}$$

$$= \text{trace } 2PX \frac{\partial}{\partial p_i} F' \tag{5.2-23}$$

Since the matrices $\frac{\partial}{\partial p_i} F$ are relatively easy to compute, Eq. 5.2-23 provides a convenient basis for evaluating the gradient, J_p, of the performance index.

In order for the first variation to vanish with respect to arbitrary perturbations in δp, δX, and δF, the following set of Canonical Equations of the First Variation must be satisfied.

Canonical Equations of the First Variation

$$FX + XF' + GQG' = 0 \tag{5.2-24}$$

$$PF + F'P + C = 0 \tag{5.2-25}$$

$$J_p = 0 \tag{5.2-26}$$

5.2.5 Satisfaction of the Necessary Conditions

The generation of weak relative minima is accomplished by a series of systematic operations which lead to a solution of the Canonical Equations.

Simultaneous solution of Eq. 5.2-24 to -26 is generally not attempted; however, Eq. 5.2-24 to -25 is usually satisfied at each iteration. A description of the more common parameter optimization algorithms is found in Appendix A with an illustrative example.

5.3 Optimization of a Vertical Positon Control System

Precision vertical guidance for the Space Shuttle is particularly important during the terminal phases of approach and landing. Beyond the terminal area, where accuracy is not a prime consideration, it is important to make the best use of the available control energy to minimize the fuel consumed in trajectory realization. This section considers the optimization of vertical-control-system trajectory accuracy subject to penalties on control-effector activity. Vertical-control-system configurations utilizing elevators and direct-lift spoilers are explored using parameter optimization techniques and some simulation results are presented.

5.3.1 Vertical Trajectory Control

The vertical velocity, $\dot{z}$, of an aerodynamic vehicle is related to the path velocity v_p, the angle of attack α, and the pitch angle θ by the equation

$$\dot{z} \approx v_p [\alpha - \theta] \tag{5.3-1}$$

for small angles. The $\dot{z}$ may be modified by changing any combination of the variables α, θ, and v_p. In conventional systems the velocity v_p is normally held constant by the airspeed control system or autothrottle. This convention will be adopted in this investigation. The vertical-control variables are thus θ and α.

The conventional method of achieving trajectory control utilizes the vehicle elevators.[6,7] The elevators produce a pitching moment about the y body axis. Control of θ is achieved by varying the pitching moment produced by the elevators. In order to satisfy the equation of static equilibrium, the aircraft weight W must balance the vertical component of lift L in the steady state.

$$L \cos [\theta - \alpha] = W \tag{5.3-2}$$

Thus a change in α is required if θ is changed. Since the airspeed v_p is constant, the change in lift is produced by a change in the angle of attack, α. The change is approximately proportional to the pitch perturbation

$$\alpha = K_{\alpha\theta}\, \theta \tag{5.3-3}$$

where $K_{\alpha\theta}$ is a positive constant less than unity in magnitude. Combining 5.3-3 and 5.3-1 gives

$$\dot{z} \approx v_p\left[K_{\alpha\theta} - 1\right]\theta \tag{5.3-4}$$

Since $\left|K_{\alpha\theta}\right| < 1$, the steady-state change in vertical velocity is proportional to the negative value of θ.

Another useful effector for vertical trajectory control is the direct-lift spoiler.[2,3] A spoiler is generally a plate hinged at its leading edge to the top surface of the wing. When retracted, the spoiler is flush with the normal surface of the wing and has no effect. When extended, the spoiler disturbs the airflow over the wing, reducing the coefficient of lift. Since v_p is constant, the lift is also reduced. This reduction in lift is countered by an increase in angle of attack which is roughly proportional to the spoiler deflection, δ_s

$$\alpha \approx K_{\alpha\delta_s}\,\delta_s \tag{5.3-5}$$

Since the spoiler, correctly placed, produces very little pitching moment, θ remains essentially unchanged; and since v_p is constant, the change in angle of attack must produce a change in $\dot{z}$. Assuming $\theta = 0$, the static relationship for $\dot{z}$ becomes

$$\dot{z} = v_p K_{\alpha\delta_s}\,\delta_s \tag{5.3-6}$$

In a control system the average deflection of the direct-lift spoilers is maintained at a fraction of the maximum spoiler range to permit positive and negative corrections in vertical velocity.

The range of θ is approximately ± 6.0 degrees in the approach and landing phases; thus, pitch-angle control can produce rather large changes in vertical velocity as opposed to the rather small changes which can be achieved by direct-lift mode-spoiler actuation. Direct-lift spoilers do offer the advantage of fast response. Thus, a vertical-position control system using direct-lift spoilers can cope more effectively with high-frequency components in the stochastic environment. Direct-lift spoilers also put the correcting force where the disturbance acts, thereby reducing structural loads.

It seems reasonable to attempt to combine the desirable properties of pitch angle and direct-lift spoiler control by using pitch attitude to effect gross changes

in trajectory while the direct-lift spoilers are used to counter high-frequency environmental disturbances. This goal may be achieved by using a control law which operates on z, $\dot{z}$, $\ddot{z}$, θ, and q to produce elevator and spoiler commands simultaneously. The spoiler command is then passed through a high-pass filter which removes the low-frequency components which characterize gross changes in vertical path.

5.3.2 Vertical Trajectory Control System Structure

The control laws for the elevator and direct-lift spoiler inputs were assumed to be of fixed structure. The structure does not necessarily represent the configuration of the final control system but indicates how a structurally similar conventional system may be improved by the addition of direct-lift spoilers and parameter optimization. The elevator servo command δ_{ec} of the form

$$\delta_{ec} = p_1 z + p_2 \dot{z} + p_3 \ddot{z} + p_4 \theta + p_5 q \tag{5.3-7}$$

The elevator control loop can provide vertical-control and/or pitch-attitude stabilization. The high-pass spoiler-command filter is assumed to have the form

$$\frac{j\omega}{j\omega + \omega_f} \tag{5.3-8}$$

where ω_f is a constant. If ω_f is sufficiently small (less than 0.1 rad/s), the filter will have negligible effect on the response of the system to stochastic disturbances and may be omitted from the analysis for the moment. The direct-lift spoiler servo input is

$$\delta_{sc} = p_6 z + p_7 \dot{z} + p_8 \ddot{z} \tag{5.3-9}$$

z, $\dot{z}$, and $\ddot{z}$ are perturbations in vertical position, velocity, and acceleration. The pitch rate, q, and angle, θ, do not appear in 5.3-9 because the spoilers are assumed to produce a very small pitching moment on the vehicle.

The feedback variables z, $\dot{z}$, and $\ddot{z}$ represent perturbations from the desired trajectory discussed in Chapters 3 and 4. The perturbations are measured by the integrated IMU-Radio Aid navigation system presented in Chapter 2. Pitch attitude may be furnished by processing IMU gimbal angles. The pitch rate q is usually measured by a body-mounted rate gyro.

5.3.3 Some Preliminary Results for the Vertical Position Control System

To illustrate the application of parameter-optimization techniques to vertical-control system synthesis a vertical controller using elevators and direct-lift spoilers was investigated.

The performance index was selected to minimize vertical-path deviations subject to penalties on the mean-square elevator and spoiler servo deflections.

$$J = w_z E(z^2) + w_e E(\delta_e^2) + w_s E(\delta_s^2) \tag{5.3-10}$$

The parameter w_z was held constant; w_e and w_s were adjusted to vary the mean-square values of the elevator and spoiler deflections.

The effect of varying the permissible levels of effector activity was investigated, utilizing three configurations.

1. Elevators only ($p_6 = p_7 = p_8 = 0$)
2. Elevators for pitch-attitude control, spoilers for vertical-position control ($p_1 = p_2 = p_3 = 0$)
3. Elevators and spoilers (all parameters nonzero).

Residual spoiler coupling into the pitch rate q equation was cancelled by adding a term proportional to δ_s to the elevator command in Eq. 5.3-8. A more detailed discussion is found in Appendix C.

The performance index was minimized for a range of w_e and w_a. The resultant mean-square vertical errors versus mean-square control-surface deflection are delineated in Fig. 5.3-1. These results show the remarkable dependence of mean-square vertical-path deviation on configuration. Spoilers alone produce the poorest control performance. An elevator-based control system can potentially reduce the maximum rms path error by a factor of 10. A hybrid system using elevators and spoilers can achieve a further reduction of at least 2, depending upon the maximum activity limits assigned to the spoilers and elevators.

Some responses of optimal vertical-position control systems are given in Ref.8.

5.4 Optimization of a Lateral Position Control System

Accurate lateral guidance is extremely important during approach and landing since permissible deviations in lateral touchdown dispersion are much smaller than

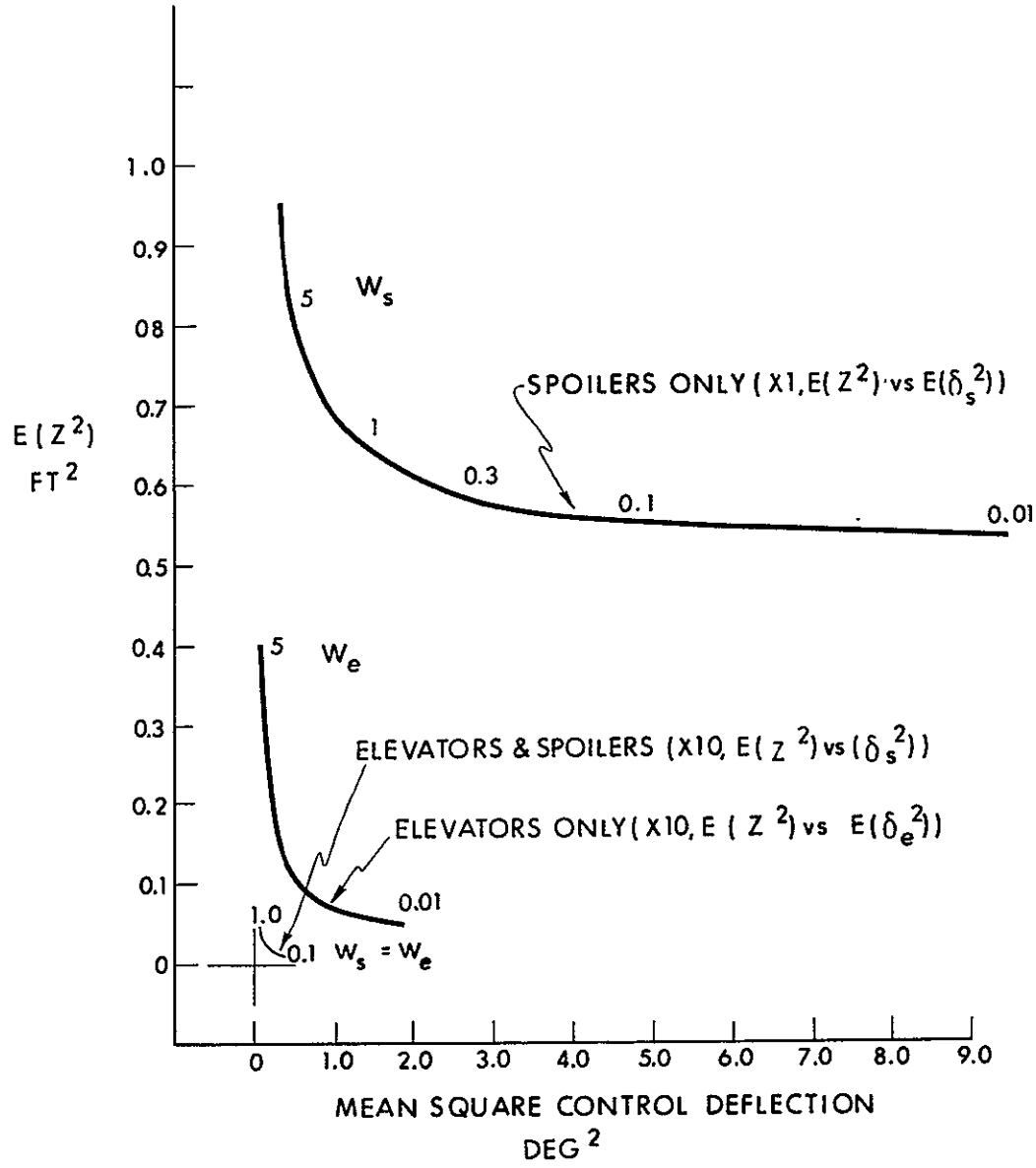

Fig. 5.3-1 Mean Square Vertical Position Error Versus Mean Square Control Surface Deflection

those along the runway surface. While precise lateral guidance outside the terminal area is probably not as critical, adequate levels of lateral control must be maintained.

This section discusses the design of a lateral-control system featuring aileron and differential-spoiler effectors.

5.4.1 Lateral Trajectory Control

Control of the position of the aircraft in the horizontal plane relative to the model position is accomplished by performing coordinated turns. If an aerodynamic vehicle is rolled about its longitudinal axis, a horizontal component of the lift vector results. If the sideslip angle β is maintained at zero, a yaw rate, $\dot{\psi}$, must be established to maintain equilibrium

$$\dot{\psi} \approx \frac{g \tan \phi}{v_p} \tag{5.4-1}$$

where v_p is the steady aircraft velocity relative to the air mass and g is the gravitational constant. The resultant yaw rate alters the direction of the velocity vector. If ψ_m is the model-heading reference, the lateral velocity of the shuttle relative to the model is

$$\dot{y} = v_p \sin(\psi - \psi_m) \tag{5.4-2}$$

Roll-angle control is achieved by establishing moments abouts the longitudinal axis. Such moments may be produced by ailerons or spoilers, operated differentially.

Ailerons and spoilers are equally effective for controlling roll rate. Turn coordination, however, is more simply produced with differential spoilers which results in a drag-produced yawing moment which aids the establishment of the desired yaw rate.

Ailerons are often designed for high-speed flight. Since their effectiveness varies as the square of the airspeed, it is often essential to provide spoiler augumentation to achieve adequate levels of low-speed control.

Since the shuttle will use spoilers as well as ailerons, it is likely that a hybrid lateral-control system with both types of effectors will be used.

5.4.2 Lateral Trajectory Control System Structure

Ailerons and spoilers are quite similar from the roll-dynamics point of view. Thus, it was decided at the outset to use similar control laws for both effectors. The aileron and spoiler effector commands δ_{ac} and δ_{sc} are linear combinations of the lateral position y, velocity $\dot{y}$, acceleration y, and roll ϕ, and roll rate p errors between the aircraft and model states.

$$\delta_{ac} = p_1 y + p_2 \dot{y} + p_3 \ddot{y} + p_4 \phi + p_5 p$$

$$\delta_{sc} = p_6 y + p_7 \dot{y} + p_8 \ddot{y} + p_9 \phi + p_{10} p \qquad (5.4\text{-}4)$$

Thus, up to 10 parameters must be defined during control synthesis. In addition, turn coordination must be assured by the computation of appropriate rudder commands.

Turn coordination was provided by closure of an additional control loop on yaw rate which also provides dutch-roll mode damping. The desired roll angle, ϕ_c, is

$$\phi_c = \left[p_1 y + p_2 \dot{y} + p_3 \ddot{y}\right] \frac{1}{p_4} + \left[p_6 y + p_7 \dot{y} + p_8 \ddot{y}\right] \frac{1}{p_9} \qquad (5.4\text{-}5)$$

so that the coordinated turn rate is

$$r_c \approx \frac{g \phi_c}{V_p} \qquad (5.4\text{-}6)$$

If the rudder command is

$$\delta_{rc} = p_{11}\left[r_c - r\right] \qquad (5.4\text{-}7)$$

the rudder will operate to make $r \approx r_c$.

The translation-error variables y, $\dot{y}$, and $\ddot{y}$ are provided by the integrated IMU-Radio Aid navigation system discussed in Chapter 2. Roll angle is provided by processing IMU gimbal angles, and roll rate is usually measured with a body-mounted rate gyro.

The effector commands are fed to control actuators which are modeled by first-order lags. The surface deflections are inputs to a set of linear vehicle equations which are detailed in Appendix C.

5.4.3 Some Preliminary Results for the Lateral Control System

Parameter optimization techniques were used to minimize the performance index

$$J = w_y E(y^2) + w_s E(\delta_s^2) + w_a E(\delta_a^2) + w_r E(\delta_r^2) \qquad (5.4\text{-}9)$$

The parameters w_y and w_r were held constant and w_s and w_a were varied to explore a range of solutions.

Two configurations were investigated.

1. Ailerons only ($p_6 \rightarrow p_{10} = 0$)
2. Spoilers only ($p_1 \rightarrow p_5 = 0$)

The mean-square lateral error for various control-surface deflection weightings is shown in Fig. 5.4-1. This shows that the rms lateral error can be improved by at least a factor of two, using spoilers instead of ailerons to effect roll control. A hybrid system reflecting activity limits on δ_a and δ_s will undoubtedly show an even more dramatic performance improvement.

To illustrate the response characteristics of parameter-optimized lateral control systems, a reference design based on an autoland system for the Convair 880 and an optimized, spoilers only, lateral control system were compared. The parameter values for the two systems are given in Table 5.4-1. The responses of the two systems to a gust input are shown in Fig. 5.4-2 — 5.4-4. Note the scale changes on y and $\dot{y}$ in Fig. 5.4-2. The well-damped response characteristics which appear to be typical for systems synthesized using parameter optimization are presented in Fig. 5.4.-5 and 5.4-6.

5.5 Conclusions

Aerodynamic vehicle-control systems are complicated by a large number of potential feedback variables and effector combinations. As a result, even the simple trajectory-control laws presented in the preceding sections required the definition of up to 11 parameters. Thus in such systems it is essentially hopeless to apply trial-and-error design procedures to the solution of the stochastic optimization

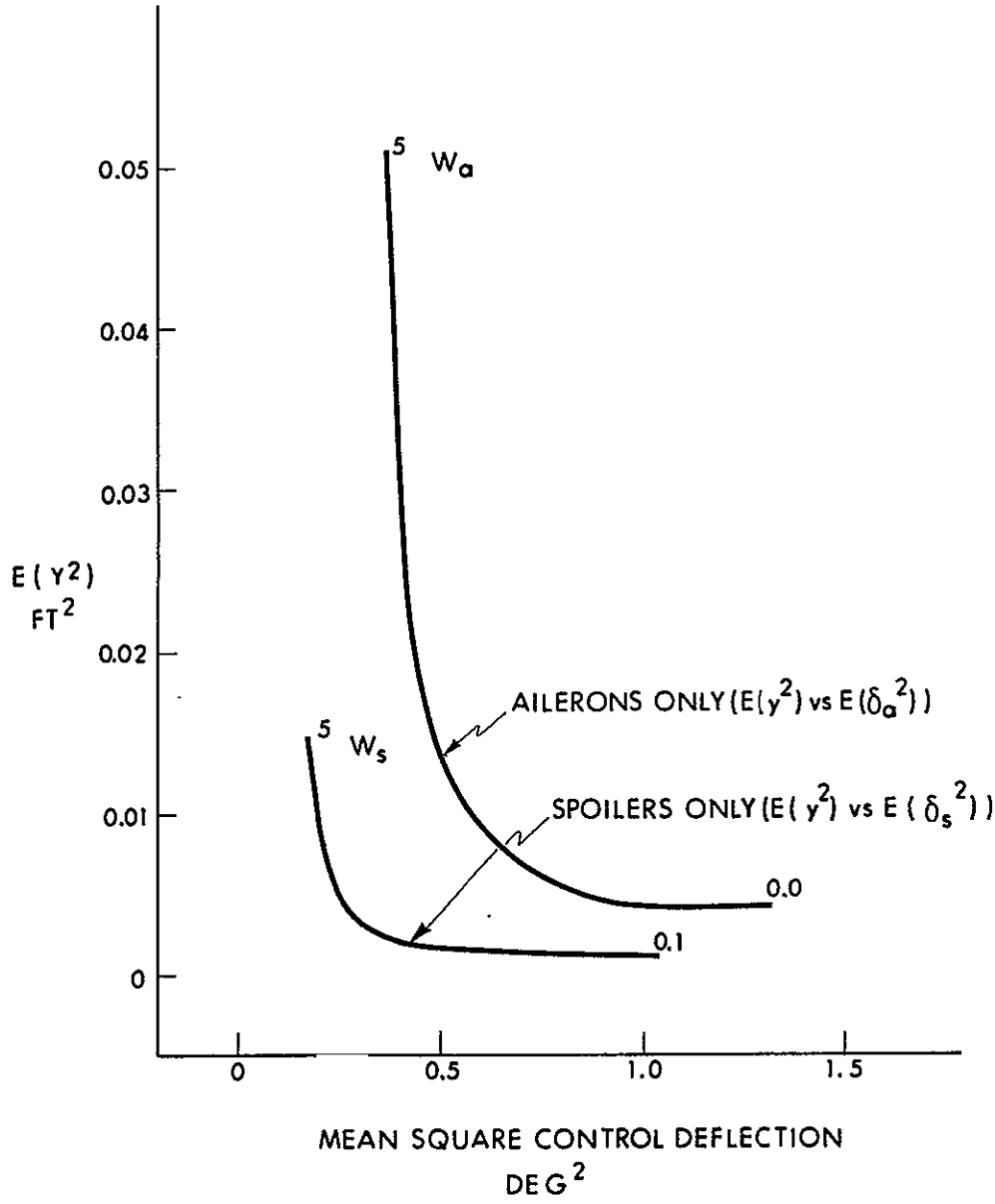

Fig. 5.4-1 Mean Square Lateral Position Error Versus Mean Square Control Surface Deflection

Table 5.4-I

Parameter Values For The Reference and Optimized Lateral Control Systems

Parameter	REFERENCE	OPTIMIZED
P_6	-0.0191	-3.69
P_7	-0.1	-23.41
P_8	0.0	-11.64
P_9	-0.853	-2.89
P_{10}	-0.526	-7.05
P_{11}	5.25	2.58

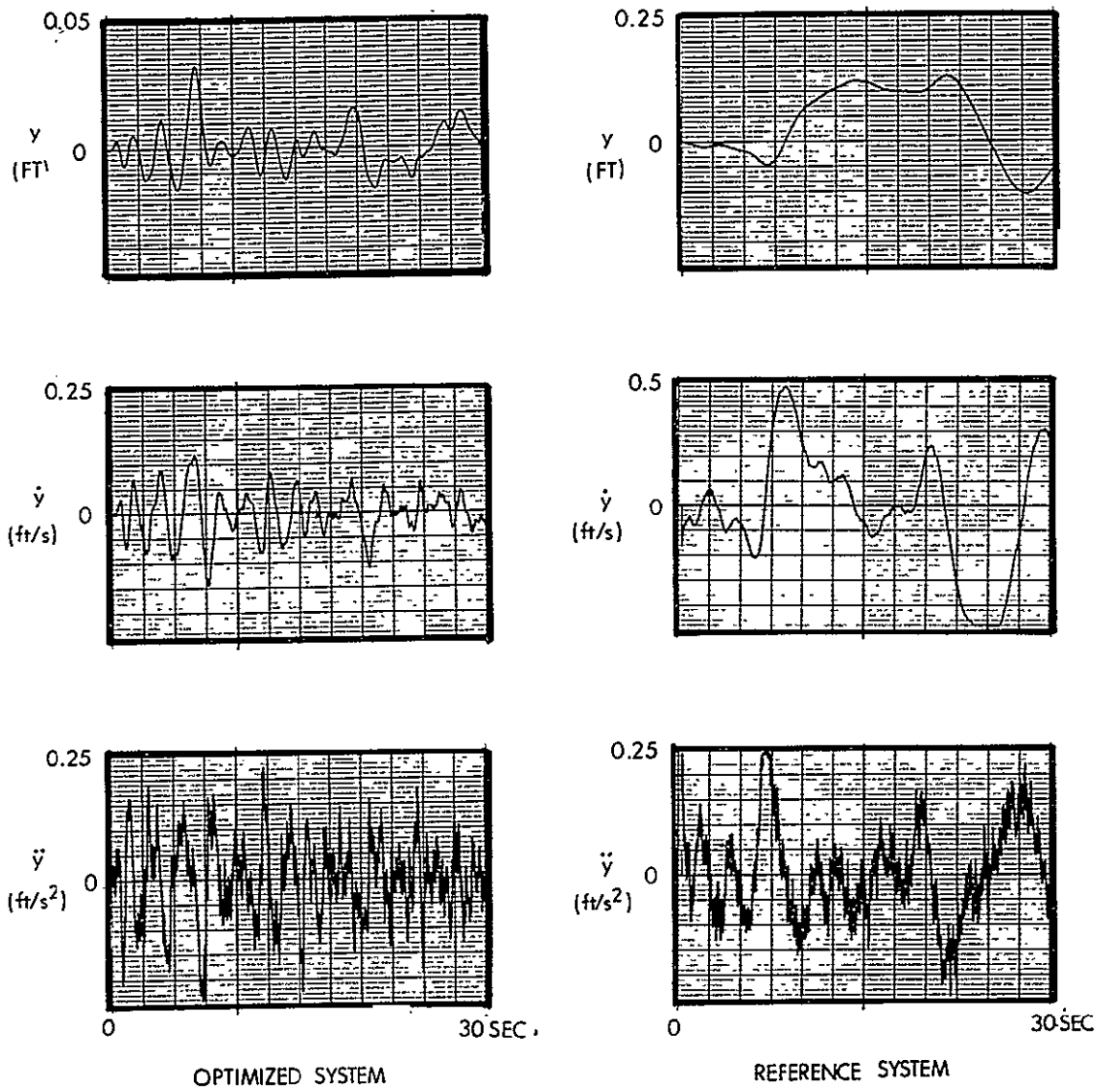

Fig. 5.4-2 Position, Velocity and Acceleration Errors in Response to Gusts for the Optimized and Reference Systems. Note the Change in y and $\dot{y}$ Scales.

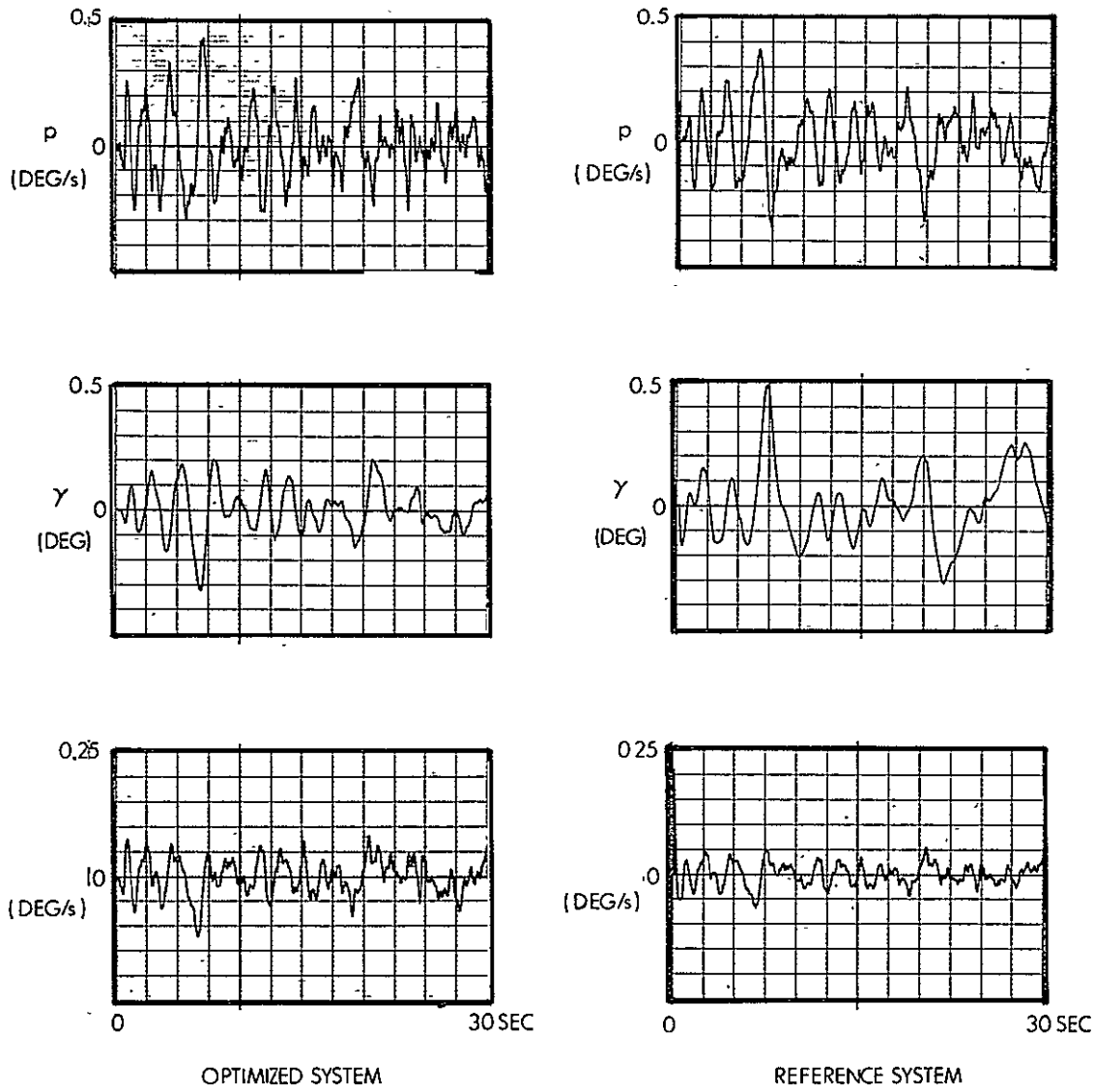

Fig. 5.4-3 Roll Rate, Roll, and Yaw Rate in Response to Gusts for the Optimized and Reference Systems

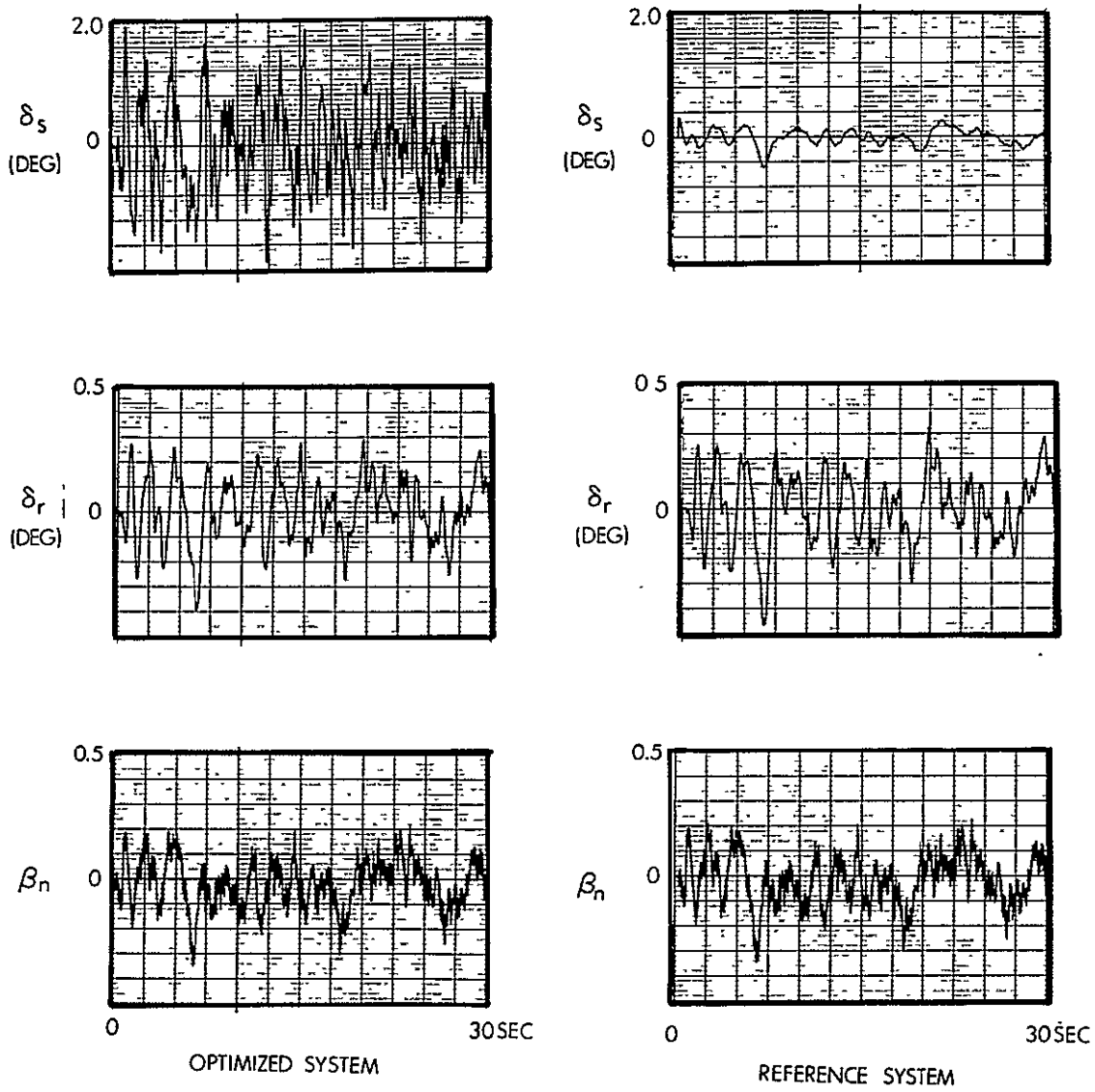

Fig. 5.4-4 Spoiler and Rudder Deflection and Gust History for the Reference and Optimized Systems

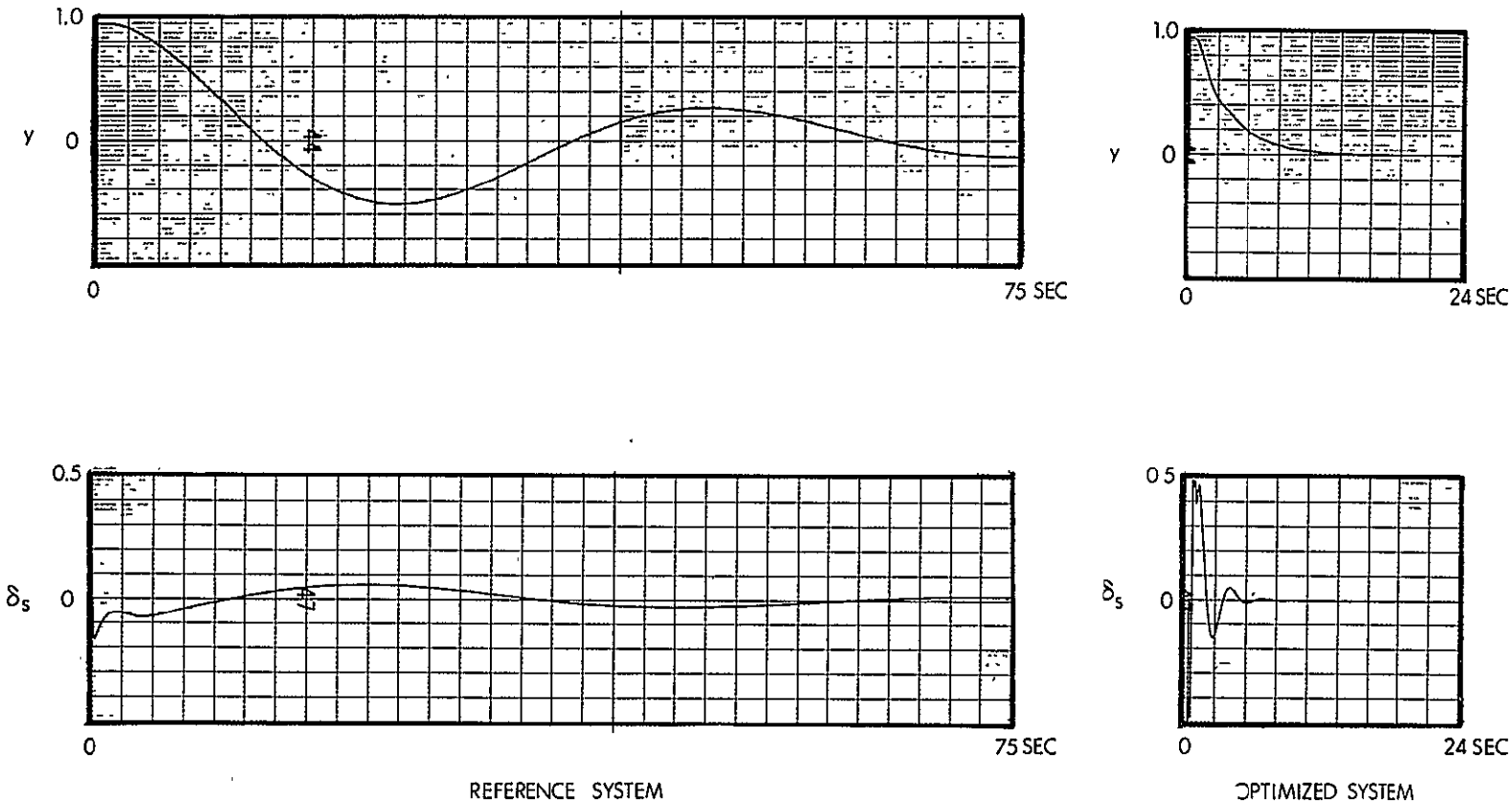

Fig. 5.4-5 Lateral Position and Spoiler Actuator Response to an Initial Error in y

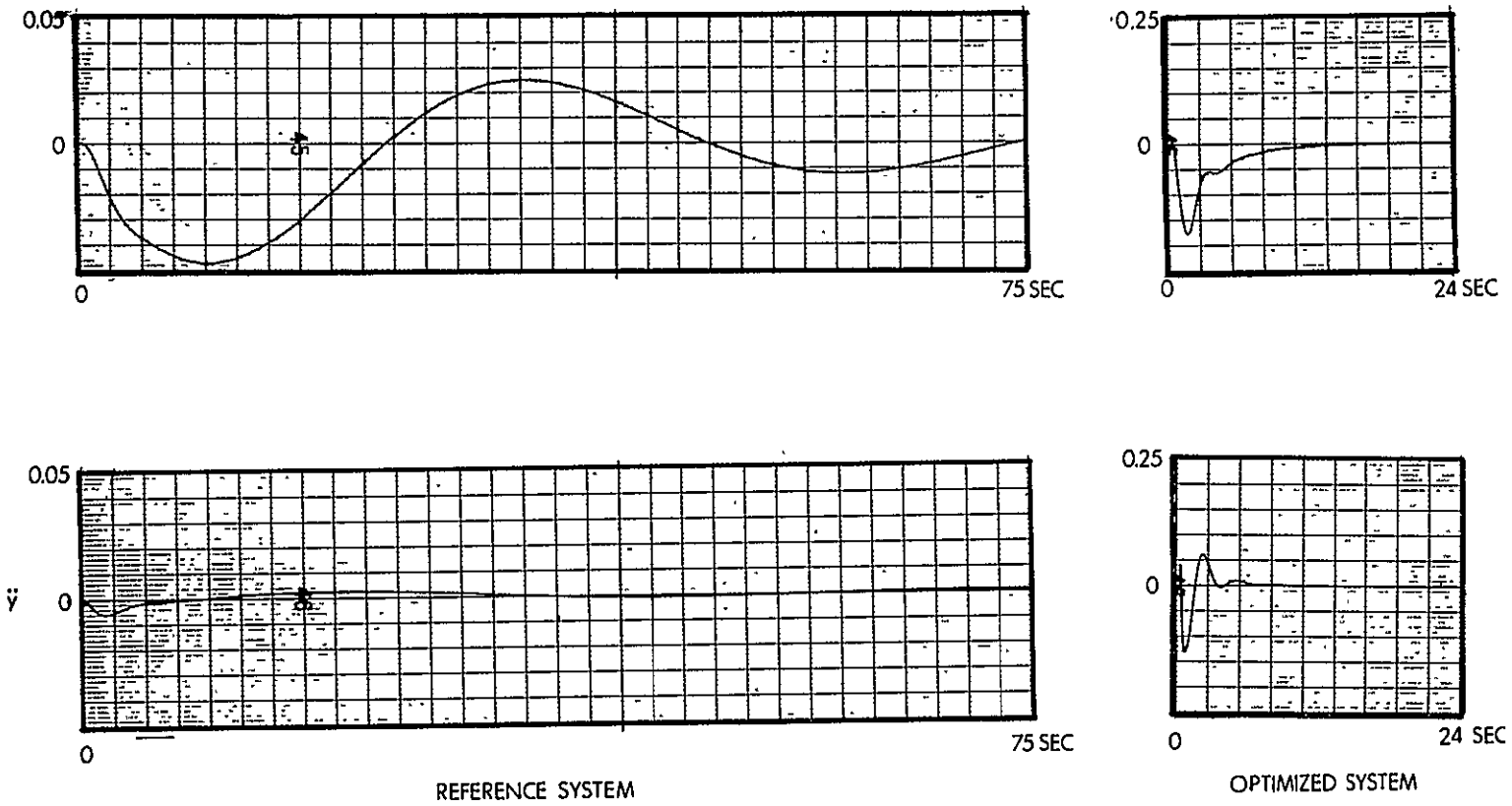

Fig. 5.4-6 Lateral Velocity and Acceleration Responses to an Initial Error in y

problem in section 5.2-2. Systematic parameter optimization using variational algorithms offers an answer to these problems.

By scanning optimal solutions for a range of control-surface activity levels, it is possible to define the best mix of effector types for a particular flight condition and control objective. The delineation of tradeoffs between effector activity and the achieved level of control provides invaluable information for the initial definition of the Space Shuttle as well as essential data for the design of a control system for an existing vehicle.

In addition to the ability of parameter optimization to handle complicated control-system design, an additional advantage is apparent in the time-domain response characteristics of the resultant control systems. Desirable features, such as short rise time and small overshoot, appear to evolve automatically during the solution of the stochastic optimization problem.

In summary, it appears that parameter optimization can play a valuable role throughout the development and design of the Space Shuttle vehicle and its trajectory-control systems.

Chapter 5 References

1. Merriam, C.W., "Optimization Theory and the Design of Feedback Control Systems", McGraw-Hill, New York, N.Y., 1964.
2. Lorenzetti, K.C., Nelson, G.L., Johnson, K.N., "Computerized Design of Optimal Direct Lift Controllers", AIAA Journal of Aircraft, Vol. 6, No. 2, March-April, 1969.
3. Lorenzetti, K.C., Direct Lift Control for Approach and Landing", presented at the NATO - AGARD Conference on Automatic Landing, Boston, Massachusetts, May, 1969.
4. Bryson, A.E., Ho, Y.C., "Applied Optimal Control", Blaisdell Publishing Company, 1969.
5. Rediess, H.A., "A New Model Performance Index for the Engineering Design of Control Systems", MIT Thesis TE-26, December 9, 1968.
6. Etkins, B., "Dynamics of Flight, Stability and Control", John Wiley and Sons, 1965.
7. Blakelock, J.H., "Automatic Control of Aircraft and Missiles", John Wiley and Sons, 1965.
8. Duncan MacKinnon, "Some Applications of Mathematical Optimization to Automatic Landing Systems", R-651, Instrumentation Laboratory, Massachusetts Institute of Technology, Cambridge, Mass., November, 1969.

APPENDIX A

NUMERICAL OPTIMIZATION ALGORITHMS

by

Duncan MacKinnon

A.1 Introduction

The parameter optimization problems discussed in Chapter 5 may be solved using a wide variety of numerical techniques. This appendix provides a description of a variety of optimization procedures which have yielded satisfactory numerical solutions. The algorithms are applied to a simple example for comparison.

A.2 Numerical Optimization Techniques

The field of numerical-optimization encompasses a large number of different algorithms and applications. To a large extent, the application of numerical optimization techniques to the solution of practical engineering problems is a relatively recent phenomenon arising from the development of high-speed, large-scale, electronic digital computers which are capable of performing the optimization computations in a reasonable length of time.

A review of the algorithms presented in the following sections reveals a structural commonality shown in Fig. A. 2-1. Each algorithm requires the computation of the value of the performance index, J, and the gradient, J_p, of J with respect to the parameter vector, p. These calculations are conveniently performed using the canonical equations of the first variation in Section 5.2.

The value of X is obtained by converting Eq. 5.2-24 to an equivalent algebraic equation of the form

$$Ay = b \qquad \text{(A.2-1)}$$

Equation A.2-1 is then solved for y using the Gaussian Elimination process. X may be constructed from y by a suitable linear transformation. The performance index is then calculated from Eq. 5.2-6.

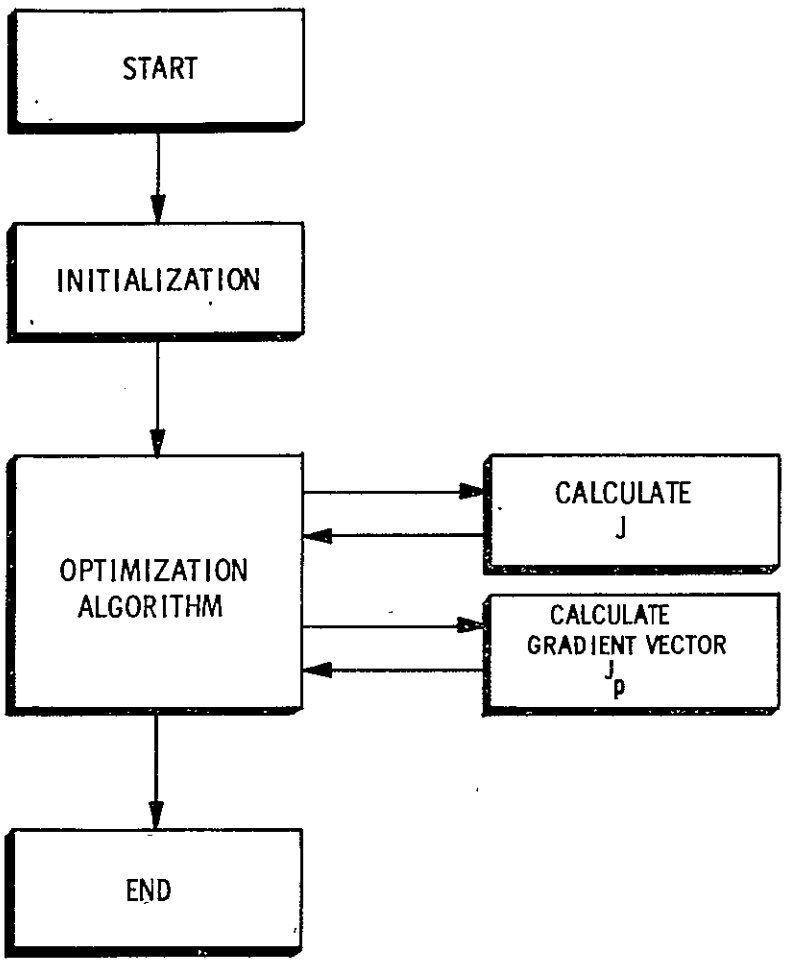

Fig. A.2-1 Structural commonality of optimization algorithms.

The gradient of the performance index J_p with respect to the parameter vector p may be calculated analytically using Eq. 5.2-23. The Lagrange Multiplier matrix P is the solution of Eq. 5.2-25 which is amenable to the same methods of solution as Eq. 5.2-24. The matrix F' is often poorly conditioned, in which case an acceptable gradient vector is calculated from the relationship

$$J_{p_i} = \frac{J(p_i + \delta p) - J(p_i - \delta p)}{2\delta p_i} \tag{A.2-2}$$

The following sections describe six algorithms for systematically generating minima.

A.3 The Method of Steepest Descent

Perhaps the most basic method of minimizing the value of a function is the method of steepest descent,[14] which is based on the Taylor series expansion of the variation δJ in the performance index due to a small perturbation, δp, in the parameter vector. If δp is sufficiently small, the value of δJ is approximately equal to

$$\delta J \approx \delta p' J_p \tag{A.3-1}$$

Suppose the change in δp is equal to

$$\delta p = -\epsilon J_p \tag{A.3-2}$$

where ϵ is a positive number. If ϵ is selected so that δp is small, the approximation A.3-1 is satisfied. Then δJ becomes

$$\delta J \approx -\epsilon J'_p J_p \tag{A.3-3}$$

Since the inner product of J_p with itself is always positive, the perturbation δJ is negative and the value of $J(p + \delta p)$ will be less than the value of $J(p)$. This process may be iterated to produce a monotonically decreasing sequence of values for J. Since the sequence is continuously decreasing, the algorithm always converges to a minimum, providing such a minimum exists.

A flow diagram of a steepest-descent algorithm is shown is Fig. A.3-1. The variable NIC counts the number of successful iterations ($\delta J < 0$) while NHC keeps track of the number of iterations in which the size of δp is too large to satisfy approximation A.3-1. If δp is too large, ϵ is halved and the evaluation of J is

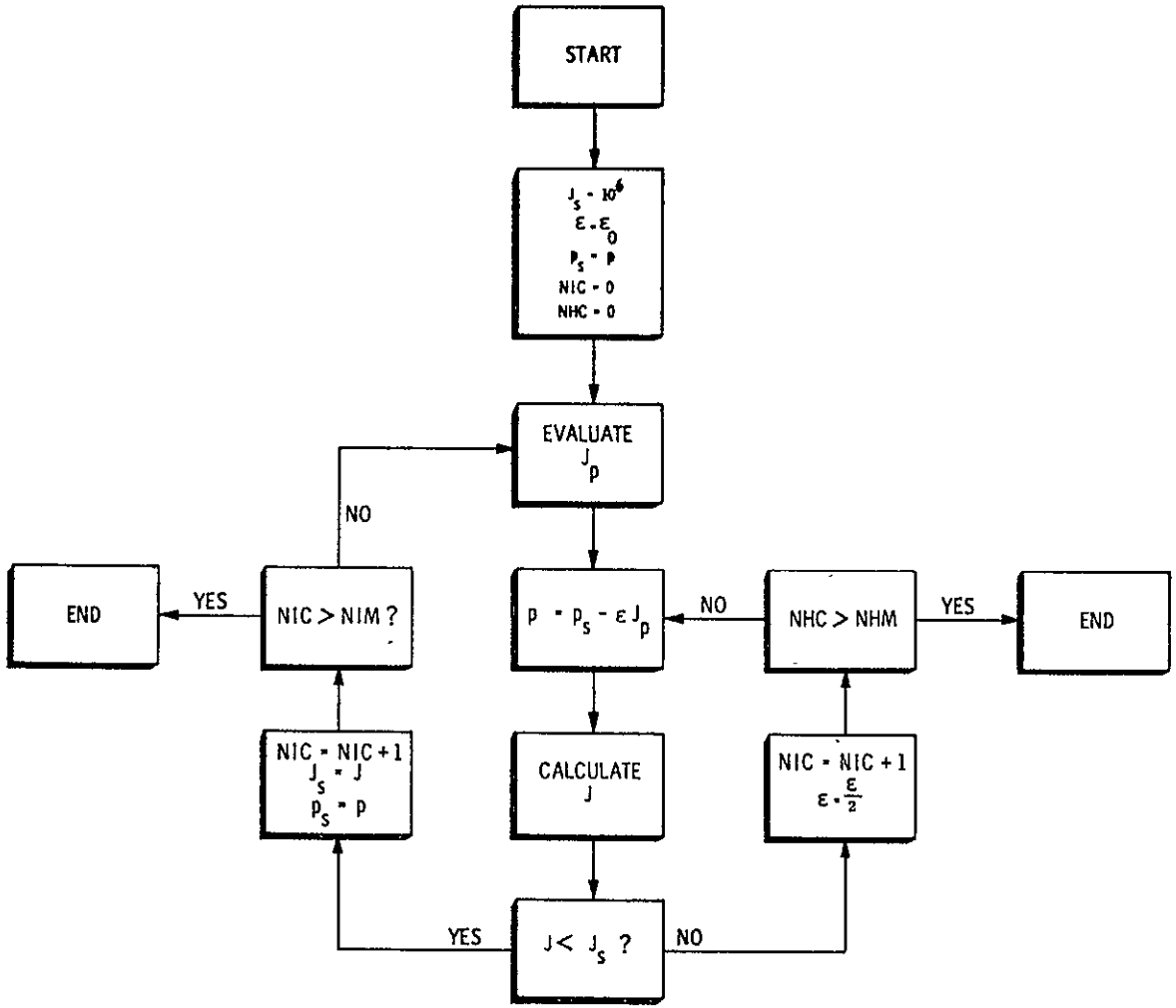

Fig. A.3-1 Method of steepest descent.

repeated. The algorithm terminates when NIC or NHC exceeds the maximum values NIM or NHM respectively.

A.4 Method of The Average Gradients

One of the important problems associated with the method of steepest descent is the "valley problem". Such a problem occurs if the orientation of the direction of maximum-descent path is approximately normal to the gradient vector at the current value of p. If the step size is too great, the value of p is transferred to the other side of the "valley" where a similar situation is often encountered. The algorithm may thus continue to traverse back and forth across the "valley", converging very slowly to the minimum. This difficulty may be advoided by using a direction which is the average of the current gradient and the gradient used in the last successful iteration.[15]

A flow diagram of the average-gradient algorithm is shown in Fig. A.4-1. The previous gradient, J_{ps}, is equal to the present gradient initially so that the first step utilizes the steepest-descent algorithm.

A.5 The Generalized Method of Newton Raphson[12]

Convergence rates can usually be improved by considering the second as well as the first variations in the performance index. The expanded perturbation in J due to δp is then of the form

$$\delta J \simeq \delta p' J_p + \frac{1}{2}\delta p' J_{pp} \delta p \qquad (A.5\text{-}1)$$

where J_{pp} is the matrix of second partial derivatives of the performance index J. J_{pp} is evaluated by finite differences or by using a combination of finite differences and closed-form generation of J_p. If the variation in J is required to vanish,

$$\delta p = -J_{pp}^{-1} J_p. \qquad (A.5\text{-}2)$$

Since the approximation A.5-1 is only valid for small δp, the step size is controlled by introducing a positive constant ϵ writing

$$\delta p = -\epsilon J_{pp}^{-1} J_p \qquad (A.5\text{-}3)$$

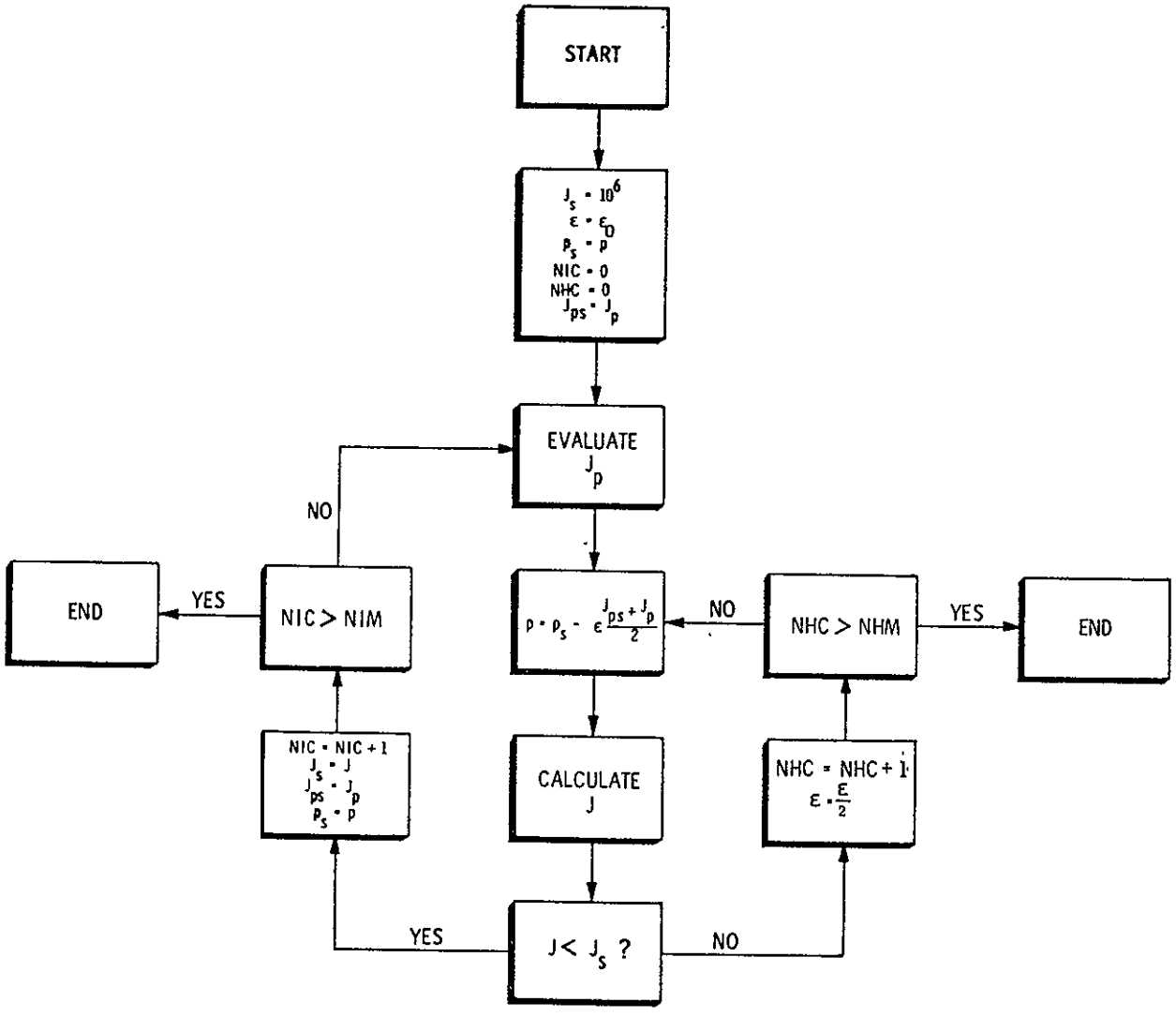

Fig. A.4-1 Method of average gradient.

If the performance index is quadratic in p and ϵ is equal to unity, the algorithm will converge in one step to the optimum value. In any case, the algorithm will exhibit one-step convergence if p is near p_{opt}.* The algorithm is illustrated in Fig. A.5-1.

A.6 Method of Conjugate Gradients[18]

This numerical technique is a systematic optimization procedure which displays some of the favorable characteristics of the Newton Raphson algorithm without the necessity of inverting the matrix of the second derivatives, J_{pp}. If the performance index, J, is quadratic in the parameter vector, p, the method will minimize J in ℓ steps, where ℓ is the dimension of p.

The algorithm operates by generating a set of "J_{pp} - orthogonal" or "J_{pp} conjugate" vectors $q_1, \ldots, q_\ell$, in the ℓ-dimensional Euclidean solution space. The matrix J_{pp} must be positive definite, in which case

$$q_i J_{pp} q_j \begin{cases} = 0 & i \neq j \\ > 0 & i = j \end{cases} \tag{A.6-1}$$

As a result, it can be shown that any vector p can be expressed as a linear combination of the vectors $q_1, \ldots, q_\ell$

$$p = \sum_{i=1}^{\ell} \beta_i q_i \tag{A.6-1}$$

where β_i is a scalar. If p_0 is the initial value of p, p_0 can be expressed in terms of the optimal value p_{opt} and the basis vectors by writing

$$[p_{opt} - p_0] = \sum_{i=1}^{\ell} \beta_i q_i, \tag{A.6-3}$$

where

$$\beta_i = \frac{[p_{opt} - p_0]' J_{pp} q_i}{q_i' J_{pp} q_i}. \tag{A.6-4}$$

*Since the performance index will be essentially quadratic in δp when p is near p_{opt}.

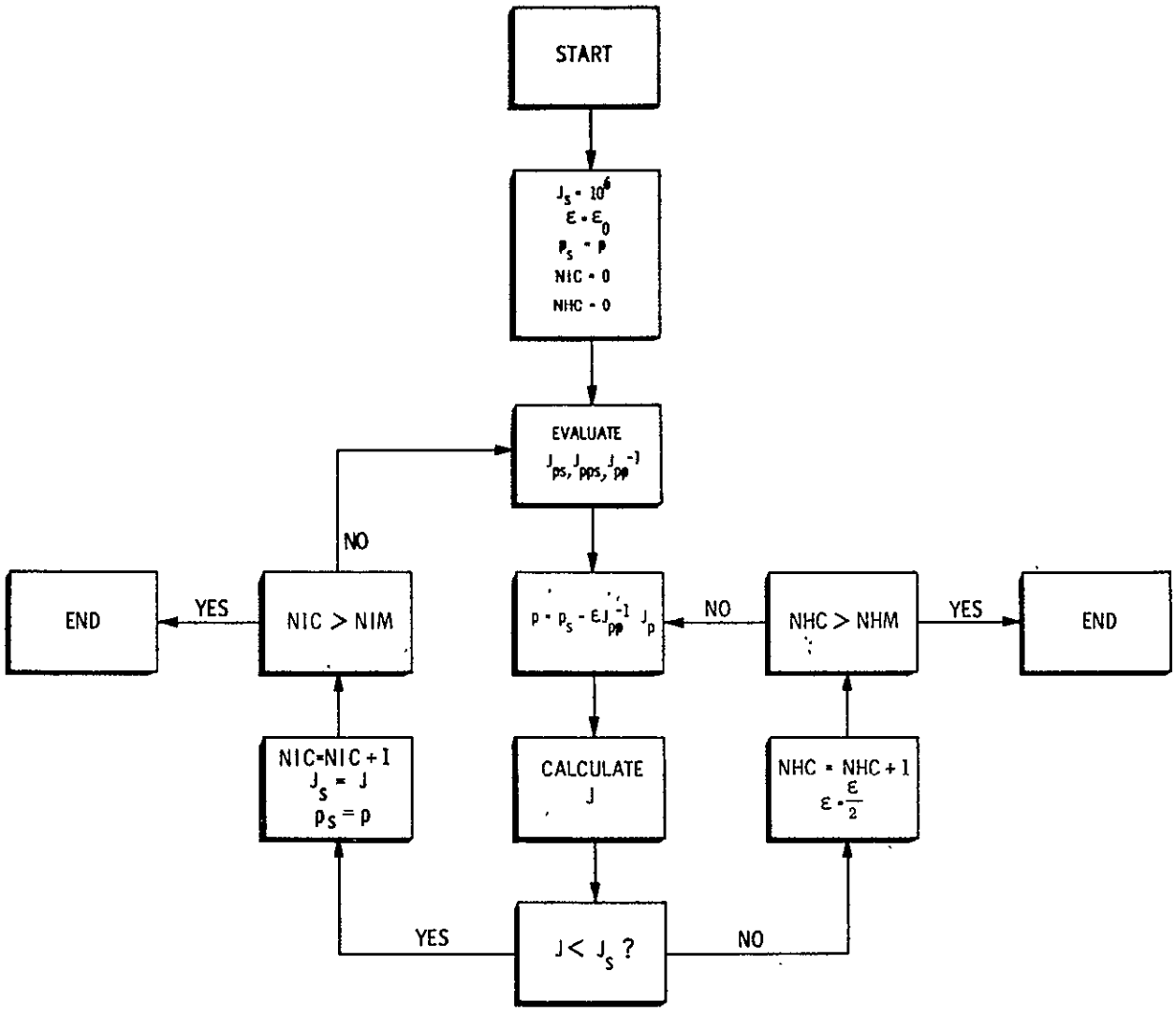

Fig. A.5-1 Generalized method of Newton Raphson.

The problems of finding the minimum thus reduces to the determination of the conjugate directions $q_1, \ldots, q_\ell$ and the Fourier coefficients $\beta_1, \ldots, \beta_\ell$.

A convenient set of "J_{pp}-conjugate" basis vectors may be constructed on the gradient vectors, J_p, using the following iterative procedure

$$p_{i+1} = -p_i + \alpha_i q_i \tag{A.6-5}$$

where

$$\alpha_1 = \frac{-q_i' J_{p_i}}{q_i' J_{pp} q_i} \tag{A.6-6}$$

The value of α_i is conveniently generated by minimizing the performance index, J, along the straight line $p = p_i + \alpha_i q_i$. The value of α which minimizes J is α_i. The new basis vector is generated by orthogonalization with respect to the subspace spanned by the vectors $q_1, \ldots, q_i$.

$$q_{i+1} = - J_{p_{i+1}} + \beta_i q_i \tag{A.6-7}$$

where

$$\beta_i = \frac{J'_{p_{i+1}} J_{p_{i+1}}}{J'_{p_i} J_{p_i}} \tag{A.6-8}$$

The result is a sequence of operations which systematically satisfies the relationship

$$p_{opt} = p_0 + \sum_{i=1}^{\ell} \alpha_i q_i. \tag{A.6-9}$$

The algorithm is illustrated in Fig. A.6-1.

A.7 Method of Davidon[17]

Another optimization technique which shares a number of the properties of the Conjugate Gradient method was suggested by Davidon[17] and further developed by Fletcher and Powell.[15] The algorithm searches iteratively for a matrix H which defines the optimum step size.

$$\delta p_{opt} = -H J_p \tag{A.7-1}$$

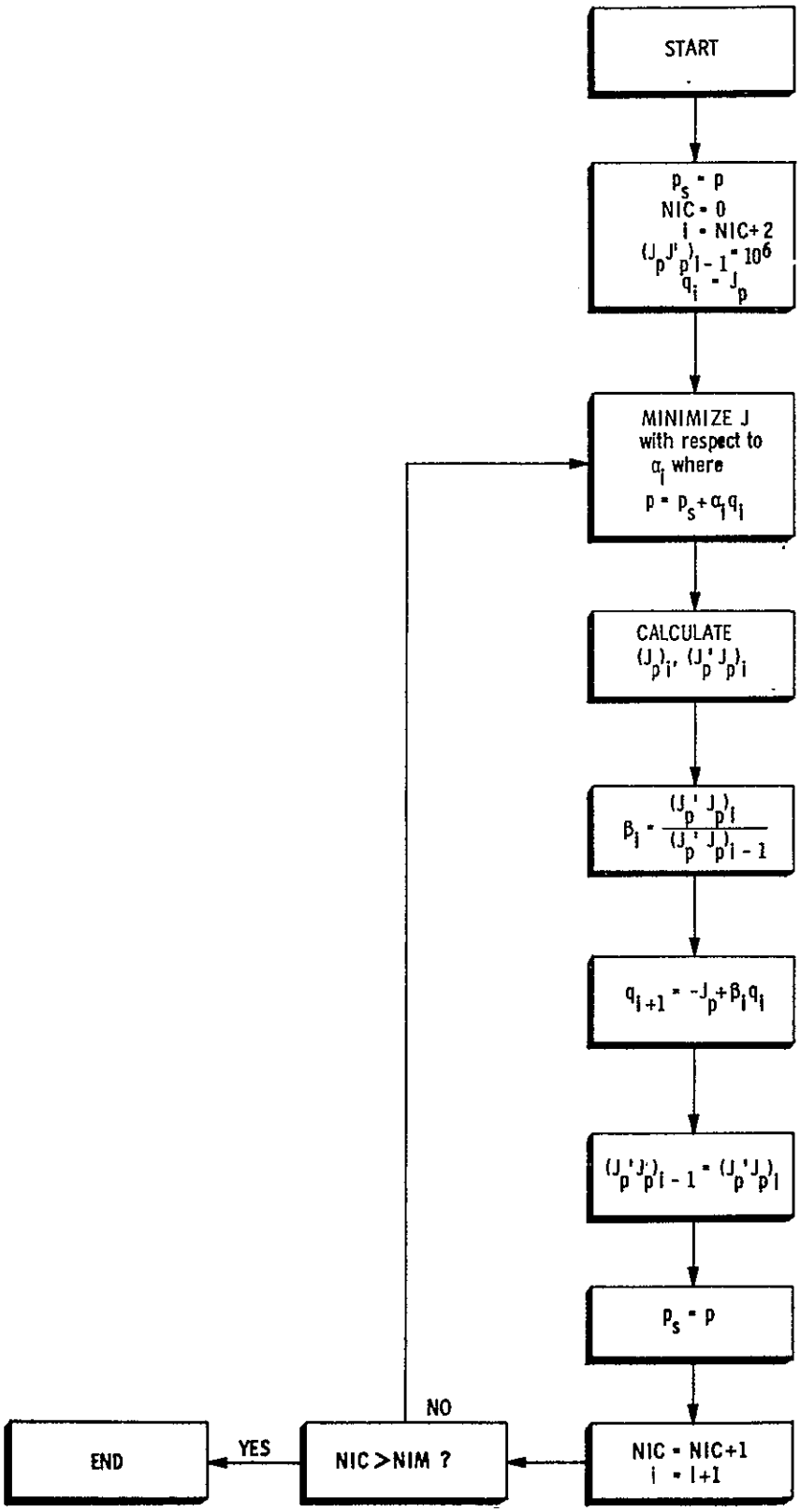

Fig. A.6-1 Method of conjugate gradients.

The matrix H is the inverse of the second variation matrix J_{pp}.

$$H = J_{pp}^{-1}. \tag{A.7-2}$$

The procedure is as follows: starting from a point p_i with gradient $J_p(p_i)$ the algorithm minimizes J with respect to a scalar ϵ where

$$p = p_i + \epsilon H_i J_p(p_i) \tag{A.7-3}$$

the optimum value of p is designated p_{i+1}.

Let

$$s_i = p_{i+1} - p_i \tag{A.7-4}$$

$$r_i = J_p(p_{i+1}) - J_p(p_i) \tag{A.7-5}$$

The matrix H_i is then refined according to the relationship

$$H_{i+1} = H_i + \frac{s_i s_i'}{s_i' r_i} - \frac{H_i r_i r_i' H_i}{r_i' H_i r_i} \tag{A.7-6}$$

The process is then repeated.

It is possible to show that, if the initial H is positive definite ($H_1 = I$ for example), the direction $H_i J_p(p_i)$ will always result in a reduction in J when the minimization with respect to ϵ is performed. Thus the algorithm generates a monotonically decreasing sequence of J's and convergence to at least a weak relative minimum is assured. If the performance index is quadratic in p, it can be shown that the algorithm will converge to a minimum in ℓ iterations, in which case the terminal value of H is J_{pp}^{-1}.

It is apparent that the algorithm will also have quadratic convergence properties when p is very close to p_{opt}. A flow diagram of the method is shown in Fig. A.7-1.

A.8 The Method of Powell[14]

This method is similar to the methods of Conjugate Gradient and Davidon, in as much as convergence can be achieved in ℓ steps where ℓ is the dimension of the

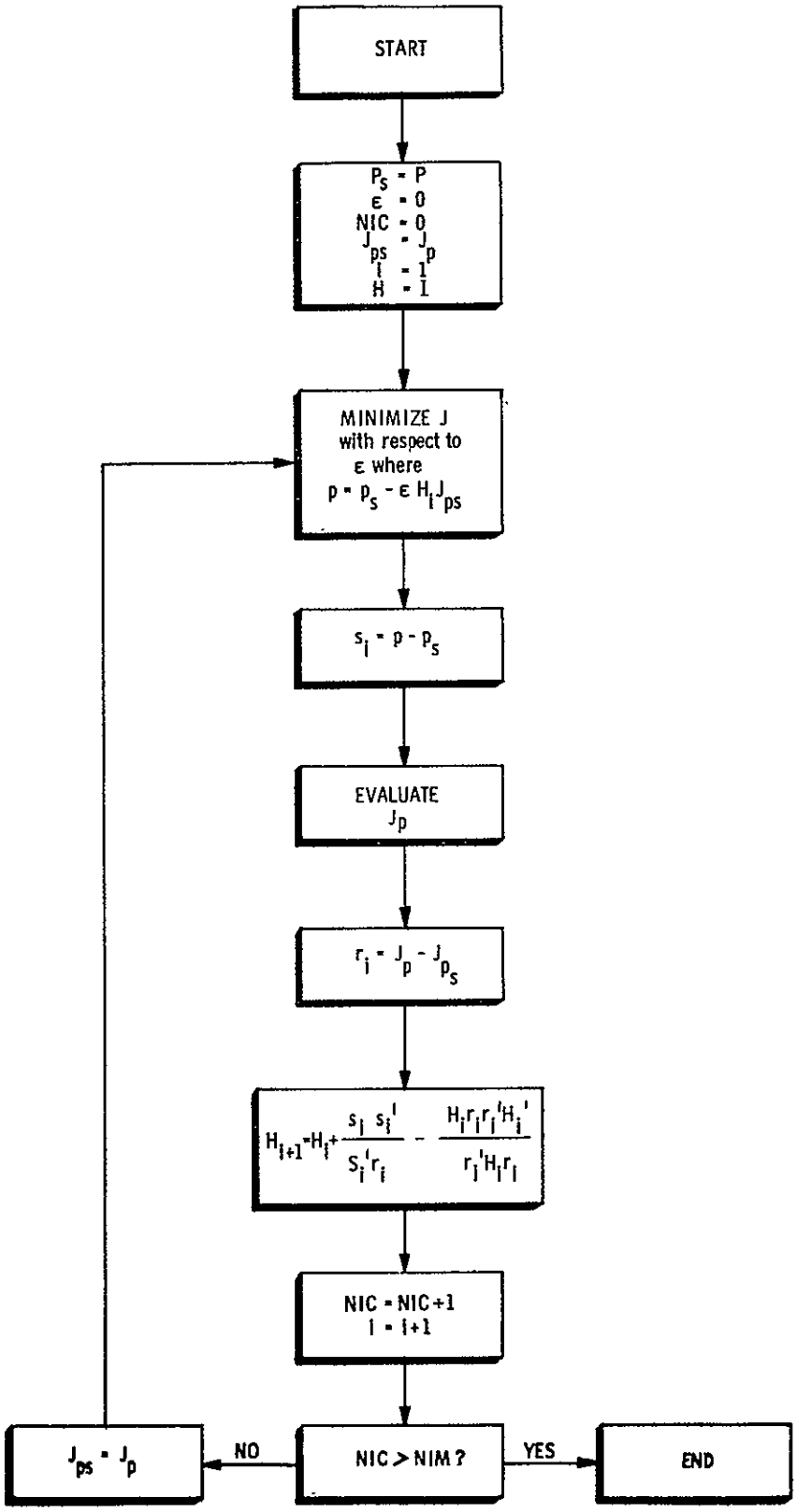

Fig. A.7-1 Method of Davidon.

parameter vector if the performance index is quadratic in p. There is also no necessity to evaluate the matrix of second derivatives J_{pp}.

In this method, each iteration requires one-dimensional minimizations down n linearly independent directions, $d_1, d_2, \ldots, d_\ell$. As a result of these minimizations, a new direction d is defined, which is linearly related to the coordinate values obtained during these minimizations. If d satisfies certain conditions, d replaces one of the original directions and the process continues.

In general, for the k^{th} iteration, the last k-1 directions used are conjugate. For quadratic functions, if p_1 is the minimum in the direction d_j, and p_2 the minimum along a direction parallel to d_j, then $p_2 - p_1$ is conjugate to d_j (parallel tangents).

The initial choice must be linearly independent. This implies that the matrix D of column vectors d_i

$$D = [d_1, d_2, \ldots . d_\ell] \tag{A.8-1}$$

must be nonsingular ($D \neq 0$). The algorithm illustrated in Fig. A.8-1 is not the original statement of Powell, but the technique now generally adopted.

The convergence tests indicated in Fig. 4.8-1 are as follows:

Define	$J_1 = J(p_1)$ and $J_{\ell+1} = J(p_{\ell+1})$.
Find	integer m, $1 \leq m \leq n$, so that $J(p_{m-1}) - J(p_m)$ is a maximum, and
Define	$\Delta = J(p_{m-1}) - J(p_m)$
Calculate	$J_2 = J(2p_{n+1} - p_1)$.
If	$J_2 \geq J_1$
or if	$[J_1 - 2J_{\ell+1} + J_2][J_1 - J_{\ell+1} - \Delta]^2 \geq \frac{1}{2}\Delta [J_1 - J_2]^2$
then set	$p_1 = p_{\ell+1}$

and use the same set of directions, $d_1, d_2, \ldots, d_\ell$. If neither holds, accept a new direction defined as

$$d = p_{\ell+1} - p_1$$

and update the direction matrix as indicated.

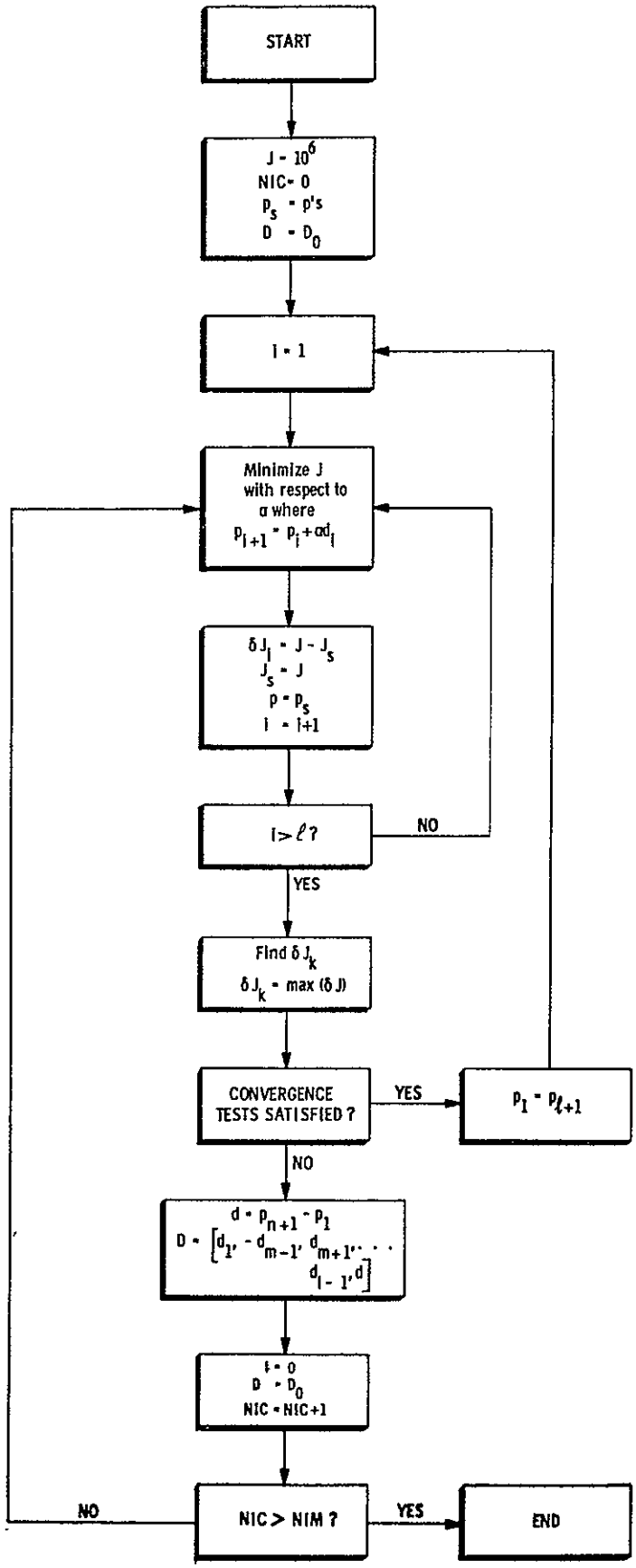

Fig. A.8-1 Method of Powell.

A.9 A Simple Illustrative Example

The foregoing material is best illustrated by application to a simple example which is characterized by a fixed control structure which operates on a subset of the components of the state vector. The system is subject to an exponentially correlated disturbance.

Consider the block diagram in Fig. A.9-1 which may be interpreted as a position control system. The vehicle equations of motion are subject to a zero-mean, exponentially correlated stochastic disturbance x_4 which produces random fluctuations in acceleration $\dot{x}_2$. The effects of the random variable u are counteracted by a control force x_3. The control law is defined by the adjustable parameter p_1.

The object of the parameter optimization is to minimize the mean-square position response $E(x_1^2)$ subject to a penalty on the mean-square control force $E(x_3^2)$.

$$\text{minimize} \quad E(x_1^2) + E(x_3^2) \tag{A.9-2}$$

The system mat be represented by

$$\dot{x} = Fx + Gu \tag{A.9-3}$$

$$x = \begin{bmatrix} x_1 \\ x_2 \\ x_3 \\ x_4 \end{bmatrix} \tag{A.9-4}$$

$$u_{vec} = u \tag{A.9-5}$$

$$F = \begin{bmatrix} 0 & 1 & 0 & 0 \\ 0 & -1 & 1 & 1 \\ p_1 & -10 & -10 & 0 \\ 0 & 0 & 0 & -1 \end{bmatrix} \tag{A.9-6}$$

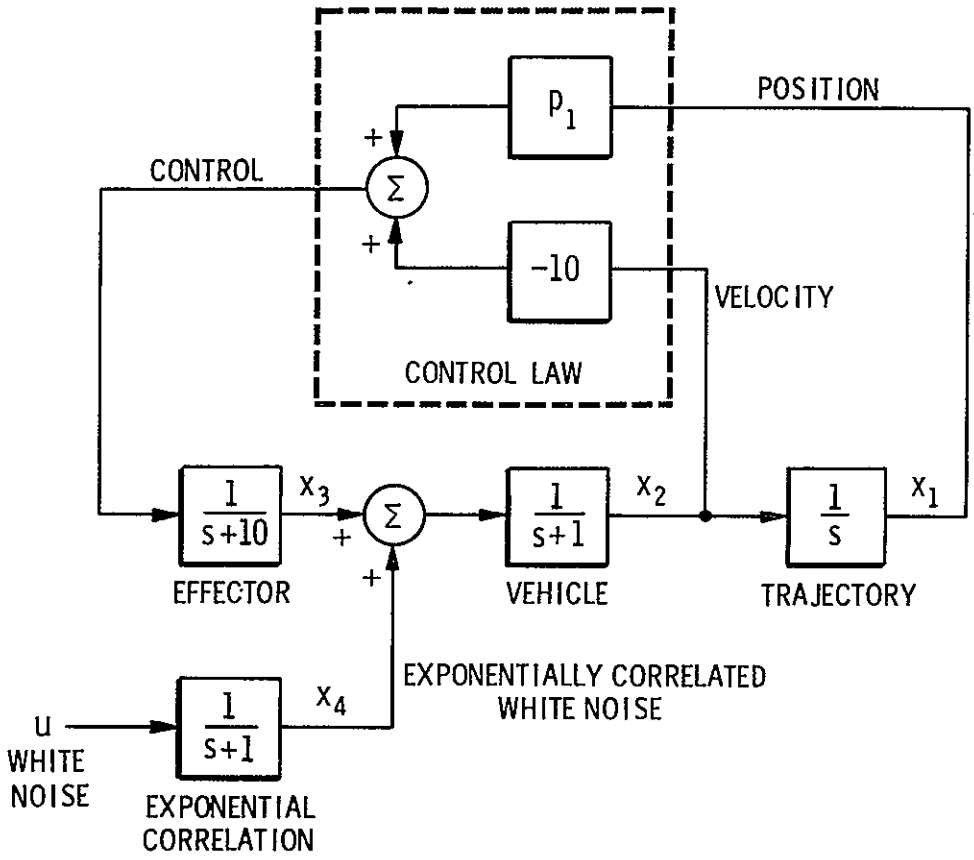

Fig. A.9-1 Position control system with fixed control structure and a stochastic disturbance.

$$G = \begin{bmatrix} 0 \\ 0 \\ 0 \\ 1 \end{bmatrix}$$

The performance index J has the form

$$J = \text{trace } CX \tag{A.9-7}$$

where

$$C = \begin{bmatrix} c_1 & c & 0 & 0 \\ c & 0 & 0 & 0 \\ 0 & 0 & 1 & 0 \\ 0 & 0 & 0 & 0 \end{bmatrix} \tag{A.9-8}$$

$$X = \begin{bmatrix} x_{11} & x_{12} & x_{13} & x_{14} \\ x_{21} & x_{22} & x_{23} & x_{24} \\ x_{31} & x_{32} & x_{33} & x_{34} \\ x_{41} & x_{42} & x_{43} & x_{44} \end{bmatrix} \tag{A.9-9}$$

The computations are initiated with a set of parameter values which result in an asymptotically stable solution. Initial solution stability is mandatory if positive definite solutions for X and P are to exist. The initial value for p_1 was

$$p_1 = -3.0 \tag{A.9-10}$$

The initial position, velocity, and effector response to a white noise disturbance are shown in Fig. A.9-2. The optimal parameter value was

$$p_1 = -13.87 \tag{A.9-11}$$

The corresponding responses for the optimal system are shown in Fig. A.9-3. The mean-square values of the initial and optimal solutions are shown in Table A.9-I.

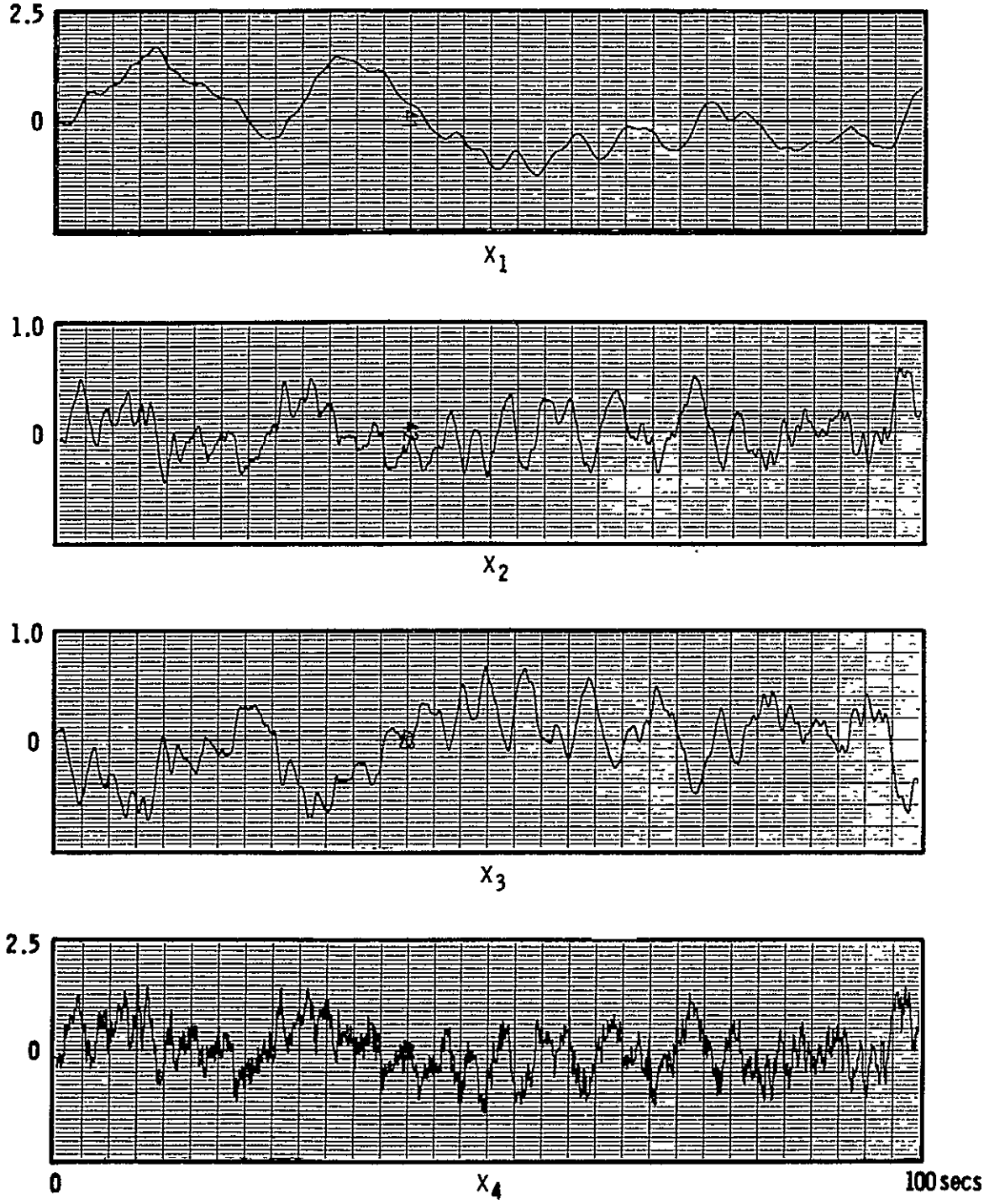

Fig. A.9-2 | Inertial system response to white noise. ($p_1 = -3.0$)

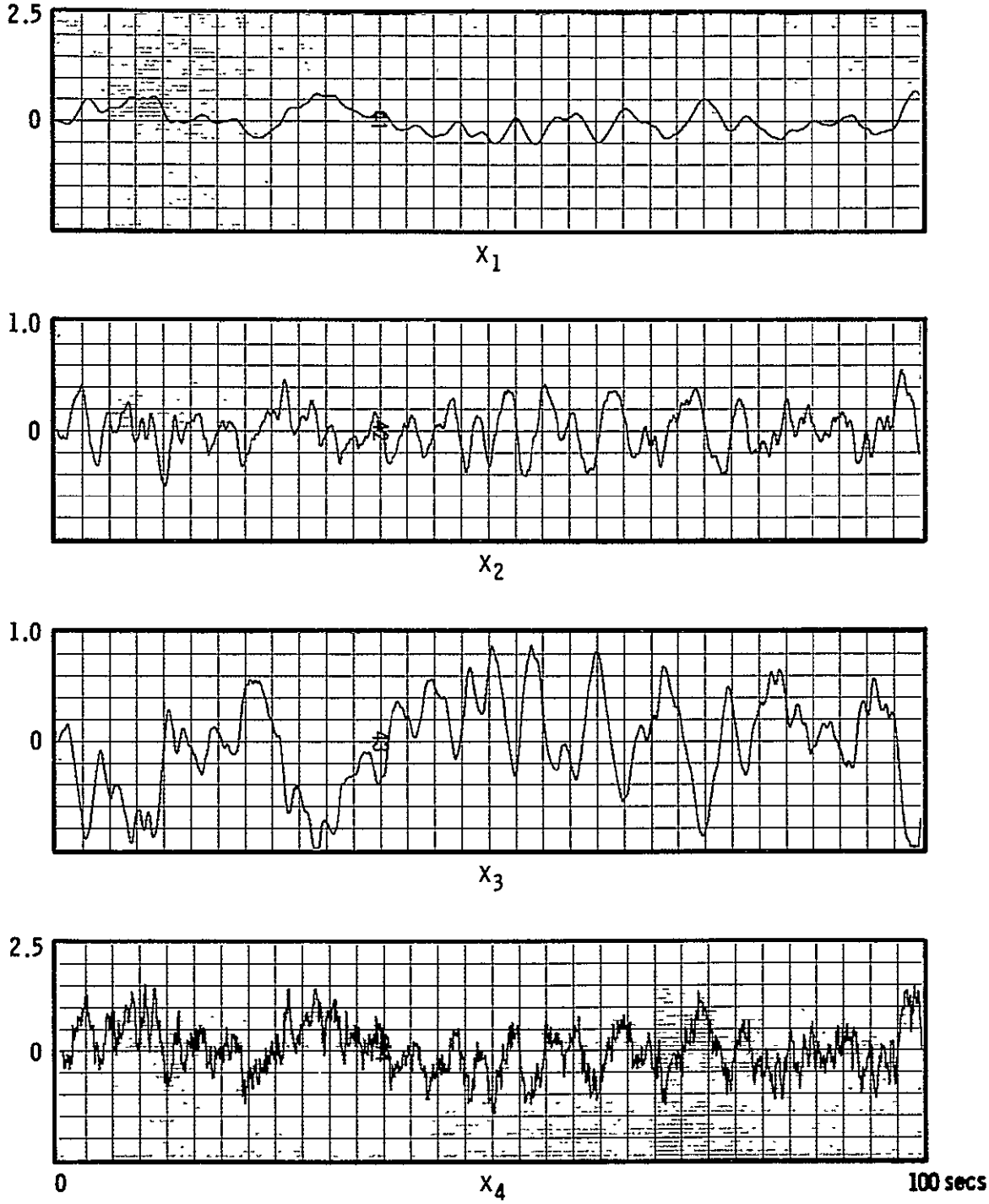

Fig. A.9-3 Optimized system response to white noise. ($p_1 = -13.87$)

Table A.9-I
Initial and Optimal Mean Square Values.

	INITIAL SOLUTION	OPTIMAL SOLUTION
x_1	0.766	0.129
x_2	0.0805	0.0652
x_3	0.148	0.311
x_4	0.500	0.500

The convergence characteristics of the various optimization algorithms may be compared by plotting J and the length of the gradient vector, $|J_p|$, and p_1 as functions of the iteration number NIC. These characteristics are illustrated in Figs. A.9-4, A.9-5, and A.9-6. The initial value of the step-size control variable was 2.0. Computation was terminated at the end of 10 iterations.

Some conclusions may be drawn from these results:

1. The Steepest Descent and Average Gradient algorithms appear to converge rapidly when p is some distance from p_{opt} (J_p large). Convergence near the optimum value is very slow (J_p small).
2. The quadratic convergence algorithms, Newton Raphson, Conjugate Gradient, Davidon, and Powell converge very quickly when p is near p_{opt} and if the problem is quadratic in p. However, more care must be taken in their application to insure solution stability.

A.10 Selection of the Optimization Algorithm

The control scientist must select an algorithm from the preceeding array to solve the problem at hand. The choice is usually determined by considerations such as:

1. Convergence rate
2. Numerical errors
3. Computation time

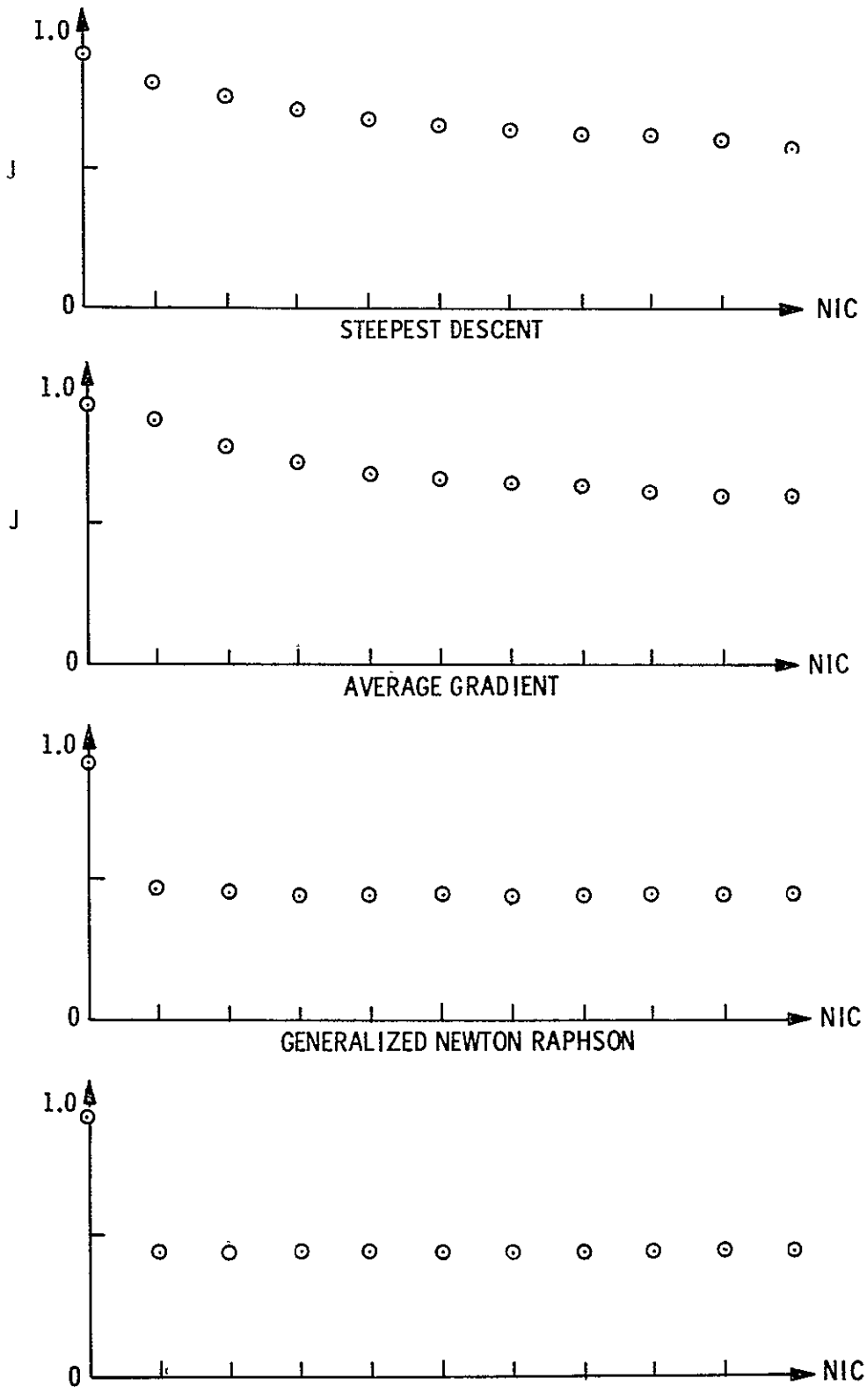

Fig. A.9-4 Performance index versus iteration number.

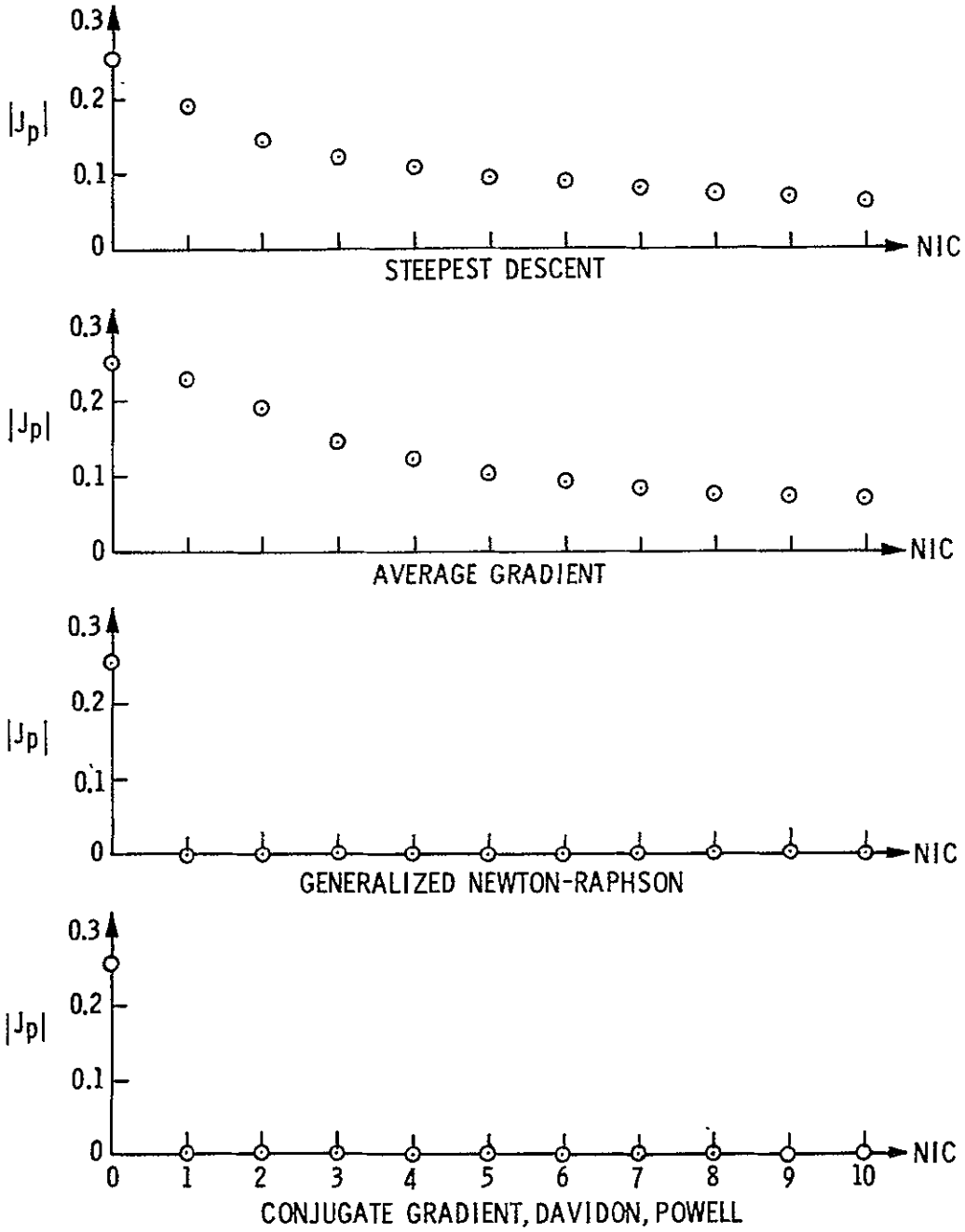

Fig. A.9-5 Gradient vector length versus iteration number.

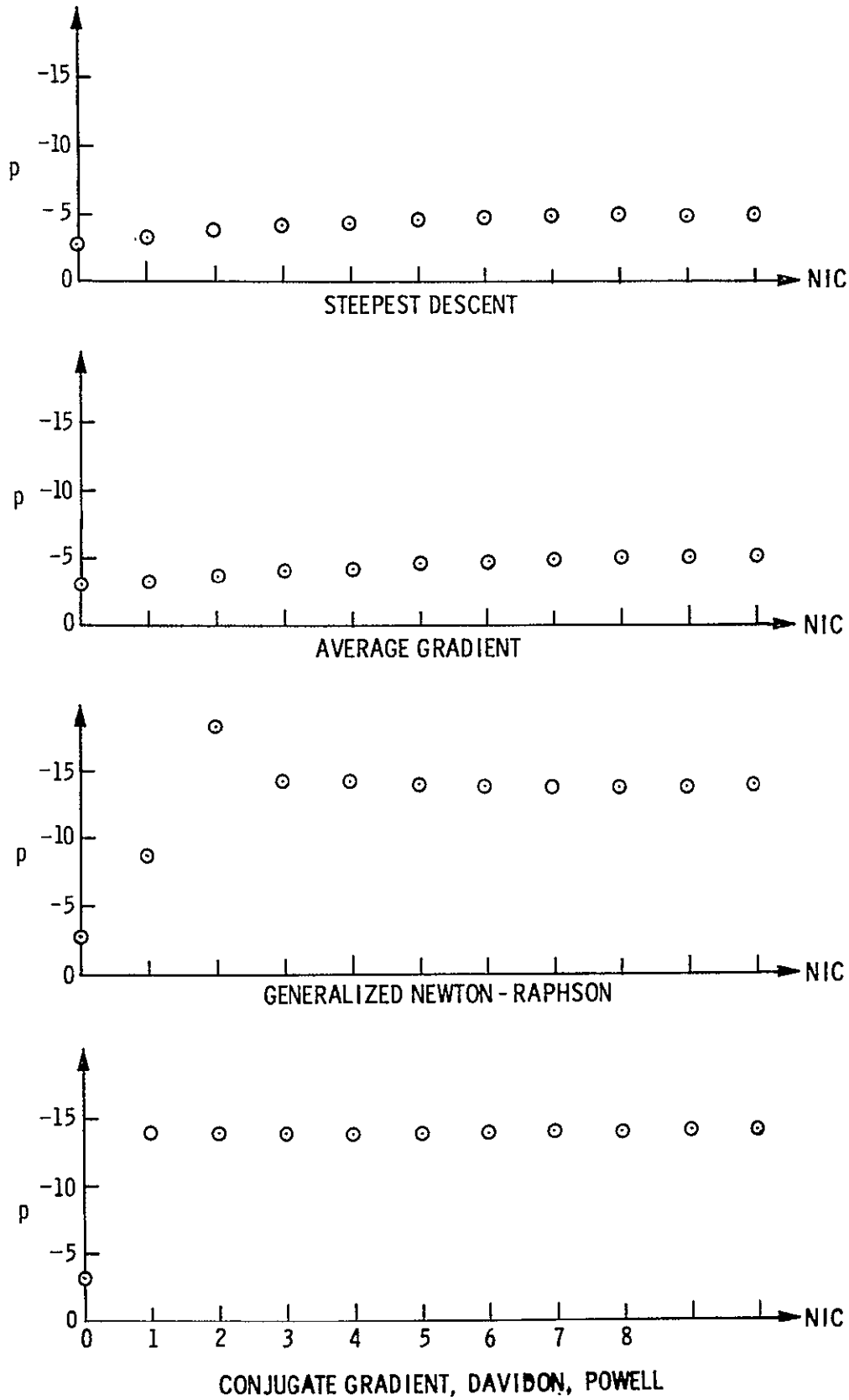

Fig. A.9-6 Parameter value versus iteration number. (p_{opt} = 13.87)

Initial optimization from a suboptimal starting solution is efficiently carried out using the Steepest Descent* or Average Gradient* algorithms which display a high rate of convergence when p is some distance from the optimum value. As the optimum is approached, the slow convergence of Steepest Descent and Average Gradient algorithms weighs heavily in favor of algorithms such as Newton Raphson, Conjugate Gradient, Davidon, and Powell, which display high rates of convergence where $\underset{\sim}{p}$ is in the vicinity of p_{opt}, justifying the increase in computation time per iteration. Numerical problems often preclude the application of the Generalized Newton Raphson technique as a result of errors arising in the estimation and inversion of the matrix J_{pp}.

Appendix A References

1. Bellman, K., (Editor), "Modern Analytic and Computational Methods in Science and Mathematics", American Elsevier Publishing Company, Inc., New York, 1968.
2. Rediess, H.A., "A New Model Performance Index for the Engineering Design of Control Systems", MIT Thesis TE-26, December 9, 1968.
3. Merrian, C.W., "Unpublished Lecture Notes", Cornell University, 1966.
4. Widnall, W.S., "Applications of Optimal Control, Theory to Computer Controller Design", MIT Research Monograph No. 48, MIT Press, 1968.

* Considerable success has been achieved using accelerated versions of Steepest Descent and Average Gradient (i.e., with algorithms which increase ϵ).

APPENDIX B N70-34335

NONLINEAR VEHICLE MODELS

by
Paul A. Madden

B.1 Introduction

Initially, the nonlinear aircraft and trajectory equations are presented without derivation. A reference frame and axis system is then defined, followed by the development of a set of perturbation equations. The latter serve as the mathematical model for simulation of aircraft flight in a noisy atmosphere from an unaccelerated reference flight condition.

All assumptions and simplifications are discussed during development of the equations. The linear aerodynamic model is outlined as is the manner in which ground effect and aerodynamic noise are incorporated. Tables listing all the equation coefficients and values for these coefficients pertinent to a specific approach-to-landing flight condition are presented.

The method of simulation of random aerodynamic noise, including wind shear, is presented and also the additional equations necessary to represent the elastic degrees of freedom of a flexible aircraft.

Finally, linearization of the nonlinear equations is discussed with particular longitudinal and lateral models being delineated in a further appendix.

Simulation of a large Space Shuttle in the landing-approach flight condition is essentially identical to simulation of any large aircraft in this flight condition. The requirement that any developed Space Shuttle should demonstrate flight characteristics similar to a conventional large jet transport in the landing approach is further evidence of this near identity.

All the elements essential to the simulation of the one are necessary for the simulation of the other.

When physical and aerodynamic characteristics of the space shuttle are better defined, there will be for the most part a one-to-one exchange with like parameters

of the jet transport. This will be so if simulation of the rigid-body response only is involved. Depending upon the Space Shuttle configuration, there may be more or less similarity in the manner in which the flexible modes are simulated and in the actual elastic-mode response.

B.2 The Aircraft Nonlinear Equations of Motion

The general rigid-body nonlinear equations of motion have been derived often in the literature, for example in ref. 1, and will not be rederived here. The equations are written with respect to an orthogonal set of axes fixed in the aircraft. The convention adopted for the axes, Euler angles, and rates is defined in Fig. B.2-1. The equations are

Lift

$$Z = -mg \cos\Theta \cos\Phi + m (\dot{W} + PV - QU)$$

Drag

$$X = mg \sin\Theta + m (\dot{U} + QW - RV)$$

Side Force

$$Y = -mg \cos\Theta \sin\Phi + m (\dot{V} + RU - PW)$$

Pitch

$$M = B\dot{Q} + RP (A - C) + E (P^2 - R^2)$$

Roll

$$L = A\dot{P} - E\dot{R} + QR (C - B) - EPQ$$

Yaw

$$N = - E\dot{P} + C\dot{R} + PQ (B - A) + EQR \qquad \text{(B.2-1)}$$

Euler angle rate equations

$$\begin{bmatrix} \dot{\Phi} \\ \dot{\Theta} \\ \dot{\Psi} \end{bmatrix} = \begin{bmatrix} 0 & \cos\Phi & -\sin\Phi \\ 1 & \sin\Phi \tan\Theta & \cos\Phi \tan\Theta \\ 0 & \sin\Phi \sec\Theta & \cos\Phi \sec\Theta \end{bmatrix} \begin{bmatrix} P \\ Q \\ R \end{bmatrix} \qquad \text{(B.2-2)}$$

Trajectory equations

The aircraft trajectory equations require that the orientation of the aircraft be specifically defined and this is done in Fig. B.2-1. It should be remembered that the trajectory equations are written with respect to an inertial frame which is not necessarily earth-fixed. To obtain the trajectory of the aircraft in earth-fixed coordinates, the velocity of the inertial frame with respect to earth must be added vectorially to the following inertial velocities.

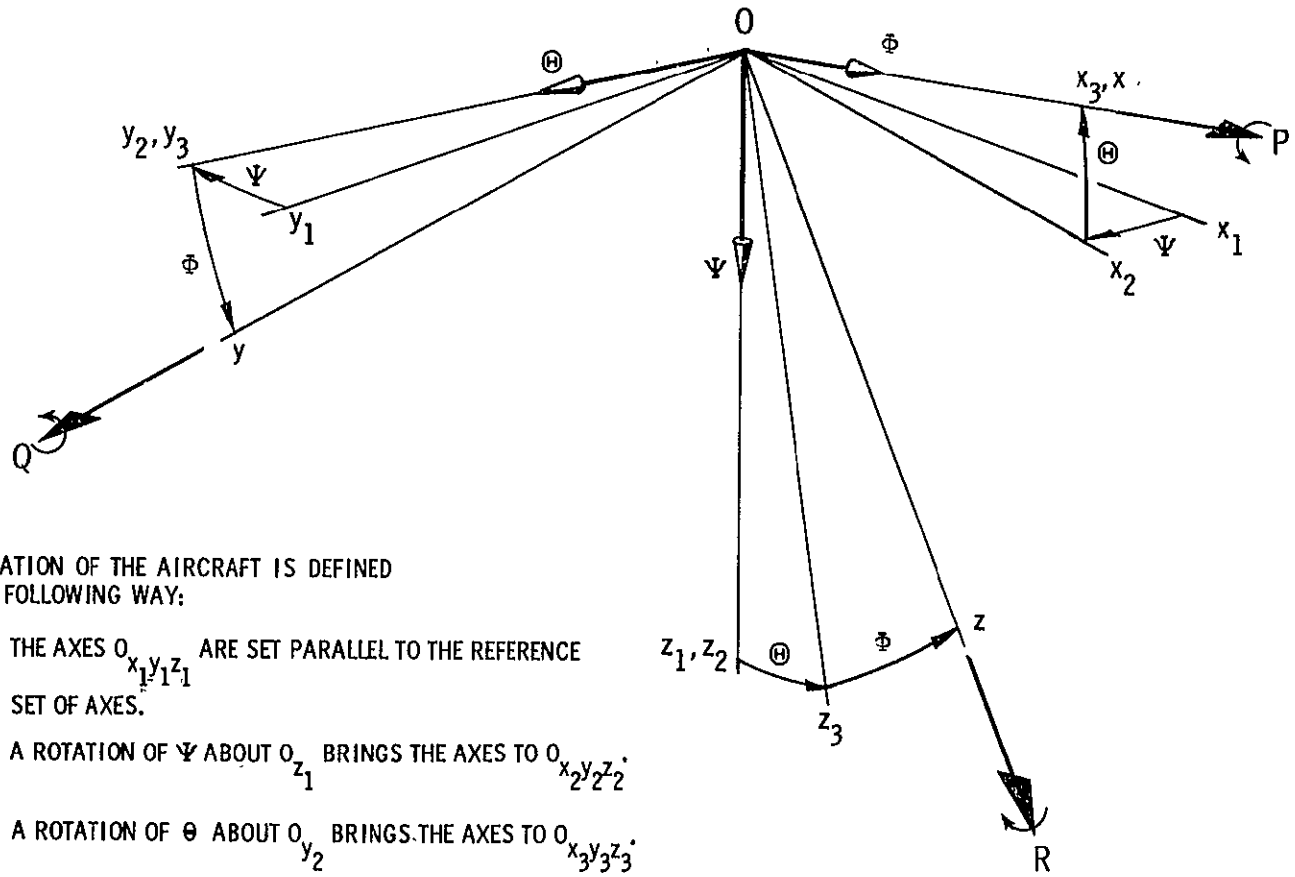

ORIENTATION OF THE AIRCRAFT IS DEFINED IN THE FOLLOWING WAY:

1) THE AXES $O_{x_1y_1z_1}$ ARE SET PARALLEL TO THE REFERENCE SET OF AXES.
2) A ROTATION OF Ψ ABOUT O_{z_1} BRINGS THE AXES TO $O_{x_2y_2z_2}$.
3) A ROTATION OF Θ ABOUT O_{y_2} BRINGS THE AXES TO $O_{x_3y_3z_3}$.
4) A ROTATION OF Φ ABOUT O_{x_3} BRINGS THE AXES TO THE FINAL POSITION, O_{xyz}.

Fig. B.2-1 Euler angle set.

$$\begin{bmatrix} \dot{x}_i \\ \dot{y}_i \\ \dot{z}_i \end{bmatrix} = \begin{bmatrix} \cos\theta\cos\psi & \sin\phi\sin\theta\cos\psi - \cos\phi\sin\psi & \cos\phi\sin\theta\cos\psi + \sin\phi\sin\psi \\ \cos\theta\sin\psi & \sin\phi\sin\theta\sin\psi + \cos\phi\cos\psi & \cos\phi\sin\theta\sin\psi - \sin\phi\cos\psi \\ -\sin\theta & \sin\phi\cos\theta & \cos\phi\cos\theta \end{bmatrix} \begin{bmatrix} U \\ V \\ W \end{bmatrix} \qquad \text{(B.2-3)}$$

Choice of Inertial Frame

The only stipulation upon choice of the inertial frame is that it be unaccelerated. For simulation of quiet-atmosphere aircraft response, the simplest set of equations result when the inertial frame is chosen to be earth-fixed. However, for simulation involving a noisy atmosphere, the most convenient equations evolve when the inertial frame is fixed in the unaccelerated air mass associated with the reference steady-state flight condition.

Choice of Axes

The equations set down in the preceding sections are valid for any orthogonal axes fixed in the aircraft, with origin at the mass center, and known as body axes.

Any set of body axes may be chosen but it is most convenient to choose O_x such that it points in the direction of motion of the aircraft in a reference condition of steady symmetric flight. In this case, the reference values of V and W are zero, and the axes are termed stability axes. These are the axes adopted in the derivations of following sections owing to their resulting simplifications in the equations of motion and aerodynamic force expressions.

B.3 Perturbation Expansion of the Equations of Motion

Changes in the time-dependent variables from the reference steady-flight condition are now introduced in the manner,

$$U(t) = U_0 + u(t) \qquad \text{(B.3-1)}$$

similarly, the aerodynamic forces and moments (including thrust components),

$$X(t) = X_0 + \Delta X. \qquad \text{(B.3-2)}$$

It is understood that an effective aerodynamic perturbation is the sum of a component due to inertial response of the aircraft and a component due to aerodynamic

noise, viz.,

$$u(t) = u_i(t) + u_n(t) \tag{B.3-3}$$

Reference Flight Condition

The initial reference state is restricted to unaccelerated flight in an unaccelerated atmosphere. The adoption of a stability axes set defines

$$\begin{aligned} V_0 &= 0 \\ W_0 &= 0 \end{aligned} \tag{B.3-4}$$

Some additional assumptions have been made about the initial reference state. Although not essential, they considerably simplify the equations of motion with no important loss of generality. These further assumptions involve the initial values of aircraft pitch, roll, and yaw rates and aircraft roll attitude, all considered zero.

$$\begin{aligned} q_0, p_0, r_0 &= 0 \\ \phi_0 &= 0 \end{aligned} \tag{B.3-5}$$

The Perturbed Equations of Motion

Substitution of the expressions for perturbed quantities, adoption of a stability axes set, and cognizance of the further assumptions (eq. B.3-5) lead to the following equations

$$\begin{aligned} Z_0 + \Delta Z &= -mg\cos\Theta\cos\Phi + m(\dot{w} + pv - qu - qU_0) \\ X_0 + \Delta X &= mg\sin\Theta + m(\dot{u} + qw - rv) \\ Y_0 + \Delta Y &= -mg\cos\Theta\sin\Phi + m(\dot{v} + rU_0 + ru - pw) \\ M_0 + \Delta M &= B\dot{q} + rp(A - C) + E(p^2 - r^2) \\ L_0 + \Delta L &= A\dot{p} - Er + qr(C - B) - pqE \\ N_0 + \Delta N &= -E\dot{p} + C\dot{r} + pq(B - A) + qrE \end{aligned} \tag{B.3-6}$$

The reference flight condition is extracted by setting the perturbation quantities equal to zero

$$\begin{aligned} Z_0 + mg\cos\theta_0 &= 0 \\ X_0 - mg\sin\theta_0 &= 0 \\ Y_0 &= 0 \\ M_0 &= 0 \\ L_0 &= 0 \\ N_0 &= 0 \end{aligned} \tag{B.3-7}$$

substitution of Eq. B.3-7 in Eq. B.3-6 and neglect of second-order terms lead to the perturbation equations which may be written

$$\begin{aligned}
\Delta Z &= mg\cos\theta_0(1 - \sec\theta_0\cos\theta\cos\phi) + m(\dot{w} + pv - qU_0 - qu)\\
\Delta X &= mg\cos\theta_0(\sec\theta_0\sin\theta - \tan\theta_0) + m(\dot{u} - rv)\\
\Delta Y &= -mg\cos\theta\sin\phi + m(\dot{v} + rU_0 + ru)\\
\Delta M &= B\dot{q}\\
\Delta L &= A\dot{p} - E\dot{r}\\
\Delta N &= -E\dot{p} + C\dot{r}
\end{aligned} \qquad \text{(B.3-8)}$$

It should be noted that, in view of Eq. B.3-3, quantities like qu, pv, are not necessarily small (second-order). An approach to landing in a noisy atmosphere involves flight through turbulence and a wind gradient (shear), the sum of which constitutes terms like u_n. The response of the aircraft is such that the effective aerodynamic perturbationexpressed as Eq. B.3-3 is always small. Inasmuch as u_n is constituted of a fluctuating component (turbulence) superimposed upon what may be a large drift component due to wind shear, the inertial quantity u_i will be nearly equal in magnitude but opposite (in sign) to u_n. It is the inertial quantities that are involved in the terms qu, pv referred to above.

B.4 The Aerodynamic Forces and Moments

A general force or moment change from the reference flight condition is represented by a Taylor series expansion

$$\Delta F \text{ (or } M) = g'x + \frac{1}{2}x'Ax + \text{higher-order terms.}$$

The first term of the expansion constitutes the quasi-steady (or linear) aerodynamic model where g is the vector of first-order derivatives (the stability derivatives) and x is the state vector.

All derivatives are evaluated at the reference flight condition; their nondimensional forms are usually referred to as the aircraft stability derivatives arising from their use in classical aircraft stability analysis. The stability derivatives together with trim aerodynamic quantities constitute the conventional characterization of the aircraft aerodynamics at a particular flight condition.

Ground Effect

An extraordinary aerodynamic perturbation occurs when the aircraft approaches close to the ground.

In this situation the ground plane inhibits the normal downward-induced flow, increasing the lifting efficiency of the aircraft. Associated with this effect is usually a nose-down pitching moment which correction reduces to some extent the gain in lifting efficiency.

The nonlinear aerodynamic corrections are accomplished in the following way.

Changes in affected stability derivatives are approximated by

$$\Delta C = K(C_{ige} - C_{oge})$$

where

C_{ige} is the coefficient value in full ground effect

C_{oge} is the coefficient value out of ground effect

and K is given by a parabolic function typical of the aircraft type. For the subsonic jet transport class

$$K \doteqdot 0.52\, s^2 - 1.21\, s + 0.75$$

where s is the aircraft altitude in semi-spans.

In addition to the derivative changes, there are net changes in the trim values of both lift and drag.

B.5 Equations of Motion as Mechanized in the Digital Simulation

Substitution of the aerodynamic force and moment changes into the perturbation equations (B.3-8) results in the following quiet-atmosphere aircraft equations of motion

Lift

$$\begin{aligned}\dot{\alpha} = \frac{1}{C}\Big[& C_\alpha \alpha + C_q q + C_u u \\ & + C_{\delta_e}\delta_e + C_{\delta_{te}}\delta_{te} + C_{\delta_s}\delta_s \\ & + C_{\beta p}\beta p + C_{qu} qu + C_{\Delta t}\Delta t \\ & + C_{L_0}(1 - \sec\theta_0 \cos\theta \cos\phi) \\ & + \langle \Delta C_L + \Delta C_D \alpha \rangle^* \Big]\end{aligned}$$

*<> terms are finite when aircraft is in ground-effect; zero otherwise.

Drag

$$\dot{u} = \frac{1}{C}\Big[C_u u + C_\alpha \alpha + C_{\delta_s}\delta_s + C_{r\beta} r\beta + C_{\Delta t}\Delta t + C_{L_0}(\sec\theta_0 \sin\theta - \tan\theta_0) + \langle \Delta C_D + \Delta C_L \alpha \rangle\Big]$$

Side Force

$$\dot{\beta} = \frac{1}{C}\Big[C_\beta \beta + C_r r + C_p p + C_{L_0}(\sec\theta_0 \cos\theta \sin\phi) + C_{\delta_s}\delta_s + C_{\delta_r}\delta_r + C_{\delta_a}\delta_a + C_{\delta_{tr}}\delta_{tr} + C_{ru} ru\Big]$$

Pitch

$$\dot{q} = \frac{1}{C}\Big[C_u u + C_{\dot{\alpha}}\dot{\alpha} + C_\alpha \alpha + C_q q + C_{\delta_e}\delta_e + C_{\dot{\delta}_e}\dot{\delta}_e + C_{\delta_{te}}\delta_{te} + C_{\delta_s}\delta_s + C_{\Delta t}\Delta t\Big] + \langle \Delta C_m \rangle$$

Roll

$$\dot{p} = \frac{1}{C}\Big[C_\beta \beta + C_p p + C_{\dot{r}}\dot{r} + C_r r + C_{\delta_a}\delta_a + C_{\delta_s}\delta_s + C_{\delta_r}\delta_r + C_{\delta_{ta}}\delta_{ta} + C_{\delta_{tr}}\delta_{tr}\Big]$$

Yaw

$$\dot{r} = \frac{1}{C}\Big[C_\beta \beta + C_p p + C_{\dot{p}}\dot{p} + C_r r + C_{\delta_a}\delta_a + C_{\delta_s}\delta_s + C_{\delta_r}\delta_r + C_{\delta_{ta}}\delta_{ta} + C_{\delta_{tr}}\delta_{tr}\Big] \qquad \text{(B.5-1)}$$

Perturbations due to Aerodymanic Noise Input

$$\Delta\dot{\alpha} = \frac{1}{C}\left[N_\alpha \alpha_n + N_q q_n + N_u u_n + N_{\dot{\alpha}} \dot{\alpha}_n\right]$$

$$\Delta\dot{u} = \frac{1}{C}\left[N_u u_n + N_\alpha \alpha_n\right]$$

$$\Delta\dot{\beta} = \frac{1}{C}\left[N_\beta \beta_n + N_r r_n + N_p p_n\right]$$

$$\Delta\dot{q} = \frac{1}{C}\left[N_u u_n + N_\alpha \alpha_n + N_{\dot{\alpha}} \dot{\alpha}_n + N_q q_n\right]$$

$$\Delta\dot{p} = \frac{1}{C}\left[N_\beta \beta_n + N_p p_n + N_r r_n\right]$$

$$\Delta\dot{r} = \frac{1}{C}\left[N_\beta \beta_n + N_p p_n + N_r r_n\right] \qquad \text{(B.5-2)}$$

Hinge Moment Equations

The dynamics of the aerodynamic effectors downstream of the control servos are represented by the hinge-moment equations. The space shuttle may employ direct force or aerodynamic effectors or a combination of both.

The hinge-moment equations associated with the aerodynamic effectors and servo tabs of a conventional aircraft are

Elevator

$$\ddot{\delta}_e = HE_\alpha \alpha + HE_{\delta_e} \delta_e + HE_{\dot{\delta}_e} \dot{\delta}_e + HE_{\delta_{te}} \delta_{te} - \dot{q}$$

Aileron

$$\ddot{\delta}_a = HA_\beta \beta + HA_p p + HA_{\delta_a} \delta_a + HA_{\dot{\delta}_a} \dot{\delta}_a + HA_{\delta_{ta}} \delta_{ta}$$

Rudder

$$\ddot{\delta}_r = HR_\beta \beta + HR_r r + HR_{\delta_r} \delta_r + HR_{\dot{\delta}_r} \dot{\delta}_r + HR_{\delta_{tr}} \delta_{tr} - \dot{r} \qquad \text{(B.5.3)}$$

where

$$\delta_{te} = \delta_e - \delta_e^s$$

$$\delta_{ta} = -\delta_a^s$$

$$\delta_{tr} = \delta_r - \delta_r^s$$

and δ_e^s, δ_a^s, δ_r^s are the elevator, aileron, and rudder control-servo outputs respectively.

Control Surface Actuators

The aileron, elevator, and rudder control surface actuators are all modeled by a second-order system with ω_n = 2.86 cps and damping ratio of 0.7. The transfer function of these servos is

$$\frac{\delta^s}{\delta^c} = \frac{324}{s^2 + 25.4s + 324}$$

The spoiler surface actuator is modeled by a first-order system with a time constant of 0.1 second.

Variables and Coefficients Defined

Define

$$\alpha = w/U_0$$
$$\beta = v/U_0$$

The variables α and β are referred to as angle-of-attack and sideslip angle respectively; a small-angle assumption is implied.

The equations of the previous section have been divided into longitudinal and lateral sets which for most aircraft are only weakly coupled for small rotational rates of motion.

Let μ, σ, and τ be defined by

	Longitudinal	Lateral
μ	$2m/\rho S\bar{c}$	$2m/\rho Sb$
σ	$\left(\frac{2}{\bar{c}}\right)^3/\rho S$	$\left(\frac{2}{b}\right)^3/\rho S$
τ	$\bar{c}/2U_0$	$b/2U_0$

Coefficients of the previous equations are defined in tables B.5-I and B.5-II in terms of the aircraft geometry, inertia constants, reference flight condition, and stability derivatives.

Table B.5-I

Coefficients Defined for the Longitudinal Equations

Coefficient \ Equation	Lift	Drag	Pitch
C	$\tau[C_{z_{\dot{\alpha}}} - 2\mu]$	$-2\tau\mu/U_0$	$\sigma\tau^2 I_{yy}$
C_α	$-C_{z_\alpha}$	$-C_{x_\alpha}$	C_{m_α}
C_q	$-\tau[2\mu + C_{z_q}]$	- - -	τC_{m_q}
C_u	$[2C_{L_0} - C_{z_u}]/U_0$	$-[C_{x_u} + C_{L_0}\tan\theta_0]/U_0$	C_{m_u}/U_0
C_{δ_e}	$-C_{z_{\delta_e}}$	- - -	$C_{m_{\delta_e}}$
$C_{\delta_{te}}$	$-C_{z_{\delta_{te}}}$	- - -	$C_{m_{\delta_{te}}}$
C_{δ_s}	$-C_{z_{\delta_s}}$	$-C_{x_{\delta_s}}$	$C_{m_{\delta_s}}$
$C_{\beta p}$	$2\tau\mu$*	- - -	- - -
C_{qu}	$-2\tau\mu/U_0$	- - -	- - -
$C_{\Delta t}$	$\sin\alpha_\epsilon/(1/2)\rho U_0^2 S$	$-\cos\alpha_\epsilon/(1/2)\rho U_0^2 S$	$z_\epsilon/(1/2)\rho U_0^2 \bar{c}\, S$
$C_{r\beta}$		$-2\tau\mu$*	- - -
$C_{\dot{\alpha}}$	- - -	- - -	$\tau C_{m_{\dot{\alpha}}}$
$C_{\dot{\delta}_e}$	- - -	- - -	$\tau C_{m_{\dot{\delta}_e}}$
N_α	$-C_{z_\alpha}$	$-C_{x_\alpha}$	C_{m_α}
N_q	$-\tau C_{z_q}$	- - -	τC_{m_q}
N_u	$[2C_{L_0} - C_{z_u}]/U_0$	$-[-C_{x_u} + 2C_{L_0}\tan\theta_0]/U_0$	C_{m_u}/U_0
$N_{\dot{\alpha}}$	$-\tau C_{z_{\dot{\alpha}}}$	- - -	$\tau C_{m_{\dot{\alpha}}}$

*μ defined for the lateral equations.

Table B.5-II

Coefficients Defined for the Lateral Equations

Coefficients \ Equation	Side Force	Roll	Yaw
C	$2\tau\mu$	$\sigma\tau^2 I_{xx}$	$\sigma\tau^2 I_{zz}$
C_β	C_{y_β}	C_{ℓ_β}	C_{n_β}
C_r	$\tau\left[C_{y_r} - 2\mu\right]$	τC_{ℓ_r}	τC_{n_r}
C_p	τC_{y_p}	τC_{ℓ_p}	τC_{n_p}
C_{δ_a}	$C_{y_{\delta_a}}$	$C_{\ell_{\delta_a}}$	$C_{n_{\delta_a}}$
$C_{\delta_{ta}}$	- - -	$C_{\ell_{\delta_{ta}}}$	$C_{n_{\delta_{ta}}}$
C_{δ_r}	$C_{y_{\delta_r}}$	$C_{\ell_{\delta_r}}$	$C_{n_{\delta_r}}$
$C_{\delta_{tr}}$	$C_{y_{\delta_{tr}}}$	$C_{\ell_{\delta_{tr}}}$	$C_{n_{\delta_{tr}}}$
C_{δ_s}	$C_{y_{\delta_s}}$	$C_{\ell_{\delta_s}}$	$C_{n_{\delta_s}}$
C_{ru}	$-2\mu\tau/U_0$	- - -	- - -
$C_{\dot{r}}$	- - -	$\sigma\tau^2 I_{zx}$	- - -
$C_{\dot{p}}$	- - -	- - -	$\sigma\tau^2 I_{zx}$
N_β	C_{y_β}	C_{ℓ_β}	C_{n_β}
N_r	τC_{y_r}	τC_{ℓ_r}	τC_{n_r}
N_p	τC_{y_p}	τC_{ℓ_p}	τC_{n_p}

Physical and aerodynamic characteristics of the aircraft adopted for the space shuttle simulation appear in Appendix C.

B.6 Structural Flexibility

When separation in frequency between the elastic degrees of freedom and the rigid-body modes is not large, significant coupling can occur.

The coupling can arise directly from the aerodynamic forces generated by aircraft rigid-body response or indirectly through control-system response to sensors mounted upon the flexible structure. The latter coupling has generally been the most important for large aircraft in the low-airspeed, landing-approach flight condition.

While there are several ways in which the dynamic equations of elastic motion may be formulated, the method chosen for the simulation was to represent the deformation of the elastic aircraft in terms of its normal modes of free vibration. This is a direct approach which requires prior knowledge of the normal modes and their frequencies.

Equations of Elastic Motion Assuming Normal Modes

For n modes, the deflection from the principal axes is

$$w(t) = \sum \phi_i q_i(t) \qquad i = 1,n \tag{B.6-1}$$

where ϕ_i are the normal modes and q_i are the generalized coordinates.

The generalized coordinates are determined from the n second-order equations (neglecting structural damping)

$$\ddot{q}_i + \omega_i^2 q_i = Q_i \qquad i = 1,n \tag{B.6-2}$$

which may be transformed into the $2n$ first-order equations

$$\begin{aligned} \dot{f}_i &= -\omega_i^2 q_i + \frac{1}{M_i} Q_i \\ \dot{q}_i &= f_i \qquad\qquad i = 1,n \end{aligned} \tag{B.6-3}$$

where M_i, Q_i are the generalized mass and generalized force, respectively, of the i^{th} mode; f_i is a transformation variable. M_i and Q_i are defined

$$M_i = \int_S \int \phi_i^2 \, m \, ds$$

$$Q_i = \int_S \int F_n \phi_i \, ds \qquad \text{(B.6-4)}$$

The simple form of Eq. B.6-2 was the direct result of the choice of normal (orthogonal) modes; the resulting simplification being the inertial and elastic decoupling of the equations. Further, the equations of elastic motion are decoupled (inertially and elastically) from the rigid-body modes which are, in fact, the zeroth normal modes of the eigensystem.

The equations, nevertheless, are coupled aerodynamically. This is because the generalized force Q_i is a function of q_i, $\dot{q}_i$(all i) though its dependence upon the elemental normal force, F_n, acting upon the aircraft. F_n includes only aerodynamic forces because of the property of inertial independence of normal modes, and hence independence from the rigid-body degrees of freedom.

Further, F_n need include only symmetric aerodynamic forces if the particular mode ϕ_i is symmetric, and only antisymmetric forces if ϕ_i is also antisymmetric.

There is additionally aeroelastic coupling back to the rigid-body equations because the elastic deflections cause aerodynamic force perturbations that must be included in the forcing of the zeroth mode equations just as the rigid aircraft response forces the elastic modes.

Evaluation of F_n is, by far, the most difficult chore in the aircraft dynamic simulation. Expressions for the aerodynamic forces due to aeroelastic effects, and similarly the importance of nonlinear aerodynamic effects, are highly configuration-dependent. Unsteady aerodynamic effects that involve attenuation and lags to the airforces must, in general, be included. However, for the lowest structural frequencies which may be of primary concern to the control and guidance problem, a quasi-steady approximation can usually be made that neglects the small phase lag and is modified to include an attenuation factor. As the frequency of the structural mode of concern increases, so does the phase lag and attenuation of the associated airforces and their inclusion is of importance. However, the response of these higher-frequency modes may not be of central concern.

Similar difficulties arise in the evaluation of airforces associated with higher-frequency gust inputs.

Currently, the CV880 digital simulation includes the two lowest frequency symmetric flexible modes with frequencies of 1.6 and 4.4 cps, respectively. Inclusion of phase shift in evaluating the aeroelastic damping at these frequencies produced no discernable change in response as compared to that obtained using the simpler modified quasi-steady theory. However, unsteady aerodynamic effects associated with gust inputs may be more important.

B.7 Atmospheric Noise

B.7.1 Introduction

The theory of flight through atmospheric turbulence has been extensively developed by many researchers and reported upon in many references. Of particular relevance are those of Etkin[1,3] and Foss and McCabe.[4]

Essentially, for typical operating speeds of aircraft, the gust field is assumed to have random spatial variation but to be frozen in time. It is further assumed to be locally homogeneous and isotropic so that only two power spectral density (PSD) functions are necessary to describe the statistics of the three gust-velocity components.

Variation of the longitudinal and vertical gust velocities over the span of the aircraft is neglected, allowing all three velocity components to be written solely as functions of the longitudinal axis coordinate.

B.7.2 Statistical description of atmospheric turbulence

The one-dimensional PSD functions used to describe the statistics of low-level turbulence are

$$\Phi_1(\omega) = \overline{w_g^2} \left(\frac{L}{\pi U_0}\right) \frac{1}{1 + (\omega \frac{L}{U_0})^2} \tag{B.7-1}$$

$$\Phi_{2,3}(\omega) = \overline{w_g^2} \left(\frac{L}{2\pi U_0}\right) \frac{1 + 3(\omega \frac{L}{U_0})^2}{\left[1 + (\omega \frac{L}{U_0})^2\right]^2} \tag{B.7-2}$$

where $\Phi_1(\omega)$, $\Phi_{2,3}(\omega)$, are the PSD functions of the longitudinal, lateral, and vertical

gust velocities respectively and where $\overline{w_g^2}$ is the mean-square gust velocity in $(\text{feet/sec})^2$, U_0 is the flight velocity in feet/sec, L is the scale of turbulence in feet, and ω is the frequency in radians/sec.

The spectrum $\Phi_{2,3}(\omega)$ may be approximated by[5]

$$\Phi_{2,3}(\omega) = \overline{w_g^2} \left(\frac{L}{3^{1/2}\pi U_0} \right) \frac{1}{1 + (\omega \frac{L}{3^{1/2} U_0})^2} \qquad \text{(B.7-3)}$$

The digital simulation makes use of the PSD functions given by Eq. B.7-1 and B.7-2. However, the linear models take advantage of the simpler first-order approximation for $\Phi_{2,3}(\omega)$ given by Eq. B.7-3

B.7.3 Simulation of atmospheric noise

Simulation of atmospheric noise implies the generation of time-varying functions whose statistics duplicate the spectrums of continuous atmospheric turbulence.

Exponentially correlated noise may be modeled by passing Gaussian white noise through a suitable shaping filter whose dynamics adjoin the existing system providing a new system subject only to white noise input.

Let the continuous white noise autocorrelation function be given by

$$\phi(\tau) = Q\delta(\tau) \qquad \text{(B.7-4)}$$

then its PSD function is

$$\Phi(\omega) = \frac{1}{2\pi} Q \qquad \text{(B.7-5)}$$

If Gaussian white noise is passed through a filter F, its output has the PSD given by

$$\Phi_n(\omega) = |F|^2_{s=i\omega} \Phi(\omega) \qquad \text{(B.7-6)}$$

For $F = \frac{a}{s + a}$, the output is

$$\Phi_n(\omega) = \frac{Q}{2\pi} \frac{1}{1 + (\frac{\omega}{a})^2} \qquad \text{(B.7-7)}$$

Equivalence of Eq. B.7-7 and the assumed empirical turbulence spectrum provides the values of correlation time and Q necessary to reproduce the spectrum. For $\Phi_{2,3}(\omega)$ given by Eq. B.7-3, this equivalence provides

$$\frac{1}{a} = \frac{L}{3^{1/2} U_0}$$

$$Q = 2 \overline{w_g^2} \left(\frac{1}{a}\right) \qquad \text{(B.7-8)}$$

The filter equation may then be written

$$\dot{n} = a(w - n) \qquad \text{(B.7-9)}$$

where n is the correlated noise output and w the Gaussian white noise input.

Evaluation of the constants involved in a second-order filter necessary to reproduce the spectrum, for example, given for $\Phi_{2,3}(\omega)$ by Eq. B.7-2 follows in a directly analogous manner.

It is not possible to provide a continuous signal representing Gaussian white noise in a digital simulation. The digital equivalent is a discrete series of uncorrelated random amplitude steps. For this step sequence, the autocorrelation function is

$$\phi(\tau) = \begin{cases} \sigma^2 \, (1 - |\tau|/\Delta T) & |\tau| \leq \Delta T \\ 0 & |\tau| > \Delta T \end{cases} \qquad \text{(B.7-10)}$$

where σ^2 is the mean-square value of the random step amplitudes and ΔT is the discrete time step. The associated PSD function, defined as

$$\Phi(\omega) = \frac{1}{2\pi} \int_{-\infty}^{\infty} \phi(\tau) \, e^{-j\omega\tau} d\tau \qquad \text{(B.7-11)}$$

is given by

$$\Phi(\omega) = \frac{\sigma^2}{2\pi} \left[\frac{\sin(\omega \Delta t)}{\omega} + j \left(\sin(\omega \Delta T) - \omega \Delta T \cos(\omega \Delta t) \right) \right] \qquad \text{(B.7-12)}$$

Considering only the long wavelengths $\left(\omega << \frac{2\pi}{\Delta t}\right)$, a small angle approximation may be used to give

$$\Phi(\omega) = \frac{\sigma^2 \Delta t}{2\pi} \qquad \omega << \frac{2\pi}{\Delta t} \qquad \text{(B.7-13)}$$

Equivalencing the above discrete-step approximation for the PSD of the white noise input with the previously given (Eq. B.7-5) continuous function provides

$$\sigma^2 = Q/\Delta T \tag{B.7-14}$$

For the example that led to the result for Q expressed by Eq. B.7-8, the root-mean-square value of the random-step amplitude would be

$$\sigma = \left[\frac{2\,\overline{w_g^2}\left(\frac{1}{a}\right)}{\Delta T}\right]^{1/2} \tag{B.7-15}$$

A block diagram, Fig. B.7-1, shows the operations which lead from a machine-generated random number sequence to a time history of gust velocity.

B.7.4 Effective Aerodynamic Noise Perturbations

The sequence of operations discussed in the last section and shown schematically in Fig B.7-1 leads to a time history of the three uncorrelated gust-velocity components u_1, u_2, and u_3.

A vertical gust produces an angle-of-attack disturbance and, because of its varying intensity along the length of the aircraft, an effective pitch disturbance. Similarly, a lateral gust-velocity component produces a sideslip and effective yaw disturbance.

The pitch and yaw disturbances may be approximately represented by effective pitch and yaw rate perturbations respectively, if the higher-frequency gust components are not admitted in evaluation of these effective rates. This is equivalent to the requirement that the gust component vary nearly linearly along the effective aerodynamic length of the aircraft. This requirement may be met with a lowpass unity-gain filter introduced in series. The break frequency of the filter is selected such that the shortest wavelength admitted is no less than about eight times the effective aerodynamic length of the aircraft. If ω_b is the break frequency, then

$$\omega_b \doteq 2\pi U_0/\lambda_{min} \tag{B.7-16}$$

with λ_{min} equal to 8 times the aircraft length.

In general, it has been observed[1,3] that neglect of the short wavelengths has negligible effect upon rigid-aircraft response; the energy content of these spectral

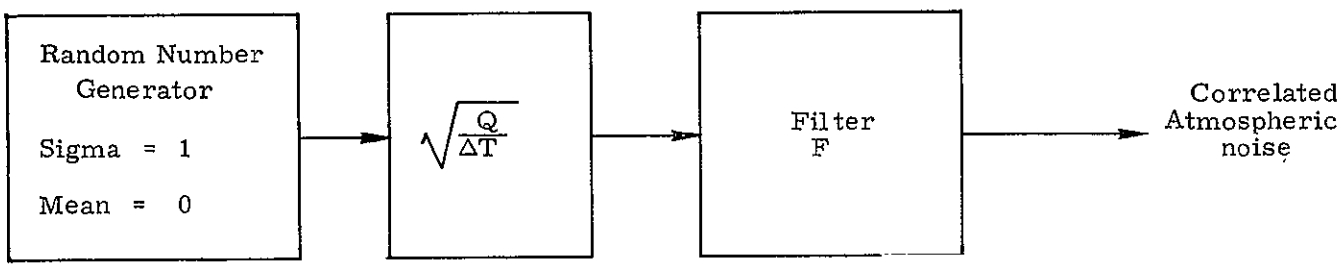

Figure B.7-1 Discrete step sequence to generate time correlated atmospheric noise component.

components is relatively small. Their inclusion, however, is of importance in the forcing of aircraft elastic modes.

It is recalled that the empirical PSD functions are functions of the longitudinal-axis coordinate only; spanwise variations in gust intensity are thereby neglected. It is not easily possible to simulate this variation with rigor. It may be approximately accounted for, however, by considering a span-averaged gust intensity.[4] The factor K is defined

$$K = \left[1 - 0.3\ \frac{b}{2L}\left(1 + \frac{b}{2L}\right)\right] \qquad b < L \tag{B.7-17}$$

where b is the wing span and L is the aircraft length. The factor K operates upon the mean-square gust intensity providing a span-averaged value. This is the gust intensity used when evaluating the vertical and longitudinal gust-velocity components. For the CV880M aircraft, K = 0.968.

The aerodynamic noise perturbations may now be expressed as functions of the gust-velocity components u_1, u_2, and u_3.

$$\begin{aligned} u_n &= u_1 \\ \alpha_n &= u_3/U_0 \\ \dot{\alpha}_n &= \dot{u}_3/U_0 \\ \beta_n &= u_2/U_0 \\ q_n &= -(\dot{u}_3)_f/U_0 \\ r_n &= (\dot{u}_2)_f/U_0 \end{aligned} \tag{B.7-18}$$

where the subscript f refers to the lowpass filtered component.

In addition to the above turbulence-induced components of aerodynamic noise, there exist also wind-shear-induced components. It is assumed that there is no mean vertical-velocity component to the air mass. The variations in mean air-mass velocity from the reference flight condition values due to wind shear must be added vectorially to the components u_n and β_n of B.7-18. The wind-shear-induced components are evaluated as the difference between the current mean wind speed (w_{mean}), developed in the next subsection, and the initial flight condition value.

B.7.5 Wind Shear

Operation of aircraft at low altitude involves flight in the thick turbulent boundary layer that extends from the surface of the earth up to an altitude of between 600 and 1500 feet, depending upon the mean wind speed at altitude, meteorological conditions, and ground terrain.

Wind shear has been modeled in basically two alternate ways. One involves constant wind shear between set altitudes, the wind-shear values and altitudes being input as data, and the other involves a wind shear inversely proportional to altitude resulting in the classical logarithmic velocity profile. The first model may be made to approximate the latter to any degree, depending upon the number of piecewise linear segments chosen.

In both models, the mean wind speed at altitude is specified and is constant above a specified altitude; the latter is chosen depending upon the strength of the former. A low wind-speed velocity profile is assumed to begin at about 600 feet while that for a strong wind may begin at about 1500 feet.

Assuming a one-segment model, the mean wind speed at any altitude h is given as

$$w_{mean} = (w_{mean})_0 - \tau_w(h_0 - h) \tag{B.7-19}$$

where τ_w is the constant wind shear and subscript 0 indicates the initial values.

For the logarithmic model, the relationship is

$$w_{mean} = (w_{mean})_0 \left[\frac{5 + 5.75 \log_{10}(h/r_0)}{5 + 5.75 \log_{10}(h_0/r_o)}\right] \tag{B.7-20}$$

where r_0 is a scale of the surface terrain roughness.

B.7.6 Estimation of the Turbulence Integral Scale Length and Intensity

At low altitudes, the turbulence resembles that in boundary layers adjacent to rough surfaces and is strongly affected by the terrain. The turbulence scale and intensity are a function of altitude, the gust field being, in general, neither homogeneous nor isotropic. The latter model, however, is probably the only acceptable

one at the present moment. Etkin,[3] after Panofsky, suggested that, based upon experiments over relatively smooth terrain, the turbulence scale length may be approximately given by

$$L \doteq 0.9\,h \tag{B.7-21}$$

up to 1000-foot altitude.

A semi-empirical relationship[3] for the variation of mean-square gust intensity with altitude and terrain roughness in unstable meterological conditions is

$$\overline{w_g^2} = \left[0.226(w_{mean}/\log_{10}(h/r_0)\right]^2 \tag{B.7-22}$$

where (w_{mean}) is the mean wind velocity at altitude h and r_0 is the scale of terrain roughness. Typical values of r_0 for low trees, crops, water or snow field are 10, 1, and 0.1 feet, respectively.

The simulation provides for an alternative model in which both gust intensity and turbulence scale length are constant-valued inputs.

B.8 Linear System Models

Linear control system studies depend upon the availability of acceptable linear models. The nonlinear aircraft and trajectory equations of previous sections can be linearized by application of a small-angle approximation and neglect of the nonlinear inertial-coupling terms. The latter grow to significant magnitude only after prolonged flight through a wind-shear condition; their exclusion in no way invalidates the equations for control-system studies.

Two linear models may be identified; both have been constructed to evaluate system response to turbulence. They are constituted as follows:

Aircraft longitudinal equations of motion
Z (altitude) trajectory equations
Control-surface actuator servos
First-order noise correlation equation for α (vertical) gusts.

Aircraft lateral equations of motion
Y (lateral) trajectory equations
Control-surface actuator servos
First-order noise correlation equation for β (side) gusts.

Some additional simplifications were made to render the models more tractable in demonstration of the parameter optimization approach to system design.

In both models, the hinge-moment equations associated with aerodynamic servo-tab-driven effectors were bypassed with the assumption of direct servo-driven effectors. The space shuttle may employ either direct force or aerodynamic effectors or a combination of both. A further simplification was the substitution of first-order for second-order actuator servo models. In all cases, perfect-state information was assumed in the feedback paths.

Insomuch as the linearized trajectory equations are linear combinations of the aircraft state equations, their inclusion implies redundancy. Consequently, the aircraft state equations were rewritten in terms of vertical and lateral acceleration rather than angle-of-attack (α) and sideslip (β). The explicit equations for the latter two variables were dropped.

All models were evaluated with a variety of control-law structures involving combinations of feedback variables to the specific effector(s) chosen for control of aircraft response.

Further assumptions and simplifications specific to the individual models are mentioned in Appendix C, where the models are fully delineated.

Appendices B and C References

1. Etkin, B., "Dynamics of Flight", Wiley, 1959.
2. "CV880M Data", Lear Siegler Report ADR-595.
3. Etkin, B., "Theory of Flight of Airplanes in Isotropic Turbulence - Review and Extension", AGARD Report No. 372, April, 1961.
4. Foss, K., McCade, W., Gust Loading of Rigid and Flexible Aircraft in Continuous Atmospheric Turbulence", (MIT) WADC Technical Report 57-704, January, 1958.

APPENDIX C

LINEAR VEHICLE MODELS

by

Paul A. Madden

C.1 Introduction

Notation common to this Appendix and Appendix B is firstly introduced in section C.2. Then the major dimensions, physical constants, and aerodynamic characteristics of the Convair 880M in a specific landing-approach flight condition are presented. This particular aircraft and flight condition serve as the basis for the space-shuttle landing simulation. The data listed in this section are derived from Ref. 2, in which the chosen flight condition was referred to as Flight Condition 1 (FC1).

The major dimensions are listed in Table C.3-I. The flight condition is defined in Table C.3-II and the related aircraft physical and aerodynamic characteristics also appear in Table C.3-II.

Two linear models designed to evaluate aircraft response to turbulence are developed in section C.4. They may be identified as a longitudinal model to evaluate response to vertical gusts, and a lateral model to evaluate response to side gusts.

The models are constituted by the linearized aircraft and trajectory equations, the servo actuator equations, and the noise correlation equation. After incorporation of the specific control law, the equations are set in the state-variable form:

$$\dot{x} = Fx + Gw$$

C.2. Notation

X, Y, Z	components of the external aerodynamic force on the aircraft
M, L, N	components of the external aerodynamic moment on the aircraft
P, Q, R	components of aircraft angular velocity
p, q, r	perturbations in P, Q, R

U, V, W	components of aircraft velocity vector
u, v, w	perturbations in U, V, W
Θ, Φ, Ψ	Euler angle set
θ, ϕ, ψ	perturbations in Θ, Φ, Ψ
A, B, C I_{xx}, I_{yy}, I_{zz}	moments of inertia about the x, y, z aircraft body axes respectively
D I_{yz}	product of inertia about y and z axes
E I_{xz}	product of inertia about x and z axes
F I_{xy}	product of inertia about x and y axes
m	mass of aircraft
g	acceleration due to gravity
ρ	air density
M	Mach number
S	reference wing area
b	wing span
$\overline{c}$	mean aerodynamic chord
z_ϵ	vertical displacement of engine thrust vector from aircraft cg.
α_ϵ	angle between the thrust vector and aircraft longitudinal body reference axis.
δ	aircraft aerodynamic effector angle
Δt	thrust perturbation

Subscripts

0	reference unaccelerated flight condition
i	inertial
n	aerodynamic noise
e	elevator
te	elevator tab
a	aileron
ta	aileron tab
r	rudder
tr	rudder tab
s	spoiler

Stability Derivatives

The aircraft stability derivatives are represented in standard NASA notation.[1]

C.3 Major Dimensions, Physical and Aerodynamic Constants of the CV880M Aircraft

Table C.3-I. Major dimensions of the Convair 880M jet transport.

Dimension	
Wing area, sq ft	2000.0
Wing span, ft	118.3
Wing mean aerodynamic chord, ft	18.94
Mean distance of engine thrust axis below cg, ft	1.0
Incidence of engine thrust axis, deg	0

C.3.1 Stability Derivatives

Some additional stability derivatives associated with the longitudinal equations are here additionally defined (for a stability-axes set).

Lift

$$C_{z_u} = -C_{L_0}(M^2/1 - M^2)$$

$$C_{z_\alpha} = -(C_{L_\alpha} + C_{D_0})$$

$$C_{z_q} = -C_{L_q}$$

$$C_{z_{\dot{\alpha}}} = -C_{L_{\dot{\alpha}}}$$

Drag

$$C_{x_u} = -2(C_{D_0} + C_{L_0}\theta_0) - MC_{D_M}$$

$$C_{x_\alpha} = C_{L_0} - C_{D_\alpha}$$

Pitch

$$C_{m_u} = MC_{m_M}$$

Table C.3-II

Physical and Aerodynamic Characteristics

Basic Flight Condition

U_0, ft/sec	280.0
Mach number	0.25
Dynamic pressure, lb/ft^2	92.6
Air density, slugs/ft^3	0.00238
Mass, slugs	3913
Weight, lb	126,000
α_{trim}, deg	4.32
Flaps, deg	30
Undercarriage	Up

Stability axes, million slug-ft^2	I_{xx}	1.15
	I_{yy}	2.45
	I_{zz}	3.59
	I_{xz}	0.

Longitudinal Derivatives		OGE	IGE
	C_{L_0}	0.68	
S	C_{D_0}	0.0799	
T	C_{L_α}	4.52	5.51
A	C_{L_q}	7.72	7.67
B	$C_{L_{\delta_e}}$	0.213	
I	$C_{L_{\delta_{te}}}$	0.0532	
L	$C_{L_{\delta_s}}$	-0.4	
I	C_{D_M}	0.0	
T	C_{D_α}	0.295	0.471
Y	$C_{D_{\delta_s}}$	0.0368	
	C_{m_α}	-0.903	-0.843
A	C_{m_q}	-12.08	-11.98
X	$C_{m_{\dot{\alpha}}}$	-4.13	
E	C_{m_u}	0.0	
S	$C_{m_{\delta_e}}$	-0.637	-0.767
	$C_{m_{\dot{\delta}_e}}$	-0.0174	
	$C_{m_{\delta_{te}}}$	-0.159	-0.192
	$C_{m_{\delta_s}}$	0.034	

Table C.3-II (Cont.)

Physical and Aerodynamic Characteristics

Basic Flight Condition

Lateral Derivatives		OGE
	C_{ℓ_β}	-0.1961
	C_{ℓ_r}	0.1983
S	C_{ℓ_p}	-0.381
T	$C_{\ell_{\delta_r}}$	0.0226
A	$C_{\ell_{\delta_a}}$	-0.0384
B	$C_{\ell_{\delta_{ta}}}$	-0.0056
I	$C_{\ell_{\delta_{tr}}}$	0.00266
L	$C_{\ell_{\delta_s}}$	0.0405
I	C_{n_β}	0.1387
T	C_{n_r}	-0.1852
Y	C_{n_p}	-0.0485
	$C_{n_{\delta_r}}$	-0.0958
	$C_{n_{\delta_a}}$	0.0172
A	$C_{n_{\delta_{ta}}}$	0.0
X	$C_{n_{\delta_{tr}}}$	-0.0192
E	$C_{n_{\delta_s}}$	0.0129
S	C_{y_β}	-0.877
	C_{y_r}	0.385
	C_{y_p}	0.0
	$C_{y_{\delta_r}}$	0.2155
	$C_{y_{\delta_{tr}}}$	0.0467
	$C_{y_{\delta_a}}$	0.0
	$C_{y_{\delta_{ta}}}$	0.0
	$C_{y_{\delta_s}}$	-0.0315

C.4 Linear Models

C.4.1 Linear Longitudinal Model Subject to Vertical Gusts

The linearized longitudinal perturbation equations may be written

$$\dot{u} = C_u u + C_\alpha \alpha + C_\theta \theta + C_{\alpha_n} \alpha_n + C_{\delta_s} \delta_s + C_{\Delta t} \Delta t \qquad \text{(C.4-1)}$$

$$\dot{\alpha} = C_u u + C_\alpha \alpha + C_q q + C_{\alpha_n} \alpha_n + C_{\delta_e} \delta_e + C_{\delta_s} \delta_s + C_{\delta_{te}} \delta_{te} \qquad \text{(C.4-2)}$$

$$\dot{q} = C_\alpha \alpha + C_{\dot{\alpha}} \dot{\alpha} + C_q q + C_{\alpha_n} \alpha_n + C_{q_n} q_n + C_{\delta_e} \delta_e + C_{\delta_{te}} \delta_{te} + C_{\delta_s} \delta_s + C_{\dot{\delta}_e} \dot{\delta}_e + C_{\Delta t} \Delta t \qquad \text{(C.4-3)}$$

$$\dot{\theta} = q$$

where u is measured in fps, g in deg/sec, and θ in degrees.

The control variables are defined as

δ_e - elevator angle, deg
δ_{te} - elevator tab angle, deg
δ_s - direct lift spoiler angle, deg
Δt - engine thrust, lb.

The coefficient values corresponding to the approach-to-landing flight condition of section C.3 are shown in Table C.4-I.

Airspeed Control

The low-frequency airspeed control dynamics are essentially decoupled from the short-period longitudinal dynamics; it is primarily the latter that are of concern when evaluating response to vertical gusts. Consequently, an airspeed control is postulated.

Reduction of the Order of the State

With the assumption of airspeed control ($\dot{u}$, u = 0), the $\dot{u}$ Eq. C.4-1 provides an expression for the change in thrust required to maintain $\dot{u}$ = 0. This expression is substituted into Eq. C.4-2 and C.4-3, together with the substitution, u = 0.

The further assumption that the aerodynamic effectors are directly controlled by the servo actuators bypasses the dynamics associated with aerodynamic servo tab controlled systems (the hinge-moment equations); the elevator tab terms, δ_{te},

Table C.4-I

Coefficient Values of Aircraft Longitudinal Equations of Motion

Coefficient \ Equation	$\dot{u}$	$\dot{\alpha}$	$\dot{q}$
C_u	-0.0271	-0.000855	0.
C_α	18.15	-0.778	-1.288
C_θ	-32.2		0.
C_q	0.	0.955	-0.586
C_{δ_e}	0.	-0.036	-0.909
$C_{\delta_{te}}$	0.	-0.009	-0.227
C_{δ_s}	-1.737	0.0678	0.0485
$C_{\Delta t}$	0.000255		0.414×10^{-6}
C_{α_n}	18.15	-0.778	-1.288
C_{q_n}	0.	0.	-0.586
$C_{\dot{\alpha}}$	0.	0.	-0.201
$C_{\dot{\delta}_e}$	0.	0.	-0.000845

are consequently dropped from Eq. C.4-2 and C.4-3.

A feedforward path is provided to the elevator to negate pitch directly due to spoiler displacement.

Trajectory Equations

The relevant linearized trajectory equations are

$$\ddot{z} = U_0 (\dot{\alpha} - q) / 57.3 \tag{C.4-5}$$

$$\dot{z} = \int_0^t \ddot{z}(\tau)\, d\tau \tag{C.4-6}$$

$$z = \int_0^t \dot{z}(\tau)\, d\tau \tag{C.4-7}$$

It is observed that Eq. C.4-5 is a linear combination of Eq. C.4-2 and C.4-4. Because angle-of-attack (α) is not required as a feedback variable (it being generally difficult to measure), the equations are rewritten in terms of vertical acceleration, $\ddot{z}$, rather than α. Substitution of Eq. C.4-2 into C.4-5 provides an expression for α in terms of $\ddot{z}$ and the remaining aircraft state variables. This expression is substituted into the remaining equations involving α.

Surface Actuator

The surface actuator servos were all modeled by first-order systems with a time constant of $\tau = 0.1$ sec.

The servo equations are

$$\dot{\delta}_e = \frac{1}{\tau}(\delta_e^c - \delta_e) \tag{C.4-8}$$

$$\dot{\delta}_s = \frac{1}{\tau}(\delta_s^c - \delta_s) \tag{C.4-9}$$

Aerodynamic Noise Correlation Equation

The first-order noise correlation equation was developed in Appendix B, section B.7, and is repeated here

$$\dot{\alpha}_n = \frac{1}{T}(w - \alpha_n) \tag{C.4-10}$$

where

α_n is the angle-of-attack disturbance, deg

T is the noise correlation time, sec

w is the Gaussian white noise input

A vertical gust produces an angle-of-attack disturbance and, because of its varying intensity along the aircraft, an effective pitch disturbance.

The latter may be approximated as an aerodynamic pitch-rate disturbance, q_n, providing the gust wavelength is such that the gust velocity varies nearly linearly along the effective length of the aircraft. As explained in Section B.7 of Appendix B, this restricts the validity of the approximation to gust wavelengths longer than about eight times the effective aircraft length. However, because most of the gust-energy content is associated with the lower frequencies, it is probable that little error is involved when all frequencies are present in q_n, at least for the evaluation of rigid-aircraft response. The resulting simplification is a linear relation between α_n and q_n, viz.,

$$q_n = -\dot{\alpha}_n$$

$$= -\frac{1}{T}(w - \alpha_n) \qquad \text{(C.4-11)}$$

The alternative to the above approximation would be provision of a filter to operate upon α_n before application of Eq. C.4-11. It is likely, however, that the aircraft itself is a satisfactory filter of the higher-frequency response involved.

Control-law Structure

The control-law structures evaluated may be identified as (1) conventional elevator control, (2) direct-lift spoiler control with pitch-attitude control, and (3) a combination of (1) and (2). They may be delineated

	Pitch axis	Z axis
(1)	q, θ, z, $\dot{z}$, $\ddot{z}$ to elevator	
(2)	q, θ to elevator	z, $\dot{z}$, $\ddot{z}$ to direct-lift spoilers
(3)	q, θ, z, $\dot{z}$, $\ddot{z}$ to elevator	z, $\dot{z}$, $\ddot{z}$ to direct-lift spoilers

Consider the control law structure associated with (3). The servo commands are

$$\delta_e^c = p_1 z + p_2 \dot{z} + p_3 \ddot{z} + p_4 \theta + p_5 q \qquad \text{(C.4-12)}$$

$$\delta_s^c = p_6 z + p_7 \dot{z} + p_8 \ddot{z} \qquad \text{(C.4-13)}$$

where p_i are the system feedback gains.

State Variable Formation

The system equations, functionally dependent upon parameters p_i, may be set in the state variable form

$$\dot{x} = Fx + Gw$$

where w is a one-dimension white noise driving term and x is an [8 x 1] state vector identified as

$$x = \begin{bmatrix} q \\ \theta \\ z \\ \dot{z} \\ \ddot{z} \\ \delta_e \\ \delta_s \\ \delta_n \end{bmatrix}$$

For the specific control law structure defined by Eq. C.4-12 and C.4-13, the [8 x 8] dimension F matrix and the [8 x 1] G matrix may be identified in Table C.4-II.

C.4.2 Linear lateral model and subject to side gusts

The linearized lateral perturbation equations may be written

$$\dot{\beta} = C_\beta \beta + C_r r + C_{\delta_s} \delta_s + C_{\delta_r} \delta_r + C_{\delta_{tr}} \delta_{tr} + C_\phi \phi + C_{\beta_n} \beta_n \qquad \text{(C.4-14)}$$

$$\dot{p} = C_\beta \beta + C_p p + C_r r + C_{\delta_a} \delta_a + C_{\delta_s} \delta_s + C_{\delta_r} \delta_r + C_{\delta_{ta}} \delta_{ta} + C_{\delta_{tr}} \delta tr + C_{\beta_n} \beta_n \qquad \text{(C.4-15)}$$

Table C.4-II

F Matrix and G Matrix

[8x 8] F Matrix

$$F = \begin{bmatrix} -0.7019 & 0.0521 & 0 & 0 & 0.0345 & -0.8416 & -0.0758 & -0.473 \\ 1.0 & 0 & 0 & 0 & 0 & 0 & 0 & 0 \\ 0 & 0 & 0 & 1.0 & 0 & 0 & 0 & 0 \\ 0 & 0 & 0 & 0 & 1.0 & 0 & 0 & 0 \\ -3.6216 & -0.01138 & 3.29p_6 & 3.26p_7 & -0.8534 & 1.931 & -3.2734 & 3.1533 \\ -1.747p_5 & -1.747p_4 & -1.747p_1 & -1.747p_2 & +3.29p_8 & & & \\ & & & & -1.747p_3 & & & \\ 10.0p_5 & 10.0p_4 & 10.0p_1 & 10.0p_2 & 10.0p_3 & -10.0 & 0 & 0 \\ & & -0.9p_6 & -0.9p_7 & 0.9p_8 & & & \\ 0 & 0 & 10.0p_6 & 10.0p_7 & 10.0p_8 & 0 & -10.0 & 0 \\ 0 & 0 & 0 & 0 & 0 & 0 & 0 & -0.807 \end{bmatrix}$$

[8 x 1] G Matrix

$$G = \begin{bmatrix} 0.473 \\ 0 \\ 0 \\ 0 \\ 0 \\ -3.1533 \\ 0 \\ 0 \\ 0.807 \end{bmatrix}$$

$$\dot{r} = C_\beta \beta + C_p p + C_r r + C_{\delta_a} \delta_a + C_{\delta_s} \delta_s + C_{\delta_r} \delta_r + C_{\delta_{tr}} \delta_{tr} + C_{\beta_n} \beta_n \quad \text{(C.4-16)}$$

$$\dot{\phi} = p \quad \text{(C.4-17)}$$

$$\dot{\psi} = r \quad \text{(C.4-18)}$$

where β, ϕ, and ψ are measured in degrees, p and r in degrees/sec.

The control variables are defined .

δ_s - spoiler deflection, deg

δ_a - aileron deflection, deg

δ_{ta} - aileron tab deflection, deg

δ_r - rudder deflection, deg

δ_{tr} - rudder tab deflection, deg

Coefficient values corresponding to the approach-to-landing flight condition of section C.3 are listed in Table C.4-III.

Reduction of the order of the state

As for the longitudinal model, the aerodynamic effectors are assumed directly controlled by the servo actuators; the aileron and rudder tab terms are consequently dropped from Eq. C.4-14, C.4-15, and C.4-16.

Trajectory equations

The relevant linearized trajectory equations are

$$\ddot{y} = U_0 (\dot{\beta} + r)/57.3 \quad \text{(C.4-19)}$$

$$\dot{y} = \int_0^t \ddot{y}(\tau)\, d\tau \quad \text{(C.4-20)}$$

$$y = \int_0^t \dot{y}(\tau)\, d\tau \quad \text{(C.4-21)}$$

Table C.4-III

Coefficient Values of Aircraft Lateral Equations of Motion

Coefficient \ Equation	$\dot{\beta}$	$\dot{p}$	r
C_{β}	-0.1485	-3.73	0.842
C_{r}	-0.987	0.8	-0.239
C_{p}	0.	-1.52	-0.0626
C_{ϕ}	0.115	0.	0.
C_{δ_s}	-0.00534	0.771	0.0785
C_{δ_a}	0.	-0.73	0.1045
$C_{\delta_{ta}}$	0.	-0.1065	0.
C_{δ_r}	0.0364	0.43	-0.581
$C_{\delta_{tr}}$	0.00792	0.0505	-0.117
C_{β_n}	-0.1485	-3.73	0.842

Evaluation of the linearized trajectory state involves a linear combination of the aircraft state equations, as seen from Eq. C.4-19. To avoid linear dependence, the equations are rewritten in terms of $\ddot{y}$ rather than β. To do this, a similar procedure of substitution to that outlined in the previous section is followed.

Surface actuator servo models

All surface actuator servos were modeled by a first-order system with a time constant of $\tau = 0.1$ sec.

The servo equations are

$$\dot{\delta}_a = (1/\tau)(\delta_a^c - \delta_a) \qquad \text{(C.4-22)}$$

$$\dot{\delta}_s = (1/\tau)(\delta_s^c - \delta_s) \qquad \text{(C.4-23)}$$

$$\dot{\delta}_r = (1/\tau)(\delta_r^c - \delta_r) \qquad \text{(C.4-24)}$$

Aerodynamic noise correlation equation

Following section B.7 of Appendix B, the first-order noise correlation equation is written

$$\dot{\beta}_n = (1/T)(w - \beta_n) \qquad \text{(C.4-25)}$$

where

β_n is the sideslip gust disturbance, deg.

T is the noise correlation time, sec.

w is a Gaussian white noise imput

Control law structure

The following control law structures were evaluated:

	Roll axis	Yaw axis
(1)	p, ϕ, y, $\dot{y}$, $\ddot{y}$ to ailerons	r to rudder
(2)	p, ϕ, y, $\dot{y}$, $\ddot{y}$ to spoilers	r to rudder
(3)	p, ϕ, y, $\dot{y}$, $\ddot{y}$ to spoilers and ailerons	r to rudder

Turn coordination feedforward to the rudder was additionally provided in all the above control structures.

Consider the control structure associated with (3) above. The aileron servo command is written

$$\delta_a^c = p_1 y + p_2 \dot{y} + p_3 \ddot{y} + p_4 p + p_5 \phi \qquad \text{(C.4-26)}$$

Assuming an identical servo actuator for the spoiler, its displacement is given by

$$\delta_s = K_s \delta_a \qquad \text{(C.4-27)}$$

where $K_s = -2.84$ for the CV880 aircraft.

The rudder servo command is

$$\delta_r^c = p_6(-r_c + r) \qquad \text{(C.4.28)}$$

where r_c is the commanded yaw rate for turn coordination.

State variable formulation

With the control law structure defined by Eq. C.4-26 and C.4-28 the aircraft, trajectory, servo-actuator, and noise-correlation equations may be set in the state-variable form

$$\dot{x} = Fx + Gw$$

where the state vector x is given by

$$x = \begin{bmatrix} p \\ r \\ \phi \\ y \\ \dot{y} \\ \ddot{y} \\ \delta_a \\ \delta_r \\ \beta_n \end{bmatrix}$$

Table C.4-IV

F Matrix and G Matrix

F Matrix

$$F = \begin{bmatrix}
-1.52 & 0.473 & -2.89 & 0 & 0 & 5.18 & -3.3 & -0.483 & 0 \\
-0.0626 & -0.1653 & 0.653 & 0 & 0 & -1.17 & -0.0325 & -0.3746 & 0 \\
1.0 & 0 & 0 & 0 & 0 & 0 & 0 & 0 & 0 \\
0 & 0 & 0 & 0 & 1.0 & 0 & 0 & 0 & 0 \\
0 & 0 & 0 & 0 & 0 & 1.0 & 0 & 0 & 0 \\
0.744p_4 & 1.765p_6 & 0.744p_5 & 0.744p_1 & 0.744p_2 & 0.744p_3 & & & \\
+0.5541 & & +0.0412 & & & -0.2227 & -0.7374 & -1.7886 & 0.581 \\
-0.203p_4p_6/p_5 & +0.7089 & -0.406p_6 & -0.203p_1p_6/p_5 & -0.203p_2p_6/p_5 & -0.203p_3p_6/p_5 & & & \\
10.0p_4 & 0 & 10.0p_5 & 10.0p_1 & 10.0p_2 & 10.0p_3 & -10.0 & 0 & 0 \\
-1.15p_4p_6/p_5 & 10.0p_6 & -2.3p_6 & -1.15p_1p_6/p_5 & -1.15p_2p_6/p_5 & -1.15p_3p_6/p_5 & 0 & -10.0 & 0 \\
0 & 0 & 0 & 0 & 0 & 0 & 0 & 0 & -0.807
\end{bmatrix}$$

G Matrix

$$G = \begin{bmatrix}
0 \\ 0 \\ 0 \\ 0 \\ 0 \\ -0.581 \\ 0 \\ 0 \\ 0.807
\end{bmatrix}$$

Appendices B and C References

1. Etkin, B., "Dynamics of Flight", Wiley, 1959.
2. "CV880M Data", Lear Siegler Report ADR-595.
3. Etkin, B., "Theory of Flight of Airplanes in Isotropic Turbulence - Review and Extension", AGARD Report No. 372, April, 1961.
4. Foss, K., McCade, W., Gust Loading of Rigid and Flexible Aircraft in Continuous Atmospheric Turbulence", (MIT) WADC Technical Report 57-704, January, 1958.

Appendix D

THE SCANNING BEAM MICROWAVE ILS TRANSFORMATION EQUATIONS AND ERROR MODEL

by

George W. Cherry

and

Donald W. Keene

The scanning beam microwave ILS is an advanced radio navigation which provides precision azimuth elevation, and range data, to approaching and landing aircraft. A prototype embodying many of the principles of the new system is presently undergoing successful testing at the Federal Aviation Administration's National Aviation Facilities Experimental Center (NAFEC). The Radio Technical Commission for Aeronautics (RTCA) has formed a special committee for specifying the data-signal format and the performance parameters of the new system. The new system could replace the current VHF ILS equipment as the international landing system as early as 1975. RTCA is endeavoring to make the new ILS compatible with all users – general aviation, civil airlines, military aircraft – and with all type of aircraft – wide-bodied jets, supersonic transports, VTOL, STOL, etc. It is anticipated that the microwave ILS will be utilized to provide the precision navigation data required to meet the all-weather landing requirements of the Space Transportation System.

The technical concept, which RTCA Special Committee 117 has chosen for the new ILS, uses ground-transmitted, scanning planar beams. There are at least two scanning beams associated with each ILS runway – an azimuth beam and an elevation beam. The ground transmitters angle-encode the transmissions to the aircraft. As the ground-transmitted scanning beams sweep past the aircraft ILS antenna, the airborne ILS receiver receives, decodes, and sends to the guidance computer the azimuth or elevation angle it obtains. The azimuth and elevation transmissions are time- or frequency-multiplexed. There will be a precision DME transceiver associated with the azimuth-beam transmitter; thus, the new ILS will provide 3-D navigation information relative to the runway. The scan frequency tentatively chosen is 15 scans per second.

The frequency bands likely to be used are C-band (5.00 to 15.7 GHz) and Ku-band (15.4 to 15.7 GHz). For runways serving sophisticated users or CAT IIIA-c landings, both frequency bands may be used: a narrow-beam, limited-angle coverage Ku-band "fine" system, and a wide-angle coverage C-band "coarse" system. See Fig. D-1 for the possible location of the various antennas and a tabulation of the accuracies and angle coverages of the "fine" and "coarse" systems.

The C-band elevation antenna is located at the typical glide-slope aiming point of most aircraft. Some runway configurations would have only this elevation antenna. The Ku-band elevation antenna is used for CAT III landing flare control on better-equipped runways. It is located farther from the runway threshold so that the aircraft will not pass the flare antenna before final runway contact. The accuracy with which the flare-initiation altitude can be inferred from the "fine" elevation beam and the precision DME signals is quite high. See Fig. D-2 for a plot of this error versus flare-antenna displacement. Notice that the rms altitude error due to 0.035-degree rms error in elevation angle and 25-ft rms error in DME range is only slightly in excess of two feet for a flare-antenna displacement of 3500 feet. The geometrically optimum location of the flare antenna locates this transmitter too close to the runway threshold to control flare through touchdown.

Measurement Geometry

Figs. D-3a and D-3b illustrate the ILS measurement geometry relative to the runway coordinate system. If the elevation antenna displacement from the runway center line is ignored, the following relationships are valid:

$$EL = h_1(x, y, z, d_0) = \tan^{-1}\left(\frac{z}{x}\right) \tag{D-1a}$$

$$AZ = h_2(x, y, z, d_0 = \tan^{-1}\left(\frac{y}{d_0 - x}\right) \tag{D-1b}$$

$$d = h_3(x, y, z, d_0) = \sqrt{(d_0 - x)^2 + y^2 + z^2} \tag{D-1c}$$

Note that these relationships are valid for both the glide-slope antenna and the flare antenna; the geometry differs only in terms of the displacement D_0.

The corresponding inverse relationships are:

$$x = \cos(EL)\left[\frac{d_0 \cos(EL) - \cos(AZ)\sqrt{d^2\,(\cos^2(EL) + \sin^2(EL)\cos^2(AZ) - d_0^2 \sin^2(EL)}}{\cos^2(EL) + \sin^2(EL)\cos^2(AZ)}\right] \tag{D-2a}$$

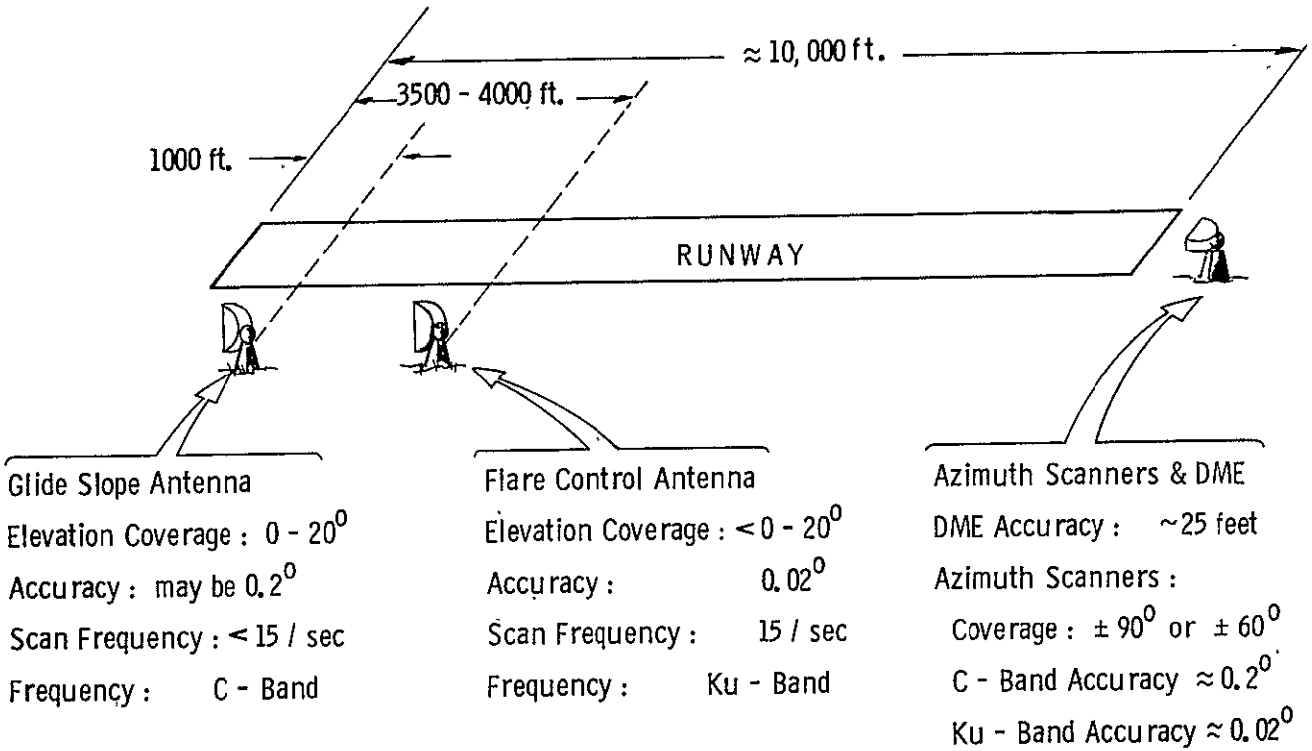

Fig. D-1 Scanning Beam Antennas: Location, Coverage, Accuracy

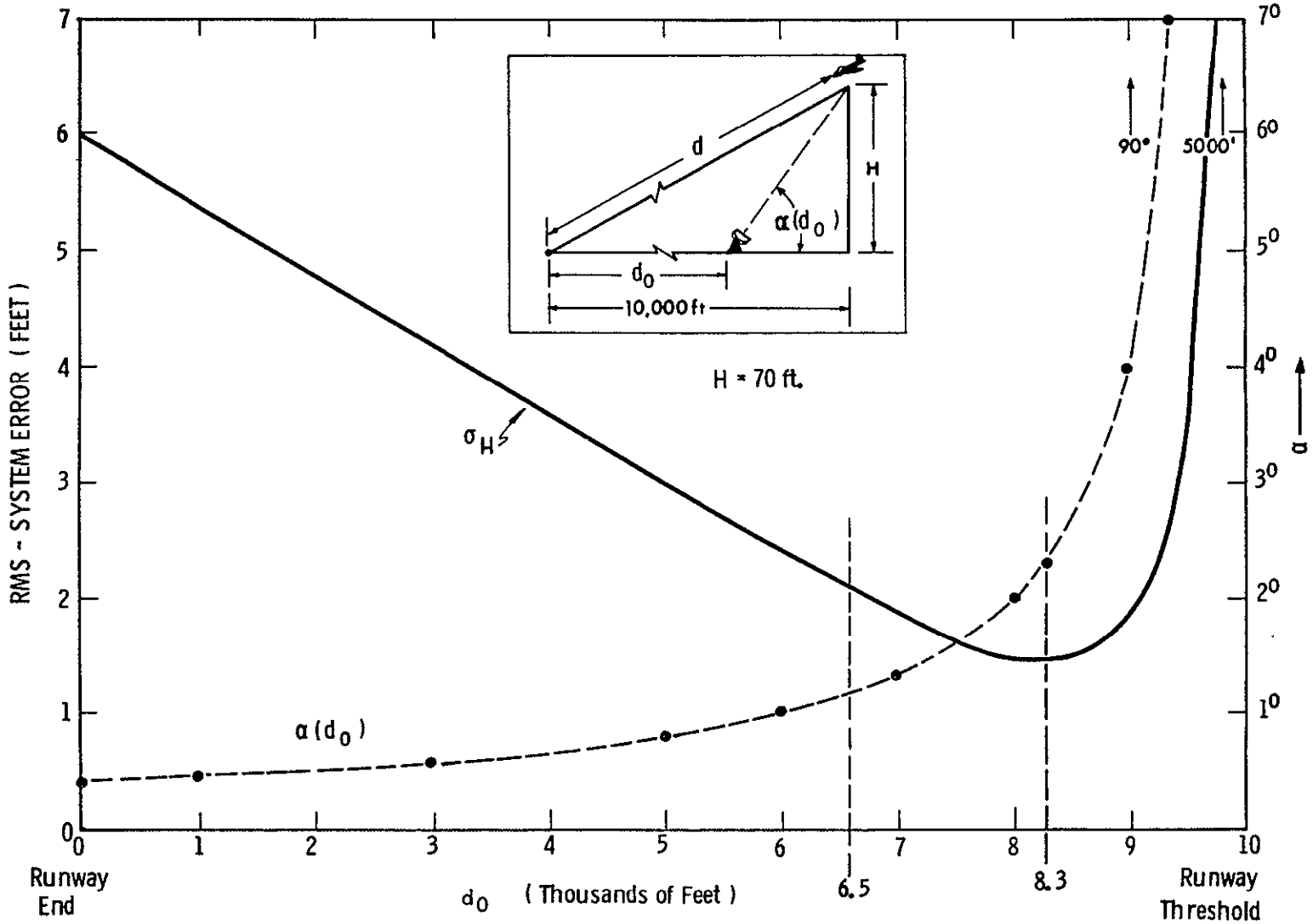

Fig. D-2 Flare Antenna Elevation Angle and Root-Mean Squared Altitude Error - Shown as a Function of Antenna Location.

EL = elevation angle

AZ = azimuth angle

d = DME range from the azimuth antenna site

d_o = displacement of the elevation antenna from the azimuth antenna site

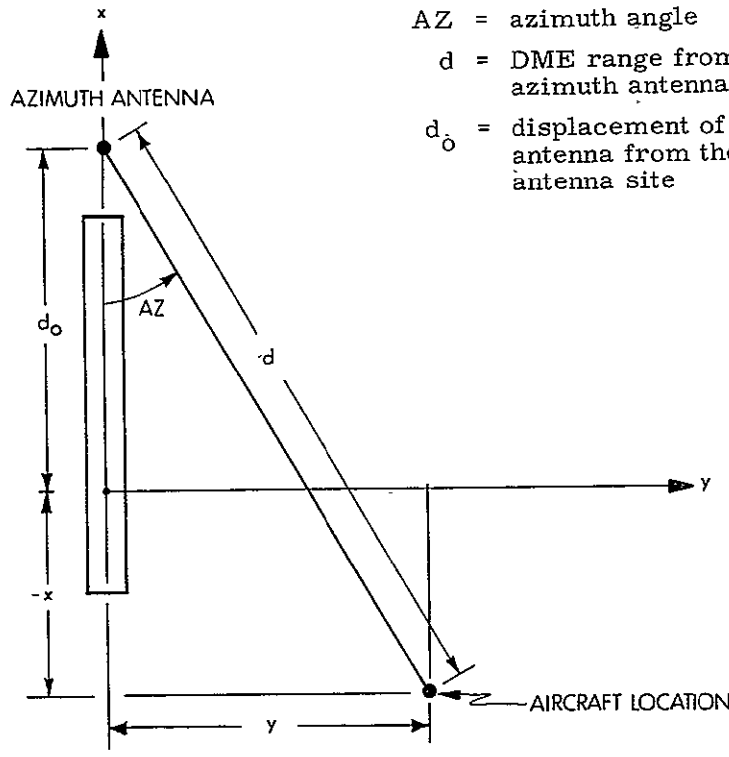

a) IN HORIZONTAL PLANE

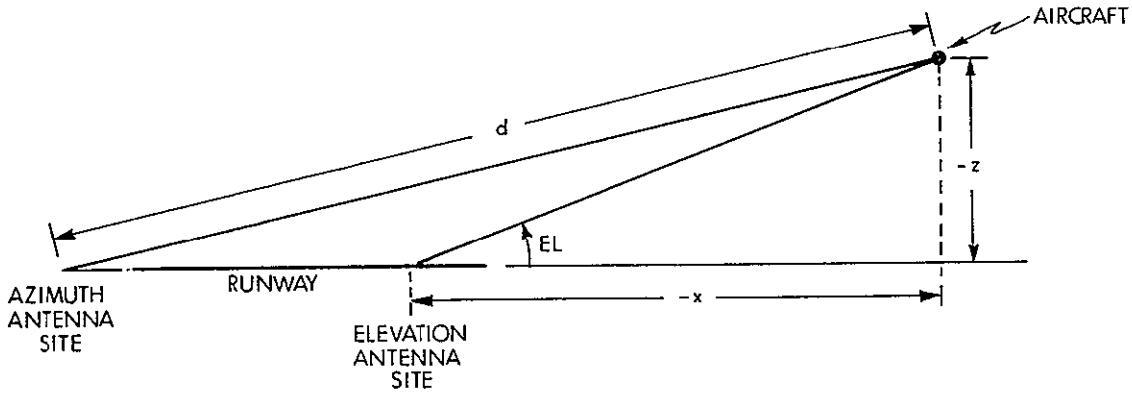

b) IN VERTICAL PLANE

Fig. D-3 Geometry of Aircraft Position

$$y = \sin(AZ)\left[\frac{d_0\cos(AZ)\ \sin^2(EL) + \cos(EL)\sqrt{d^2(\cos^2(EL) + \sin^2(EL)\cos^2(AZ)) - d_0^2\sin^2(EL)}}{\cos^2(EL) + \sin^2(EL)\cos^2(AZ)}\right] \quad \text{(D-2b)}$$

$$z = \sin(EL)\left[\frac{d_0\cos(EL) - \cos(AZ)\sqrt{d^2(\cos^2(EL) + \sin^2(EL)\cos^2(AZ)) - d_0^2\sin^2(EL)}}{\cos^3(EL) + \sin^2(EL)\cos^2(AZ)}\right] \quad \text{(D-2c)}$$

The differential relationships between measurement deviations and the position deviation are summarized in the following equation:

$$\delta\underline{m} = \left[\frac{\delta\underline{h}}{\delta\underline{x}}\right]\delta x \quad \text{(D-3)}$$

where

$$\delta\underline{m} = \begin{bmatrix} \delta(EL) \\ \delta(AZ) \\ \delta d \end{bmatrix}$$

$$\delta\underline{x} = \begin{bmatrix} \delta x \\ \delta y \\ \delta z \end{bmatrix}$$

$$\frac{\delta\underline{h}}{\delta\underline{x}} = \begin{bmatrix} -\frac{z}{x^2 + z^2} & 0 & \frac{x}{x^2 + z^2} \\ \frac{y}{(d_0 - x)^2 + y^2} & \frac{d_0 - x}{(d_0 - x)^2 + y^2} & 0 \\ \frac{x - d_0}{\sqrt{(d_0 - x)^2 + y^2 + z^2}} & \frac{y}{\sqrt{(d_0 - x)^2 + y^2 + z^2}} & \frac{z}{\sqrt{(d_0 - x)^2 + y^2 + z^2}} \end{bmatrix}$$

The exact relationship (Eq. D-2a, b, c) could be used to establish the initial position fix upon aqusition of the ILS signal. The differential relation (Eq. D-3) will be used for incorporating measurements in the navigation filter estimates.

System Accuracy

The anticipated accuracy of the air-derived data for the scanning-beam microwave ILS is summarized in Fig. D-1. For comparison, the performance requirements for the developmental system at NAFEC are summarized in Table D-I. Note that this system includes a precision-approach radar capability. Ground tests have confirmed that the range, elevation, and azimuth accuracies are within the specified tolerances. Data compiled from a series of flight tests conducted at NAFEC have yielded the following results (from Reference D.1):

Elevation-angle error, rms	0.028°
Azimuth-angle error, rms	0.021°
Range error, rms	75 ft

The elevation azimuth, and range errors are uncorrelated with respect to each other and are essentially uncorrelated from measurement to measurement. Thus the covariance matrix for the measurement errors can be written as:

$$V_n = \begin{bmatrix} \sigma_{EL}^2 & 0 & 0 \\ 0 & \sigma_{AZ}^2 & 0 \\ 0 & 0 & \sigma_d^2 \end{bmatrix}$$

where σ_{EL}, σ_{AZ}, and σ_d can be considered constant over the space scanned by the microwave ILS. Flight tests have also shown that the measurement errors are substantially unaffected by multipath propagation.

REFERENCE FOR APPENDIX D

D.1 Advanced Scanning Beam Guidance System for All Weather Landing, Federal Aviation Administration Report No. RD-68-2, February, 1968.

Table D-I

Air-Derived Guidance-Signal Characteristics

Elevation angle error	Standard deviation of less than 0.03 degree
Azimuth angle error	Standard deviation of less than 0.05 degree
Range error	Standard deviation not exceeding 100 feet or 1 percent of range, whichever is greater
System range	15 miles from touchdown
Elevation angle coverage	0 to 10 degrees
Azimuth angle coverage	±5 degrees of runway centerline
Azimuth clearance coverage	5 to 35 degrees each side of runway centerline
DME coverage	±5 degrees of runway centerline

Radar-Operation Performance Requirement

Range (for a 20-meter square target,
10 mm/hour uniform rainfall
over the path)

Elevation	9 miles
Azimuth	13 miles
Accuracy	Adequate to define a point target on a 3.0-degree glide slope at 2000 feet from the glide-slope origin to within ±15 feet in azimuth and elevation and ±50 feet in distance.

External:

NASA/RASPO (1)

MSC:

National Aeronautics and Space Administration (40 & 1R)
Manned Spacecraft Center
Houston, Texas 77058
ATTN: BG/731 (47) (1)
EG 23 (9 & 1R)
BM-6 (4)
BM-7 (1)
K. Cox (25)

Internal:

D. Hoag
W. Stameris
G. Mayo
N. Sears
A. Laats
L. Larson
R. Battin
E. C. Hall
R. Crisp
G. Silver
J. Gilmore
G. Ogletree
J. Barker
R. O'Donnell (KSC)
J. Hand
T. Lawton (MSC)
J. Nevins
T. Fitzgibbon
S. Copps
M. Hamilton
G. Cherry (50)
G. Levine
D. Fraser
P. Felleman
R. Weatherbee
CSDL Technical Documentation Center (10)
Apollo Library (2)